BOLT BERANEK AND NEWMAN INC

CONSULTING • DEVELOPMENT • RESEARCH

A THEORETICAL AND EXPERIMENTAL MODEL-STUDY OF THE SOUND-INDUCED VIBRATION TRANSMITTED TO A SHROUD-ENCLOSED SPACECRAFT

Jerome E. Manning

Contract No. NAS5-10302
Report No. 1891

1 May 1970

Submitted to:

National Aeronautics and Space Administration
Goddard Space Flight Center
Greenbelt, Maryland

FINAL REPORT

20 January 1967 – 20 July 1969

A THEORETICAL AND EXPERIMENTAL MODEL-STUDY OF THE SOUND-INDUCED VIBRATION TRANSMITTED TO A SHROUD-ENCLOSED SPACECRAFT

Contract No. NAS5-10302

Goddard Space Flight Center

Contracting Officer: A.L. Essex
Technical Officer: J.P. Young, 321

Prepared by:

Bolt Beranek and Newman Inc.
50 Moulton Street
Cambridge, Massachusetts 02138

Project Manager: Jerome E. Manning

for

Goddard Space Flight Center
Greenbelt, Maryland 20771

ABSTRACT

Results are presented from a three year study of the vibration transmitted to a shroud-enclosed spacecraft from an external acoustic field. The study included both a theoretical prediction of the vibration transmission and an experimental study of a 1/2-scale model of a typical spacecraft assembly. The theoretical predictions were obtained using a statistical energy analysis. Data from the experiments are compared with the predictions to establish the validity and accuracy of the prediction technique. Experiments were also conducted to determine the effect of changes in the model configuration on the vibration transmission. The results of the study indicate that the vibrations transmitted via the internal acoustic space and those transmitted via the mounting trusses are comparible.

TABLE OF CONTENTS

LIST OF FIGURES

LIST OF TABLES

A THEORETICAL AND EXPERIMENTAL MODEL-STUDY OF THE SOUND-INDUCED VIBRATION TRANSMITTED TO A SHROUD-ENCLOSED SPACECRAFT

1. INTRODUCTION

1.1 Program Review

During the past three years, Bolt Beranek and Newman Inc. (BBN) has conducted a theoretical[1] and experimental[2] model-study of the sound-induced vibrations transmitted to a shroud-enclosed spacecraft. The spacecraft-shroud assembly used for the study is shown schematically in Fig. 1. The major structural and acoustical elements of this assembly are identified in Fig. 2.

In the study, the source of vibration was taken to be a diffuse field of acoustic noise; the frequencies of excitation of the full-scale assembly were taken to be in the range of 200 Hz to 6,000 Hz. Frequencies of excitation for the experimental study were doubled since a one-half scale model was used. Vibrations transmitted from the boost vehicle to the spacecraft were not considered, since the frequency content of these vibrations is typically below 200 Hz.

Two paths of vibration transmission exist from the external acoustic field to the spacecraft: (1) an acoustic path involving the external acoustic space, the shroud and the internal acoustic space; and (2) a mechanical path involving the external acoustic space, the shroud, the ring frame and the mounting trusses. One purpose of our study was to develop a technique to predict the vibrations transmitted to the spacecraft by these two paths.

The second purpose of our study was to determine the effect of structural parameter changes on the amount of vibration transmitted

to the spacecraft. Theoretical predictions of this vibration transmission were obtained using statistical energy analysis.[3] This type of analysis has been used in the past to study the interaction of an acoustic field with a structure and to study the vibration transmitted between two structures; however, the study described in this report represents the first attempt to use statistical energy analysis to predict the interaction of a large number of structural elements. The theoretical predictions for this study are derived in Ref. 1. However, the derivation of these predictions is reviewed in Section 3 below.

Experiments were conducted on a one-half scale model of a typical spacecraft-shroud assembly to provide data which could then be compared with the theoretical response predictions. The OGO spacecraft assembly was chosen as the basis for this model, and simple structural elements were chosen to represent approximately the actual elements in the OGO assembly. The model for the shroud is a ribbed cylindrical shell; the model for the spacecraft is an array of four honeycomb panels. The model shroud is connected to the model spacecraft by four channel trusses and a ring frame. A detailed description of the entire model is presented in Section 2.

Structural properties of the one-half scale model only approximate the properties of the OGO assembly elements. We do not intend that the vibration levels measured for this model be indicative of vibration levels in the actual assembly; but, data from our model should serve to establish the validity of the theoretical prediction technique for a spacecraft-shroud assembly.

Two kinds of experiments were conducted with the one-half scale model. First, experiments were conducted to measure the flow of vibratory energy in individual structural elements of the model and in combinations of the elements coupled together. Second, experiments were conducted to measure the vibratory response of the individual assembly elements when the model shroud is excited by an external acoustic field of noise. Ref. 2 describes many of the experiments that were conducted in this study. Unfortunately, some of the data presented in Ref. 2 are inaccurate.* Therefore, all of the experimental data are presented in this report.

1.2 Summary of Results

Spectra of the vibration transmitted to elements of the spacecraft-shroud assembly are shown in Figs. 24 - 35. Data from the experiments are in reasonable agreement with the theoretical predictions; although, agreement between the predictions and the measurements for acoustic path transmission is somewhat better than for mechanical path transmission. The measured vibration transmission to the spacecraft by the mechanical path is as much as 5 to 10 dB from the theoretical predictions for many frequency bands.

The spectra of vibration transmitted to the spacecraft by the mechanical path and by the acoustic path are comparable in amplitude. This result is, of course, limited to our particular model; but, clearly, both paths of vibration transmission must be considered in designing or analyzing the environment of an actual spacecraft. The spectrum of vibration transmitted to the *mounting trusses* by the mechanical path far exceeds that transmitted by the acoustic path.

---

*See Appendix 1.

In addition to the above results, the effects of changing the model configuration have been investigated. Changes that were investigated include:

1. Excitation of the shroud by a directive acoustic field;
2. Removal of the absorptive liner from the shroud;
3. Addition of covers to the top and bottom of the spacecraft;
4. Addition of an adaptor to the spacecraft assembly;
5. Excitation of the spacecraft by a simulated acoustic field and a multi-modal fixture.

Techniques to measure the damping of a structure were thoroughly investigated using the decay-rate technique described in Sec. 4.1. However, in measuring the damping of the model spacecraft, certain inconsistencies were noted and, therefore, the technique of directly measuring the power input from a point-drive shaker and the resulting response of the structure was investigated. It was found that this technique is more reliable and should be used whenever possible.

2. DESCRIPTION OF THE MODEL

2.1 General Description

A typical spacecraft assembly consists of six structural and acoustical elements:

1. External acoustic space;
2. Shroud;
3. Internal acoustic space;
4. Spacecraft;
5. Ring frame which connects to the boost vehicle; and
6. Mounting trusses (or a mounting shell) to connect the spacecraft to the ring frame.

We have chosen rather simple structural elements to represent the six actual components. The model shroud (shown in Figs. 3 and 4) is taken to be a thin-walled ribbed cylindrical shell. We have not included the conical section of an actual shroud with our model, since we do not feel that it has a great effect on the vibration transmission characteristics of the shroud, and since theoretical predictions of vibration transmission by a cone have not been worked out at this time. The model consists of an 0.087-inch-thick NEMA grade G-11 fiberglass-epoxy laminate shell. Ribs of aluminum channel have been epoxied in position at the locations shown. The ends of the shell are sealed with 0.75-inch plywood baffles that are mechanically isolated from the shell.

The shroud of an actual spacecraft assembly is often lined with a thermal blanket which controls the absorption in the internal acoustic space. For our model, we selected a one-inch-thick porous fiberglass blanket to line the shroud.

Although an actual spacecraft is a very complicated structure, for our study we selected a simple rectilinear box composed of four honeycomb panels (shown in Figs. 5, 6 and 9). In modeling the spacecraft, we have not included instruments or other components that are connected to the main structure. However, the addition of a large number of components to the spacecraft would, no doubt, change its vibrational characteristics.

The model chosen to represent the ring frame (shown in Figs. 7 and 9) consists of an aluminum channel ring with two aluminum angles connected to it by a rigid epoxy and a number of small screws.

In our model, the spacecraft is supported on the ring frame by the four mounting trusses. These trusses (shown in Figs. 5, 7, 8 and 9) are simple aluminum channel beams stiffened by gussets at each end and in the middle of the truss.

2.2 Structural Parameters of the Model

A list of structural parameter values for the elements of the one-half scale model is given in Table 1. The test frequencies for the one-half scale model are twice those for the actual assembly.

3. THEORY

3.1 Use of Statistical Energy Analysis

Statistical Energy Analysis holds, as its basic hypothesis, that the time-average power flow between two groups of resonant modes is proportional to the difference in their average modal energy,

$$\Pi_{ij} \propto (\theta_i - \theta_j) \quad , \tag{1}$$

where Π_{ij} is the time-average power flow between group i and group j and θ_i is the average energy per mode in group i. This basic hypothesis can be proven when each group has one mode excited by an independent white-noise source;[4] and the hypothesis can be shown to be a good approximation when the coupling is small and when there is modal overlap in the frequency domain, i.e., when the separation between resonance frequencies is less than the resonance bandwidth of each mode.[5] We will assume that the basic power-flow relation is a satisfactory approximation for *all* cases, supporting our assumption by the agreement between Statistical Energy Analysis predictions and experiments.[6]

When the modes of each group have resonance frequencies in a narrow band, the power-flow relation (1) can be written as*

$$\Pi_{ij} = \omega \eta_{ij} n_i \Delta\omega \left[\frac{E_i}{n_i \Delta\omega} - \frac{E_j}{n_j \Delta\omega} \right] \quad , \tag{2}$$

*Note, since $\Pi_{ij} = -\Pi_{ji}$, that $\eta_{ij} n_i = \eta_{ji} n_j$.

where ω is the center frequency of the band, η_{ij} is by definition the coupling loss factor, n_i is the modal density of group i, $\Delta\omega$ is the frequency bandwidth, and E_i is the time-average total energy of all modes in group i.

To obtain power-balance equations, we must equate the power flow to and from each mode group, with the power dissipated in the group and the power supplied by external sources. The time-average power dissipated is given by

$$\Pi_{id} = \omega\eta_{id} n_i \Delta\omega \left(\frac{E_i}{n_i \Delta\omega}\right), \tag{3}$$

where η_{id} is the dissipation loss factor for group i. The dissipation loss factor is defined by Eq. 3.*

Consider now a set of inner-connected mode groups (Fig. 10). Power balance for group i can be written as

$$\Pi_{id} + \sum_j \Pi_{ij} = \Pi_i^{in}, \tag{4}$$

where Π_i^{in} is the power supplied to group i from external sources. Equation 4 can be written in terms of the loss factors as

$$\omega\eta_{id} n_i \Delta\omega \frac{E_i}{n_i \Delta\omega} + \sum_j \omega\eta_{ij} n_i \Delta\omega \left[\frac{E_i}{n_i \Delta\omega} - \frac{E_j}{n_j \Delta\omega}\right] = \Pi_i^{in}. \tag{5}$$

It will be convenient to rewrite Eq. 5 as

$$-\eta_{itot} \frac{E_i}{n_i} + \sum_{j}^{j\neq i} \eta_{ij} \frac{E_j}{n_j} = -\frac{1}{\omega} \frac{\Pi_i^{in}}{n_i}, \tag{6}$$

*Note that the definition of coupling loss factor, Eq. 2, has been made to conform to the classical definition of dissipation loss factor, Eq. 3.

where η_{itot} is the total loss factor defined as

$$\eta_{itot} = \eta_{id} + \sum_{j}^{j \neq i} \eta_{ij} \quad . \tag{7}$$

Power balances for other mode groups give a set of simultaneous algebraic equations that can be solved for the total energies E_i in terms of the loss factors and modal densities. The power balance equations can be written in matrix form as*

$$-\left[\eta_{ij}\right]\left[\frac{E_j}{n_j}\right] = \frac{1}{\omega}\left[\frac{\Pi_i^{in}}{n_i}\right] \quad , \tag{8}$$

where

$$\eta_{ii} \equiv -\eta_{itot} \quad . \tag{9}$$

The expressions for mode-group energy found by solving Eqs. 8 are in terms of coupling loss factors, dissipation loss factors, and modal densities. To obtain these parameters, it is important that the modes of each group have the same energy. Modes within a group will have the same energy if they have similar dissipation loss factors and similar coupling loss factors to modes in other groups, or if they are closely coupled together.[6]

Applications of the power-balance equations will be given in the following sections.

---

*For the special case in which the energy of one mode group is maintained at a set level by external sources, the power supplied to the mode groups can be set to zero and Eqs. 8 can be solved for the unknown energies of the mode groups in terms of the specified mode-group energy.

Acoustic Space-Plate

Consider the problem of a plate immersed in a closed acoustic space. The energy in the acoustic space in each 1/3-oct band is maintained at a set level. We will find the resulting energy in the plate in 1/3-oct bands.

For this problem, Eqs. 8 become

$$\eta_{ptot} \frac{E_p}{n_p} - \eta_{pa} \frac{E_a}{n_a} = 0 \quad , \tag{10}$$

where η_{ptot} is the total loss factor of the plate at frequency ω, η_{pa} is the coupling loss factor between the plate and the acoustic space at ω, n_a is the modal density of the acoustic space at ω, n_p is the modal density of the plate at ω, E_p is the energy of the plate in the 1/3-oct band centered around ω, and E_a is the specified energy in the acoustic space in the 1/3-oct band centered around ω. Equation 10 can be solved to give

$$\frac{E_p}{n_p} = \frac{E_a}{n_a} \left(\frac{\eta_{pa}}{\eta_{ptot}} \right) . \tag{11}$$

Acoustic Space - Cylindrical Shell - Acoustic Space

Consider the problem of a cylindrical shell, baffled on each end, immersed in an acoustic space. The energy in the acoustic space in each 1/3-oct band is maintained at a set level. We will find the resulting 1/3-oct-band energy in the shell and in the interior acoustic space.

Resonant modes of the cylindrical shell should be divided into two groups - acoustically fast (AF) modes that are well-coupled

to the acoustic spaces and acoustically slow (AS) modes that are not well coupled to the acoustic space. Equations 8 become

$$-\begin{bmatrix} -\eta_{AFtot} & \eta_{AFAS} & \eta_{AFi} \\ \eta_{ASAF} & -\eta_{AStot} & \eta_{ASi} \\ \eta_{iAF} & \eta_{iAS} & -\eta_{itot} \end{bmatrix} \begin{bmatrix} \frac{E_{AF}}{n_{AF}} \\ \frac{E_{AS}}{n_{AS}} \\ \frac{E_i}{n_i} \end{bmatrix} = \begin{bmatrix} \eta_{AFe} \\ \eta_{ASe} \\ \eta_{ie} \end{bmatrix} \frac{E_e}{n_e} , \qquad (12)$$

where E_e is assumed to be known and AF, AS, e, and i signify the AF mode group, the AS mode group, the external-acoustic-space mode group, and the internal-acoustic-space mode group, respectively. Equations 12 can be solved exactly. However, in many practical cases, simplifications are valid.

In our analysis we take the modes of the undamped cylindrical shell to be those of a simply-supported undamped shell in vacuum. For such an idealized case the modes of the shell are uncoupled. A more realistic model of an actual structure would require complex boundary conditions, some form of damping, and many types of discontinuities in the shell such as ribs, stringers, equipment mounting fixtures, etc. The vibrations of this complex model can be studied in terms of the modes of the simply-supported undamped shell in vacuum if we allow the modes to be coupled in the describing equations of motion. Unfortunately, an understanding of modal coupling has not advanced to the point where we can quantitatively evaluate the coupling loss factor between AF and AS modes, η_{AFAS}, in Equation 12. For a cylindrical shell in which no longitudinal discontinuities (stringers)

are present, we can assume that the intermodal coupling is very small so that

$$\eta_{AFAS} \approx 0 \quad . \tag{13}$$

For a shell with longitudinal discontinuities the intermodal coupling will be large. For this case we can assume that the coupling loss factor η_{AFAS} is larger than the total loss factors of the AF and AS modes so that the AF and AS modes will have equal modal energy. The validity of these assumptions cannot be supported, however, until further studies of modal coupling are undertaken.

The one-half scale model shroud used for our study has no longitudinal discontinuities. Therefore, we will assume in the remaining sections of this report that Equation 13 holds true. The case of strong modal coupling is discussed in Appendix 2.

When the internal-space modal energy is much less than the external-space modal energy,

$$\frac{E_i}{n_i} << \frac{E_e}{n_e} \quad , \tag{14}$$

then Eqs. 12 give

$$\frac{E_{AF}}{n_{AF}} = \frac{\eta_{AFe}}{\eta_{AFtot}} \frac{E_e}{n_e} - \frac{\eta_{AFi}}{\eta_{AFtot}} \frac{E_i}{n_i} \approx \frac{\eta_{AFe}}{\eta_{AFtot}} \frac{E_e}{n_e} \quad , \tag{15}$$

and, similarly,

$$\frac{E_{AS}}{n_{AS}} = \frac{\eta_{ASe}}{\eta_{AStot}} \frac{E_e}{n_e} - \frac{\eta_{ASi}}{\eta_{AStot}} \frac{E_i}{n_i} \approx \frac{\eta_{ASe}}{\eta_{AStot}} \frac{E_e}{n_e} \quad . \tag{16}$$

The total energy in the shell is the sum of E_{AF} and E_{AS}. When Eqs. 13 and 14 hold, the energy in the internal space is

$$\frac{E_i}{n_i} = \frac{\eta_{ie}}{\eta_{itot}} \frac{E_e}{n_e} + \frac{\eta_{iAF}}{\eta_{itot}} \frac{E_{AF}}{n_{AF}} + \frac{\eta_{iAS}}{\eta_{itot}} \frac{E_{AS}}{n_{AS}}$$

$$\approx \left[\frac{\eta_{ie}}{\eta_{itot}} + \frac{\eta_{iAF}\eta_{AFe}}{\eta_{itot}\eta_{AFtot}} + \frac{\eta_{iAS}\eta_{ASe}}{\eta_{itot}\eta_{AStot}} \right] \frac{E_e}{n_e} \quad . \tag{17}$$

In Eq. 17, the coupling loss factor η_{ie} represents coupling between the interior space and the exterior space through non-resonant shell modes. This loss factor is related to the mass-law transmission coefficient[7]:

$$\eta_{ie} = \frac{c_o}{4\omega} \frac{A_s}{V_i} \bar{\tau} \quad , \tag{18}$$

where c_o is the speed of sound in the acoustic space, A_s is the surface area of the shell, V_i is the volume of the interior acoustic space, and $\bar{\tau}$ is the mass-law transmission coefficient.

The second and third terms of Eq. 17 represent response and subsequent radiation of resonant modes of the shell.

Spacecraft Assembly

We now consider the complex problem of a spacecraft supported by mounting trusses inside a shroud which is exposed to an acoustic field, as shown in Fig. 1. This problem was previously studied by the author in Ref. 1. The results in Ref. 1 agree with those presented here; however, the formalism of this section is more complete. The structural elements for the spacecraft assembly

are shown in Fig. 2. Appropriate groups of resonant modes are shown in Figs. 11 and 12. In theory, each mode group is coupled to every other mode group; resonant modes of adjacent structures are coupled through boundaries; resonant modes of nonadjacent structures are coupled through nonresonant modes of intermediate structures. Equations 8 for this assembly are

$$-\left[\eta_{ij}\right]\left[\frac{E_j}{n_j}\right] = \left[\eta_{il}\right]\frac{E_1}{n_1} \quad , \tag{19}$$

where i and j = 2AF, 2AS, 3, 4, 5tors, 5hflex, 5vflex, 6tors, 6hflex, 6vflex, and $\eta_{ii} = -\eta_{itot}$ by convention. The notations 5tors, 5hflex, etc., refer to torsional motions and bending motions about the two principle axes of the ring frames and the mounting trusses as shown in Fig. 13. We have assumed that the external acoustic field is contained in a test chamber. The modal energy in the chamber is related to the average mean-square pressure, $\langle p^2\rangle_{x,t}$, by

$$\frac{E_1}{n_1} = \frac{\frac{1}{\rho_0 c_0^2} V_1 \langle p^2\rangle_{x,t}}{\frac{4\pi f^2}{c_0^3} V_1} = \frac{c_0}{\rho_0}\frac{1}{4\pi f^2}\langle p^2\rangle_{x,t} \tag{20}$$

Since the volume of the chamber does not enter in the modal energy and since the acoustic field is diffuse in a large chamber, we can also use Eqs. 19 and 20 when the external acoustic field is a diffuse field of travelling waves in an infinite space.

As in the previous example, Eqs. 19 can be solved exactly. However, we choose to simplify the equations by making certain approximations following the approach of Ref. 1.

3.2 Separation into Acoustic and Mechanical Paths

The first set of approximations allows the acoustic and mechanical paths to be treated separately (Fig. 2). We assume that

a. power flow from the shroud to the ring frame is small in comparison to power dissipated in the shroud;

b. the internal acoustic space is not coupled to the ring frame or the mounting trusses; and

c. the modal energy in the spacecraft is less than that in other mode groups, i.e., the spacecraft does not act as a source of excitation for the trusses (this assumption was verified experimentally, see Section 5).

In this case, the acoustic and mechanical transmission paths can be treated separately provided we use the exact η_{4tot} in both calculations. The modal energy of the spacecraft is the sum of the modal energy from acoustic-path transmission and from mechanical path transmission.

3.3 Other Simplifications

Acoustic-Path Transmission

Equations 8 for the acoustic-path mode groups are

$$\begin{bmatrix} -\eta_{AFtot} & \eta_{AFAS} & \eta_{AF3} & \eta_{AF4} \\ \eta_{ASAF} & -\eta_{AStot} & \eta_{AS3} & \eta_{AS4} \\ \eta_{3AF} & \eta_{3AS} & -\eta_{3tot} & \eta_{34} \\ \eta_{4AF} & \eta_{4AS} & \eta_{43} & -\eta_{4tot} \end{bmatrix} \begin{bmatrix} \frac{E_{AF}}{n_{AF}} \\ \frac{E_{AS}}{n_{AS}} \\ \frac{E_3}{n_3} \\ \frac{E_4}{n_4} \end{bmatrix} = \begin{bmatrix} \eta_{AF1} \\ \eta_{AS1} \\ \eta_{31} \\ \eta_{41} \end{bmatrix} = \frac{E_1}{n_1} \qquad (21)$$

In solving Eqs. 21, we assume that

$$\eta_{AFAS} = \eta_{AF4} = \eta_{AS4} = \eta_{41} = 0 \ , \qquad (22)$$

and $\eta_4+\eta_{43} >> \eta_{45}+\eta_{46}$ so that $\eta_{4tot} \approx \eta_4+\eta_{43}$. These assumptions are valid for our model spacecraft assembly; however, they are not generally valid for all assemblies. The coupling between AF modes and AS modes is zero only when there are no vertical stringers; otherwise this coupling loss factor is quite large so that AF and AS modes have equal energies. The coupling loss factors η_{AF4} and η_{AS4} represent coupling between resonant modes of the shroud and resonant modes of the spacecraft through nonresonant modes of the acoustic space. These coupling loss factors cannot be set to zero if the spacecraft panels are close to the shroud wall — closer than approximately 1/6 of an acoustic wavelength. The coupling loss factor η_{41} represents coupling between resonant modes of the external space to resonant modes of the spacecraft through nonresonant modes of both the shroud and the internal acoustic space. This loss factor is very small and can be set to zero.

In dealing with coupling loss factors involving nonresonant modes of intervening structures some caution must be used. It is possible for the nonresonant modes for two adjacent structures to form a new resonant set of modes that were not initially considered. For example, when the spacecraft is very close to the shroud wall it is possible for the nonresonant mass-law modes of the spacecraft and shroud and the nonresonant spring-law modes of the acoustic space to form new resonant modes corresponding to a mass-spring-mass system.

With the assumptions given by Eqs. 22, Eqs. 21 can be solved to give

$$\frac{E_{AF}}{n_{AF}} = \frac{\eta_{AF1}}{\eta_{AFtot}} \frac{E_1}{n_1} + \frac{\eta_{AF3}}{\eta_{AFtot}} \frac{E_3}{n_3} \quad , \tag{23}$$

where $\eta_{AFtot} = \eta_{AFd} + \eta_{AF1} + \eta_{AF3}$. Similarly, the solution for E_{AS}/n_{AS} is

$$\frac{E_{AS}}{n_{AS}} = \frac{\eta_{AS1}}{\eta_{AStot}} \frac{E_1}{n_1} + \frac{\eta_{AS3}}{\eta_{AStot}} \frac{E_3}{n_3} \quad . \tag{24}$$

Equations 23 and 24 agree with Eqs. 92 and 93 of Ref. 1. In most practical cases, the second terms of these equations are negligible. Equations 21 can be solved for E_4/n_4 to give

$$\frac{E_4}{n_4} = \frac{\eta_{43}}{\eta_{4tot}} \frac{E_3}{n_3} \quad . \tag{25}$$

This equation agrees with Eqs. 100 and 101 of Ref. 1.* Finally, Eqs. 21 can be solved for E_3/n_3:

$$\frac{E_3}{n_3} = \frac{\eta_{31}}{\eta_{3tot}} \frac{E_1}{n_1} + \frac{\eta_{3AF}}{\eta_{3tot}} \frac{E_{AF}}{n_{AF}} + \frac{\eta_{3AS}}{\eta_{3tot}} \frac{E_{AS}}{n_{AS}} + \frac{\eta_{34}}{\eta_{3tot}} \frac{E_4}{n_4} \quad . \tag{26}$$

Combining Eqs. 23 - 26, we get the final solution

$$\frac{E_3}{n_3} = \left[\frac{\eta_{31}}{\eta_{3tot}} + \frac{\eta_{3AF}\eta_{AF1}}{\eta_{3tot}\eta_{AStot}} + \frac{\eta_{3AS}\eta_{AS1}}{\eta_{3tot}\eta_{AStot}} \right] \left[1 - \frac{\eta_{3AF}\eta_{AF3}}{\eta_{3tot}\eta_{AFtot}} - \frac{\eta_{3AS}\eta_{AS3}}{\eta_{3tot}\eta_{AStot}} - \frac{\eta_{34}\eta_{43}}{\eta_{3tot}\eta_{4tot}} \right]^{-1} \frac{E_1}{n_1} . \tag{27}$$

*Note: AF and AS modes of the spacecraft do not both occur in the same frequency band. They do in the shroud.

Equation 27 can be algebraically manipulated into a form similar to Eq. 75 in Ref. 1 by making use of Eqs. 7 and 9, and by assuming that

$$\eta_{AF1} = \eta_{AF3}$$

and (28)

$$\eta_{AS1} = \eta_{AS3} \quad .$$

Using these assumptions in Eq. 27 gives*

$$\frac{E_1}{E_3} = \frac{n_1}{n_3} \frac{\eta_{AS1}n_{AS} + \eta_{AF1}n_{AF} + \eta_{3eq}n_3}{n_3\eta_{31} + \frac{\eta_{AS1}^2 n_{AS}}{\eta_{AStot}} + \frac{\eta_{AF1}^2 n_{AF}}{\eta_{AFtot}}} \quad , \tag{29}$$

where

$$\eta_{3eq} = \eta_{31} + \eta_3 + \frac{n_4}{n_3}\frac{\eta_4\eta_{43}}{\eta_{4tot}} \quad . \tag{30}$$

Equations 29 and 30 are identical to Eqs. 75 and 76 of Ref. 1 if $\eta_{31} = 0$.**

Mechanical-Path Transmission

Equations 8 can now be used to study vibration transmission by elements of the mechanical path. According to assumptions a, b and c of page 15, we can assume the modal energy of the shroud

*The Noise Reduction is given by $NR = 10 \log_{10}[(E_1/n_1)/(E_3/n_3)]$.

**Note: In Ref. 1, transmission by nonresonant shell modes was calculated separately so that Eqs. 75 and 76 of Ref. 1 include only transmission by resonant shell modes, i.e., $\eta_{31} = 0$.

has been determined from an analysis of the acoustic path transmission. In addition we will assume that*

a. the spacecraft, being an open box of four panels, responds only to moments about an axis parallel to the axis of revolution of the cylindrical shell.
b. the bending modes of the mounting trusses are not well coupled to the spacecraft and, therefore, can be neglected.

Assumption (a) allows us to neglect bending modes of the mounting trusses and the ring frame that have motion in a vertical plane and torsional modes of the ring frame. Assumption (b) allows us to consider only torsional modes of the mounting trusses. Using these assumptions, Eqs. 8 become

$$-\begin{bmatrix} -\eta_{5tot} & \eta_{56} & \eta_{54} \\ \eta_{65} & -\eta_{6tot} & \eta_{64} \\ \eta_{45} & \eta_{46} & -\eta_{4tot} \end{bmatrix} \begin{bmatrix} \frac{E_5}{n_5} \\ \frac{E_6}{n_6} \\ \frac{E_4}{n_4} \end{bmatrix} = \begin{bmatrix} \eta_{5AF} \\ \eta_{6AF} \\ \eta_{4AF} \end{bmatrix} \frac{E_{AF}}{n_{AF}} + \begin{bmatrix} \eta_{5AS} \\ \eta_{6AS} \\ \eta_{4AS} \end{bmatrix} \frac{E_{AS}}{n_{AS}} , \quad (31)$$

where 5 represents bending modes of the ring frame with motion in horizontal plane,

$$E_5 = E_{5hflex} , \quad (32)$$

6 represents torsional modes of the mounting trusses,

*The validity of these assumptions has been studied experimentally, see Sections 4 and 5.

$$E_6 = E_{6tors} \quad , \tag{33}$$

No distinction was made in Ref. 1 between AF and AS shell modes in the treatment of mechanical-path transmission. The formalism in Ref. 1 is in error since the AF and AS modes have different energies. This error will be limited to frequencies below the ring frequency since this is the only frequency range in which both AF and AS modes occur.

The solution of Eqs. 31 for the modal energy of the ring frame is

$$\frac{E_5}{n_5} = \frac{\eta_{5AF}}{\eta_{5tot}} \frac{E_{AF}}{n_{AF}} + \frac{\eta_{5AS}}{\eta_{5tot}} \frac{E_{AS}}{n_{AS}} + \frac{\eta_{56}}{\eta_{5tot}} \frac{E_6}{n_6} + \frac{\eta_{54}}{\eta_{5tot}} \frac{E_4}{n_4} \quad . \tag{34}$$

We assume in the frequency range below the ring frequency that

$$\eta_{5AF} >> \eta_{5d} + \eta_{5AS} + \eta_{56} + \eta_{54} \quad , \tag{35}$$

and in the frequency range above the ring frequency that

$$\eta_{5AS} >> \eta_{5d} + \eta_{56} + \eta_{54} \quad . \tag{36}$$

With these assumptions, Eq. 34 becomes

$$\frac{E_5}{n_5} \approx \frac{E_{AF}}{n_{AF}} \quad \text{for} \quad f < f_R \text{ or } f > f_c \quad , \tag{37}$$

where f_R is the ring frequency, and

$$\frac{E_5}{n_5} = \frac{E_{AS}}{n_{AS}} \quad \text{for} \quad f > f_R \text{ and } f < f_c \quad . \tag{38}$$

To solve Eqs. 31 for the modal energies of the mounting trusses and the spacecraft, we assume that

$$\begin{aligned} \eta_{6AF} &= 0 \\ \eta_{4AF} &= 0 \\ \eta_{6AS} &= 0 \\ \eta_{4AS} &= 0 \end{aligned} \tag{39}$$

The general validity of these assumptions has not been studied. However, they should be valid for our model as long as the ring frame has resonant modes in the frequency band being considered. If we make the assumptions of Eqs. 39, Eqs. 31 can be solved to give

$$\frac{E_6}{n_6} = \frac{\eta_{4tot}\eta_{65} + \eta_{64}\eta_{45}}{\eta_{6tot}\eta_{4tot} - \eta_{64}\eta_{46}} \frac{E_5}{n_5} \tag{40}$$

where E_5/n_5 is given by Eqs. 37 and 38. The solution for the modal energy of the spacecraft is

$$\frac{E_4}{n_4} = \frac{\eta_{6tot}\eta_{45} + \eta_{65}\eta_{46}}{\eta_{6tot}\eta_{4tot} - \eta_{64}\eta_{46}} \frac{E_5}{n_5} \tag{41}$$

This equation can be compared with those of Ref. 1. However, in Ref. 1, transmissions by resonant and nonresonant mounting truss modes are treated separately. If we set $\eta_{45} = 0$ in Eq. 41, it agrees exactly with Eq. 153 in Ref. 1. If we set $\eta_{46} = 0$ in Eq. 41, it agrees exactly with Eq. 160 in Ref. 1. The separate treatment of resonant mode transmission and nonresonant mode transmission is not generally valid. However, for the particular

problem of Ref. 1,

$$\eta_{43} + \eta_4 >> \eta_{46} + \eta_{45} , \tag{42}$$

so that separate treatment is a valid approximation. This concludes our calculation of energy distribution in a spacecraft assembly.

The great number of approximations were necessary to keep the level-of-effort of the study within bounds. Additional research is required to eliminate the need for these approximations.

3.4 Summary of Theoretical Results

Solution of the power balance equations requires knowledge of the modal densities, coupling loss factors, and dissipation loss factors of the different resonant mode groups. A complete discussion of the derivation of these parameters is given in Ref. 1. We will present only a summary of results.

3.4.1 Modal Densities

The modal density, n(f), gives the average number of resonant modes per unit frequency. It is analogous to the mass density of a material, where the microscopic variations from molecule to molecule are averaged out. The average number of modes in a frequency band, N(f), is given by

$$N(f) = \int_{f_1}^{f_2} df\, n(f) . \tag{43}$$

N(f) will be a close approximation to the exact number of modes in the band for a particular structure if N(f) >> 1.

The modal densities for the elements of the model spacecraft assembly are listed in Table 2, and plotted in Fig. 14.

3.4.2 Coupling Loss Factors

The coupling loss factor relates the time-average power flowing between two groups of modes with resonant frequencies in a given band to the *difference* in their time-average total energies,

$$\Pi_{ab} = \omega \eta_{ab} n_a \left\{ \frac{E_a}{n_a} - \frac{E_b}{n_b} \right\} \quad . \tag{44}$$

Π_{ab} is the time-average power, ω is the band-center-frequency, η_{ab} is the coupling loss factor, n_a is the modal density for group a, and E_a is the time-average total energy of all modes in group a. Equation 44 is valid only if the modes in each group "look alike", i.e., if they have the same time-average energy.[3] The resonant modes of the elements of the model spacecraft assembly can be divided into groups of similar modes, as shown in Figs. 11 and 12. The coupling loss factors between these groups of modes are calculated in Ref. 1. The theoretical values of these coupling loss factors are given in Table 3 and are plotted in Fig. 15.

3.4.3 Dissipation and Total Loss Factors

The dissipation loss factor relates the time-average power dissipated by a group of modes with resonant frequencies in a given band to their time-average energy,

$$\Pi_{a,diss} = \omega \eta_{a,diss} E_a \quad . \tag{45}$$

$\Pi_{a,diss}$ is the time-average power dissipated, ω is the band-center frequency, $\eta_{a,diss}$ is the dissipation loss factor, and E_a is the time-average energy of all modes in the group. The dissipation loss factor is simply related to the critical damping ratio,

$$\eta_{a,diss} = 2\zeta_a \quad , \tag{46}$$

where ζ_a is the critical damping ratio.

The dissipation loss factor of a structural element must be estimated empirically. In built-up structures, the material damping is insignificant compared to the damping at joints. Therefore, the best empirical estimate of the dissipation loss factor of a built-up structure is

$$\eta_{diss} = 0.01 \quad . \tag{47}$$

This value will be used for each group of modes in the spacecraft assembly.

The total loss factor relates the time-average power dissipated and transmissed to all other groups of modes to the time-average energy of the group being considered. Thus,

$$\eta_{a,total} = \eta_{a,diss} + \sum_i \eta_{a,i} \tag{48}$$

where $\eta_{a,total}$ is the total loss factor, $\eta_{a,diss}$ is the dissipation loss factor, $\eta_{a,i}$ is a coupling loss factor, and the summation

is over all other groups of modes. In many cases the dissipation loss factor is sufficiently large that the summation of coupling loss factors in Eq. 49 can be neglected. However, this is not always the case, and all terms in Eq. 49 must be considered.

4. MEASUREMENT OF THE COUPLING AND TOTAL LOSS FACTORS

4.1 Measurement Techniques

The coupling loss factor for two coupled groups of modes with resonant frequencies in a given band relates the time-average power flowing between the groups to the difference in their time-average total energy,

$$\Pi_{ab} = \omega \eta_{ab} n_a \left\{ \frac{E_a}{n_a} - \frac{E_b}{n_b} \right\} \tag{49}$$

where Π_{ab} is the time-average power, ω is the band center frequency, η_{ab} is the coupling loss factor, n_a and n_b are the modal densities of group a and group b, and E_a and E_b are the time-average total energies of groups a and b.

The time-average total energies of mode groups a and b are twice the time-average kinetic energies of the groups since each mode is responding at resonance. Therefore, if all resonant modes of a given structure are similar and can be placed in one group, we can measure the time-average total energy of the mode group by measuring the time-average kinetic energy of the structure. When the modes of a structure must be separated into two or more groups, it is difficult to measure the time-average kinetic energy of just one group. Special correlation techniques could be used for this purpose but, at this time, they have not been developed to the extent where they could be used for this study.

The modal densities in Eq. 49 can be measured by slowly sweeping a sinusoidal excitation and counting the number of resonances. The technique can be used only when the separation between the modes

exceeds the modal bandwidth due to damping. For typical structures this requirement limits the technique to low frequencies and does not allow measurement over much of the frequency range of interest. Usually, one relies on theoretical estimates of the modal density.

Techniques to measure directly the power flowing between two groups of modes have not been developed. Therefore, the coupling loss factor must be inferred from experiments in which the total energies can be measured and all other parameters are known or can be measured.

The best technique to measure coupling loss factors is to isolate the two groups of modes being considered, excite one group with an external source and measure the time-average total energy in the two groups. The coupling loss factor can then be related to the total loss factor of the non-excited group by the equation

$$\frac{E_b}{E_a} = \frac{n_b}{n_a} \frac{\eta_{ba}}{\eta_{b,total}} \tag{50}$$

where a refers to the excited group, b refers to the nonexcited group and $\eta_{b,total}$ is the total loss factor of group b. For this special case in which we have isolated two groups of modes, the total loss factor of one group is simply the dissipation loss factor of that group plus the coupling loss factor between that group and the other. Thus, Eq. 50 can be rewritten as

$$\frac{E_b}{E_a} = \frac{n_b}{n_a} \frac{\eta_{ba}}{\eta_{b,diss} + \eta_{ba}} \tag{51}$$

When the coupling loss factor is much larger than the dissipation loss factor, a small error in the measurement of the total loss factor or in the measurement of the total energies of the mode groups results in very large errors in the experimental determination of the coupling loss factor. Cases in which the coupling loss factor is greater than the dissipation loss factor should be avoided if possible. This can usually be done by the addition of damping to the nonexcited group of modes.

We were able to use the above technique of isolating the two groups of modes being studied to measure the coupling loss factor between the model shroud and an acoustic space for frequencies at which only AF or AS modes are present, and that between the model spacecraft and an acoustic space. We could not measure other coupling loss factors by this technique because it was not possible to isolate the different groups of modes. We attempted to measure the coupling loss factors between the different groups of modes in the mounting trusses and the modes of the model spacecraft without isolating the different groups being studied. But unfortunately, the results of this attempt, which is described in Section 4.3, are questionable.

Measurement of the coupling loss factor requires that we first measure the total loss factor of each group of modes. The total loss factor of a group of modes relates the power dissipated in the group plus all power transmitted to other groups to the time-average total energy of the group. Thus,

$$\eta_{a,\text{total}} = \eta_{a,\text{diss}} + \sum_i \eta_{ai} \qquad (52)$$

where $\eta_{a,total}$ is the total loss factor of mode group a, $\eta_{a,diss}$ is the dissipation loss factor, η_{ai} is the coupling loss factor for group a to group i, and the summation is over all other groups of modes.

To measure the total loss factor, we excite one group of modes with an external source. The time-average power input from the source is related to the time-average total energies in the different mode groups by the equation,

$$\Pi_{in} = \omega \eta_{a,total} E_a - \omega \sum_i \frac{n_a}{n_i} \eta_{ai} E_i \qquad (53)$$

where a is the group being excited, and the summation is over all other coupled groups of modes. If the damping in the nonexcited modes is sufficiently high, the modal energies of the nonexcited groups will be small and we can ignore the summation term in Eq. 53.

Two techniques exist for measuring the total loss factor when the summation term in Eq. 53 can be neglected. First, we can use the decay rate technique. Using this technique, the source of vibration is suddenly stopped and the rate of decay of energy in the mode group is measured. The decay rate is related to the total loss factor by the equation

$$\eta_{a,total} = \frac{2.2}{f\, T_{rev}} \qquad (54)$$

where f is the band center frequency and T_{rev} is the reverberation time - the time, in seconds, for the vibration level to decay 60 dB. This technique has proven to be reliable in the past.

However, we found that it cannot be used to measure the total loss factor of the model spacecraft panels. An explanation is given in Section 4.2.

The second technique is to measure the power input and energy of the excited mode group directly. The power input is measured by using a mechanical shaker and an impedance head. The time-average product of force applied by the shaker and velocity at the drive point is found by using a digital correlator. The time-average total energy is found by measuring the time-average kinetic energy. Then, we can find the total loss factor from Eq. 53, since the summation term is negligible.

We found that the second technique was very reliable and could be used to find the total loss factor of the model spacecraft. We conclude, as a result of this study, that a direct measurement of the power input is preferable to use of the decay rate technique.

4.2 Evaluation of the Coupling Loss Factors

4.2.1 Shroud to Acoustic Space

We have measured the coupling between the model shroud AF and AS modes and the external acoustic space modes. We assume that this coupling is equal to that between the shroud modes and the internal acoustic space modes. For our experiments, the external acoustic space was a 2900 cubic foot reverberant room. To measure the loss factor between the model shroud modes and the modes of this room, we excited the shroud in one-third octave bands with a point drive shaker, and measured the mean-square acceleration at many points on the structure and the mean-square sound pressure at many points in the room. The average power input to the AF

modes is the same as that to the AS modes. Thus, the average response of the AF modes is given by

$$\theta_{2AF} = \frac{\Pi_{in}}{\omega \eta_{2AF,tot}} \tag{55}$$

where θ_{2AF} is the average energy of an AF mode, Π_{in} is the average power input to the mode, ω is the band center frequency, and $\eta_{2AF,tot}$ is the AF mode total loss factor. The average response of the AS modes is given by a similar equation,

$$\theta_{2AS} = \frac{\Pi_{in}}{\omega \eta_{2AS,tot}} \tag{56}$$

The acoustical power radiated by the AF and AS modes is given by

$$\Pi_{rad} = \omega \eta_{2AF1} \, n_{2AF} \, \theta_{2AF} + \omega \eta_{2AS1} \, n_{2AS} \, \theta_{2AS} \, , \tag{57}$$

where we have assumed that θ_1 and $\theta_3 << \theta_{2AF}$ and θ_1 and $\theta_3 << \theta_{2AS}$. This power must equal the power dissipated in the reverberant chamber, given by

$$\Pi_{diss} = \omega \eta_{1tot} \, E_1 \tag{58}$$

where Π_{diss} is the dissipated power, η_{tot} is the total loss factor of the chamber, and E_1 is the energy in the chamber, Eq. 57, with Eqs. 55 and 56, can be rewritten as

$$\Pi_{rad} = \omega \eta_{2eq1} \, E_2 \, , \tag{59}$$

where E_2 is the energy of all shroud modes and

$$\eta_{2eq1} = \frac{\eta_{2AF1}\dfrac{n_{2AF}}{\eta_{2AFtot}} + \eta_{2AS1}\dfrac{n_{2AS}}{\eta_{2AStot}}}{\dfrac{n_{2AF}}{\eta_{2AFtot}} + \dfrac{n_{2AS}}{\eta_{2AStot}}} \qquad (60)$$

Equating Eqs. 58 and 59 gives

$$\eta_{2eq1} = \eta_{1tot}\frac{E_1}{E_2} \qquad (61)$$

The chamber energy is related to the space-average mean-square pressure while the shroud energy is related to its space-average mean-square acceleration, see Eqs. 75 and 78. Thus, Eq. 61 can be written as

$$10LOG_{10}\eta_{2eq1} = 10LOG_{10}\eta_{1tot} + 20LOG_{10}f \qquad (62)$$

$$+ 10LOG_{10}\frac{V_1}{M_2} - 161 + SPL_{re0.0002\mu bar} - AL_{re1g}$$

where V_1 is the chamber volume in ft^3, M_2 is the shroud mass in pounds and

$$SPL_{re0.0002\mu bar} = 10LOG_{10}\frac{\langle p^2\rangle}{(0.0002)^2}(479)^2 \qquad (63)$$

where $\langle p^2\rangle$ is the spatial average mean-square pressure in $(lbs/ft^2)^2$ and

$$AL_{re1g} = 10LOG_{10}\langle a^2\rangle \qquad (64)$$

where $\langle a^2\rangle$ is the spatial average mean-square acceleration in g^2's.

The total loss factor of the reverberant chamber was measured by exciting the chamber in frequency bands with an electromagnetic speaker and measuring the decay rate of the mean-square sound pressure at many points in the chamber after the input to the speaker was removed. The total loss factor is given by

$$\eta_{1tot} = \frac{2.2}{fT_{rev}} \tag{65}$$

where T_{rev} is the average reverberation time - the time for 60 dB of decay*, and f is the band center frequency.

Measured values for η_{2eq1} are plotted in Fig. 16 where they can be compared with the theoretical prediction using the expressions given in Table 3. Note that our theoretical results predict a sharp drop in the loss factor just above the ring frequency. This sharp drop is not usually observed in experimental results, so that we have smoothed the prediction over one octave of frequency. The agreement between theory and measured values is quite good. We feel that the deviations at 630 and 800 Hz may be due to a lack of AF modes in these bands. The deviations at 10,000 and 12,500 occur because the absorption in the chamber is so high that the acoustic field is not reverberant.

We were not able to measure the radiation loss factors of the AF and AS modes separately because we could not excite the modes separately.

*Usually the reverberation time is inferred by extrapolating from the first 10 to 30 dB of decay.

4.2.2 Spacecraft-acoustic space

We have measured the coupling between the spacecraft modes and the modes of the reverberant test chamber. We assume that this coupling is equal to that between the spacecraft and the internal acoustic space. This assumption is valid for our model spacecraft-shroud assembly since the internal acoustic space contains many resonant modes in each frequency band of interest.

The procedure for measurement of the spacecraft-acoustic space coupling loss factor is the same as that used for the shroud-acoustic space coupling loss factor. However, in this case each frequency band contains only one type of modes so that the spacecraft-acoustic space coupling loss factor is directly given by Eq. 62.

Measured values for the spacecraft-acoustic space coupling loss factor are plotted in Fig. 17 where they can be compared with the theoretical prediction. The agreement between theory and measured values is good. The cause of the deviations that do occur are not known.

4.2.3 Truss-spacecraft

Measurement of the truss-spacecraft coupling is difficult because the three types of truss modes cannot be excited separately. We attempted to measure the three coupling loss factors between one truss and the spacecraft by conducting three experiments in which the truss was excited differently. For these experiments the trusses and spacecraft were removed from the assembly. In the first experiment one truss was excited at its end by a point drive shaker. The shaker was aligned so that the applied force

was in a direction corresponding to bending in the vertical plane. In the second experiment the truss was excited in a direction corresponding to bending in the horizontal plane. And, finally, in the third experiment the truss was excited off center to induce mostly torsion and bending in the vertical plane. In each experiment we measured the bending vibration in the two directions and the torsional vibration in the middle of the truss where it is supported by a gusset. Measurements at other points were not meaningful since there were no other gussets to inhibit deformations of the truss cross-section. The measured values for the modal energies showed that the modes were not strongly coupled and equal partition of energy between the different modes groups did not occur. Thus, separate treatment of the different groups of truss modes is justified. The measurements also showed, however, that it was not possible to excite only one type of mode.

Measurements of the mean-square acceleration at many points on the spacecraft were also taken. For each experiment the power flow between the truss and the spacecraft is given by

$$\Pi_{64} = \omega\eta_{6t4}\, n_{6t} \left[\theta_{6t} - \theta_4\right] + \omega\eta_{6fh4}\, n_{6fh} \left[\theta_{6fh} - \theta_4\right] + \omega\eta_{6fv4}\, n_{6fv} \left[\theta_{6fv} - \theta_4\right] \quad (66)$$

where Π_{64} is the total power flow, 6t refers to truss torsion, 6fh refers to bending (flexure) in the horizontal plane and 6fv refers to bending in the vertical plane.* The power flow must equal the power dissipated plus that radiated by the spacecraft. This power is given by

*See Fig. 13.

$$\Pi_{4tot} = \omega \eta_{4tot} n_4 \theta_4 \tag{67}$$

where, in this case,

$$\eta_{4tot} = \eta_{4diss} + \eta_{4rad} \, . \tag{68}$$

The measurement of η_{4tot} is described in Section 4.3.3.

Combining Eqs. 66 and 67 gives

$$\eta_{6t4} E_{6t} + \eta_{6fh4} E_{6fh} + \eta_{6fv4} E_{6fv} = \left[\eta_{4tot} + \frac{n_{6t}}{n_4} \eta_{6t4} + \frac{n_{6fh}}{n_4} \eta_{6fh4} + \frac{n_{6fv}}{n_4} \eta_{6fv4} \right] E_4 \tag{69}$$

By conducting three independent experiments and measuring E_{6t}, E_{6fh}, E_{6fv}, and E_4 we obtain a set of simultaneous equations which can be solved for the coupling loss factors η_{6t4}, η_{6fh4}, and η_{6fv4}. Following this procedure gives values of η_{6t4} which are negative for every band.

Negative loss factors are not allowed within the context of Statistical Energy Analysis. Therefore, we interpreted this result as meaning that η_{6t4} should be zero. We set η_{6t4} equal to zero in Eq. 66, disregarded the third experiment, and solved for η_{6fh4} and η_{6fv4}. The results are presented in Fig. 18 where they can be compared with theoretical predictions for η_{6t4} and η_{6fh4}. Remember that we have assumed η_{6fv4} is zero. The large deviations between measured results and theory indicate that the theory is invalid. Our assumption that the spacecraft responds only to moments about the vertical axis is apparently incorrect. It should be pointed out, however, that the experimental technique described above is questionable.

4.3 Evaluation of the Total Loss Factors

4.3.1 Shroud

The shroud total loss factor was measured in the reverberant chamber using the decay-rate technique. We excited the shroud with a point drive shaker in one-third octave bands until a steady vibration level was reached. Then the shaker input was removed and the decay of the mean-square acceleration was measured at many points on the shroud. We did not attempt to measure the decay of AF or AS modes separately. For our experiment all modes were excited equally. However, since there are many AS modes and since they are not as highly damped by radiation to the acoustic space as AF modes, the measured decay rate should be attributed to the AS mode decay. Thus,

$$\eta_{2AS,tot} = \frac{2.2}{fT_{rev}} \tag{70}$$

where f is the band center frequency and T_{rev} is the average reverberation time.* Measured values for the total loss factor are plotted in Fig. 19.

The theoretical prediction for the AF mode total loss factor is

$$\eta_{2AF,tot} = \eta_{2AF,diss} + \eta_{2AF,1} + \eta_{2AF,3} \tag{71}$$

where $\eta_{2AF,diss}$ is again taken to be 0.01 based on empirical evidence. In this case, however, the prediction is dominated by the sum $\eta_{2AF,1} + \eta_{2AF,3}$. The prediction for $\eta_{2AF,tot}$ is also plotted in Fig. 19 where it can be compared with the prediction for $\eta_{2AS,tot}$ and with measured values. Note that the measured values

*See note on page 33.

fall in between the predictions for $\eta_{2AF,tot}$ and $\eta_{2AS,tot}$. As explained earlier, we expect that the decay-rate measurements to give a value for $\eta_{2AS,tot}$. Thus, we interpret the deviation between the measured values and the prediction for $\eta_{2AS,tot}$ to mean that $\eta_{2AS,diss}$ for the model shroud is higher than 0.01. Prediction of this result would be quite difficult, which points out a great problem in any prediction scheme — the estimation of damping.

4.3.2 Internal acoustic space

The total loss factor of the internal acoustic space was also measured by the decay-rate technique. We excited the internal space with a small electromagnetic loudspeaker in one-third octave bands. The space was excited to its steady state sound pressure level. Then the excitation was stopped and the decay-rate of the mean-square sound pressure at many points in the space was measured. The total loss factor is given by Eq. 72,

$$\eta_{3,tot} = \frac{2.2}{fT_{rev}} . \qquad (72)$$

Measured values for $\eta_{3,tot}$ are plotted in Fig. 20. We did not try to predict this loss factor and, therefore, we present only a "best" fit to the data which will be used in response predictions.

The total loss factor of the internal space is, no doubt, dominated by dissipation at the absorptive liner.

4.3.3 Spacecraft

The spacecraft total loss factor proved to be very difficult to measure. We first used the decay-rate technique. Since the

spacecraft-acoustic space coupling loss factor is large, it was necessary to conduct our measurements in an anechoic chamber so that excitation of the spacecraft by the acoustic field would not interfere with the measurements. The total loss factor measured by the decay-rate technique is plotted in Fig. 21. Lack of agreement between our empirical prediction using $\eta_{4diss} = 0.01$ and the measured values is clear. But even more significantly, the total loss factors in many bands are less than the spacecraft-acoustic space loss factors plotted in Fig. 17 - a result which is inconsistent with the basic ideas of Statistical Energy Analysis. In order to gain an understanding of this inconsistency, we remeasured the total loss factors by directly measuring the power input from the shaker and the energy of the spacecraft. The total loss factor is given by

$$\eta_{4,tot} = \frac{\Pi_{in}}{\omega E_4} \quad , \tag{73}$$

where Π_{in} is the power input to the structure and is given by

$$\Pi_{in} = \langle fv \rangle_t \tag{74}$$

where $\langle fv \rangle_t$ is the time-average of the force applied by the shaker times the velocity of the drive point. This product can be measured using a multiplier or a correlator. We used a digital polarity coincidence correlator which provided reliable results even at high frequencies where the force and velocity correlation coefficient is small. The instrument can measure correlation coefficient as low as 0.01.

The total loss factors measured by the power input technique are plotted in Fig. 21. These loss factors agree well with the

empirical prediction and satisfy the requirement that they be larger than the spacecraft-acoustic space coupling loss factors. Deviations between measured values using the decay-rate technique and the power-input technique are quite large.

To investigate the cause of these deviations we measured the total loss factor of a single panel from the spacecraft using both techniques. The panel was mounted in a rigid frame in a large baffle. The boundary condition can be best described as a simple-support. The total loss factors for the single panel are plotted in Fig. 22. Values measured using the two techniques are in agreement and the total loss factors are larger than the spacecraft-acoustic-space coupling loss factors. Thus, for the simply-supported single panel, either measurement technique is valid.

We continued our investigation by measuring the total loss factor of a single panel mounted on the light frame used for the model spacecraft. The boundary condition for this configuration is close to unsupported since the edges of the honeycomb panels are much stiffer than the frame. For this configuration the measured values from the two techniques do not agree, as shown in Fig. 23.

We conclude, therefore, that the decay-rate technique is not valid for the panels as they are mounted in the model spacecraft.

The edges of the spacecraft panel are reinforced with 5/16" x 3/4" solid bars. These bars vibrate and, apparently, the rate of vibration decay on the panels is governed by the rate at which these bars provide energy to the panels. Thus, the decay-rate technique gives the coupling loss factor between the bars and the panels, not the total loss factor of the panels. When the panel edges are restrained the bar vibration and this effect are greatly reduced.

5. RESPONSE MEASUREMENTS

5.1 Measurement Techniques

Techniques to measure the response of a structure or of an acoustic space are well developed and offer no problems. Acceleration at one point on a structure is measured using a light weight accelerometer, a preamplifier, and a vibration analyzer which filters the signal into a band of frequencies and takes the mean-square response. A spatial average is found by measuring the mean-square response at many points on the structure and averaging.

When the frequency band of the measurement is narrow, the mean-square velocity can be simply related to the mean-square acceleration so that

$$E = \frac{M\langle a^2\rangle}{\omega^2} , \tag{75}$$

where E is the total energy of the structure, M is its mass, ω is the band-center frequency and $\langle a^2\rangle$ is the spatial-average mean-square acceleration.

To provide an accurate estimate of the acceleration at high frequencies the accelerometer mass must be sufficiently small that it does not inhibit the motion of the structure. The accelerometer loading frequency - above which loading is a problem - is given by

$$f_\ell = \frac{8\rho_s \kappa c_\ell}{2\pi M} \tag{76}$$

The accelerometer mass must be small enough that f_ℓ is above

the highest frequency of interest. We used a 2 gram accelerometer. However, even with this light-weight unit, the loading frequency was 5500 Hz so that data above this frequency had to be corrected for the loading effect according to the equation

$$\frac{\langle a^2 \rangle}{\langle a_m^2 \rangle} = 1 + \left(\frac{f}{f_\ell}\right)^2 \quad , \tag{77}$$

where $\langle a^2 \rangle$ is the actual mean-square acceleration which we are trying to measure, $\langle a_m^2 \rangle$ is the acceleration read by the accelerometer, and f is the center frequency of the band in which the measurement is being taken. The correction given by Eq. 77 should be applied with caution and should not be used for $f > 2f_\ell$.

Sound pressure is measured with the same instrumentation using a microphone instead of an accelerometer. The total energy in an acoustic space is given by

$$E = \frac{V \langle p^2 \rangle}{\rho_o c_o^2} \tag{78}$$

where E is the total energy, ρ_o is the acoustic density, c_o is the speed of sound, V is the volume of the space, and $\langle p^2 \rangle$ is the spatial average mean-square pressure.

Techniques to measure the response of a group of modes when there are two or more groups with different modal energies in a given narrow band of frequencies are not well developed. Perhaps correlation techniques could be used for this purpose if there are not too many modes. We made no attempt to use these techniques in this program.

Excitation for a structure or an acoustic space can be provided by a point drive shaker or a small electromagnetic speaker. These sources excite all modes in approximately the same way. When two or more groups of modes with different properties are resonant in a given band of frequencies it would be desirable to excite the different groups independently. This could possible be done using phased multiple sources. However, at the present time, this technique is not well developed and was not used for this program.

Our approach was to place the entire spacecraft-shroud assembly in a reverberant chamber, to excite the chamber with a sound source, and measure the spatial average response of each structural element in the assembly. By following this approach we were sure that each group of modes in the assembly would be properly excited.

The sound field established in the reverberant chamber is approximately diffuse. Correlation measurements in the chamber were not taken to establish the diffusivity of the field. However, the variations in sound pressure level from point to point in the field were less than ± 1.5 dB which indicates that the field was diffuse.

5.2 Shroud Response to Acoustic Excitation

We measured the shroud response to acoustic excitation by placing the shroud in the reverberant chamber and exciting the chamber in one-third octave bands to a spatial-average sound pressure level of 90 dB. The acceleration level at 12 points on the shroud were measured for each one-third octave band. The variations of the levels from point to point were within ± 2½ dB at high frequencies. The measured response for frequencies above 5500 Hz was affected by accelerometer loading. Therefore, we corrected these measured values to account for the loading.

The spatial-average acceleration levels of the shroud relative to the exciting sound pressure levels are plotted in Fig. 24. The theoretical prediction given by the sum of Eqs. 23 and 24 is also plotted in Fig. 24. Below the ring frequency, f_R, and above the critical frequency, f_c, the theoretical prediction is dominated by AF mode response. Just above f_R there are no AF modes, so that the theoretical prediction of the response drops significantly from one band to the next. This rapid drop is usually not observed so that we modified the theoretical prediction by smoothly connecting the response levels below f_R with those above f_R - see Fig. 24.

The agreement between the theoretical predictions and the measured values is very good except at low frequencies. The deviation at these frequencies is due to errors in our empirical estimate for the shroud total loss factor - see Fig. 19.

5.3 Shroud Noise Reduction

The shroud Noise Reduction was measured at the same time that the shroud response was measured. Air-tight baffles were connected to each end of the shroud so that no acoustic transmission through the ends could take place. Sound pressure levels were measured at six points within the internal acoustic space. Variations in the levels ranged from $\pm$ 8 dB in the low frequency bands to $\pm$ 3 dB in the high frequency bands. Measured values for Noise Reduction are plotted in Fig. 25.

The theoretical prediction, given by Eq. 29, is also plotted in Fig. 25. The "mass law" Noise Reduction is the Noise Reduction obtained by considering only the acoustic energy transmitted by the "mass law" nonresonant shroud modes. The complete expression

for the Noise Reduction is dominated by the "mass law" noise reduction in the frequency range 1950 Hz to 6300 Hz. In this frequency range the level of the shroud response - which is governed by resonant modes - will not control the amount of acoustic energy transmitted to the interior space. This conclusion is verified in Section 6.1.

The theoretical expression for Noise Reduction is directly dependent on the absorption in the interior acoustic space. For our particular set-up the absorption at high frequencies is very large so that the Noise Reduction is also large. As we will see in Section 6.3, the Noise Reduction is significantly less when the absorptive liner is removed.

The comparison between theory and experiment is not as good as we expected. At low frequencies the prediction is high, in part, because our empirical prediction of shroud total loss factor is low, see Fig. 19. The cause of the remaining deviation at low frequencies is probably due to a lack of AF and "mass law" modes. The deviations at high frequencies are not understood.

5.4 Spacecraft Reponse to Acoustic Excitation

The spacecraft response to acoustic excitation was measured for two different acoustic fields. First, the spacecraft was suspended in the reverberant chamber. The chamber was excited in one-third octave bands to a spatial-average sound pressure level of 90 dB, and the response at 12 points on the spacecraft was measured. The average response level relative to the exciting sound pressure level is plotted in Fig. 26. The second measurement of spacecraft response was taken with the spacecraft trusses disconnected and the

spacecraft suspended by string inside the shroud. The shroud was placed in the reverberant chamber and excited acoustically. The average acceleration levels of the spacecraft relative to the average sound pressure levels of the interior acoustic space are plotted in Fig. 26. The response levels to the two different fields are somewhat different. However, the average difference between the two response levels for all bands is small.

The theoretical prediction for spacecraft response to diffuse field excitation, given by Eq. 25, is plotted in Fig. 26. At high frequencies the modal density of the honeycomb panels of the spacecraft increases above the prediction for a thin panel because of shear deformations and rotary inertia of the panel. To estimate this effect we measured the driving point impedance of one of the panels. The average impedance in a band of frequencies is inversely proportional to the modal density. Therefore, we increased the level of our theoretical prediction by the amount the measured impedance was below that predicted for a thin panel.

The measured values for spacecraft response are consistently above the prediction. To determine the cause of this deviation we measured the response of a panel mounted in a baffle with two different boundary conditions. The response of the simply-supported panel agrees closely with the prediction. However, the response of the unsupported panel is consistently 3 dB above that of the supported panel in the frequency range 3200 to 10,000 Hz. We have concluded that this difference accounts for the deviations between prediction and measured values in Fig. 26. However, we do not have an explanation as to why the unsupported-panel response should be greater than the supported panel response at high frequencies.

5.5 Spacecraft Response to Vibration Transmitted by the Acoustic Path

To conclude our study of the response of elements in the acoustic path, we suspended the spacecraft inside the shroud using string. The mounting trusses were disconnected so that no mechanical path transmission was present. Then we placed the shroud in the reverberant chamber, excited the chamber in one-third octave bands and measured the spatial-average vibration level of the spacecraft. The measured values are plotted in Fig. 27 where they can be compared with the theoretical prediction from Section 3. The theoretical predictions are high at both low and high frequencies. Most of the deviation at these frequencies occur because our prediction of Noise Reduction is well below the measured values, see Fig. 25. The measured level in the band centered at 630 Hz is 15 dB below our prediction. In this band the spacecraft does not have many modes and apparently the few modes that are resonant in this band are not well excited by the sound field in the internal acoustic space.

5.6 Ring Frame Response

The ring frame response was measured while the shroud was excited by an acoustic field in the reverberant chamber. Two sets of measurements were taken. The first set was taken with the trusses and spacecraft connected to the ring frame. The second set was taken with the trusses disconnected. The vibration levels for the two sets of measurements were the same within 1½ dB.

Vibration measurements were taken at 10 locations around the ring frame. At each location, three measurements were taken corresponding to points A, B and C as shown in Fig. 28. The ten measure-

ment locations were selected so that none of the locations were near a truss-ring frame attachment point. We expect that the vibration levels at such an attachment point is very sensitive to details of the connection point. The spatial-average vibration levels at points A, B and C relative to the spatial-average vibration level of the shroud are plotted in Fig. 28. The levels at point A are much higher than those at points B and C for frequencies above 2000 Hz. These differences in level are a result of cross-sectional deformations of the ring-frame. We feel that the levels at points B and C are indicative of the ring frame bending motions. The levels at point B correspond to bending with motions in the horizontal plane, while those at point C correspond to bending with motions in the vertical plane.

Theoretical predictions for the three types of ring-frame motion, from Eqs. 37 and 38, are plotted in Fig. 28. The predictions for vertical and horizontal bending are equal since the modal densities for these two types of modes are equal. The prediction for torsional motion is somewhat higher since the modal density for torsional modes is higher. The agreement between theoretical prediction and measured values for horizontal and for vertical bending is quite good considering the approximations made in the theory. Measurements of ring frame torsion were not taken and, therefore, a comparison with theory cannot be made.

5.7 Truss Response

We measured the response of the mounting trusses to vibrations transmitted by the ring frame and to vibrations transmitted through the internal acoustic space and spacecraft. To measure the truss response to vibrations transmitted by the ring frame we placed the entire assembly in the reverberant chamber and excited the shroud

acoustically. The spacecraft was enclosed in a sound-proof box so that vibrations transmitted through the internal acoustic space were negligible.

The truss response in torsion, bending in the vertical plane, and bending in the horizontal plane were measured at the center point of each truss. Vibration measurements at other points on the truss were not made because deformations of the truss cross-section would dominate the measured levels. The center point of each truss is reinforced by a gusset so that cross-section deformations are not present. The measured response for different mode groups of the truss are plotted in Fig. 29. Vibration levels for the different mode groups are approximately equal.

To measure the response to vibrations transmitted through the internal acoustic space and spacecraft, we used the setup described above except that we excited the spacecraft acoustically rather than the shroud. A small speaker was placed inside the sound-proof box and the levels in this box were increased until the spacecraft levels were the same as those measured for acoustic path transmission. The measured truss response levels relative to the shroud levels measured for acoustic path transmission are plotted in Fig. 29. The truss response due to vibration transmitted by the ring frame is larger than the response due to vibration transmitted by the acoustic path elements. This result supports the assumption made in the theoretical study on page 15.

The theoretical prediction for truss torsion, from Eq. 40, is plotted in Fig. 29. A comparison of this prediction with the measured values for torsion are in reasonable agreement except in the 8000 Hz band. For this frequency band the assumption that

truss damping is zero is probably not valid. The effect of truss damping would be to lower the theoretical prediction. Predictions for bending motions of the truss were not made because our theoretical calculations indicated that the vibration transmitted to the spacecraft by truss bending is negligible.

5.8 Spacecraft Response to Vibration Transmitted by the Mechanical Path

The vibration transmitted to the spacecraft by the mechanical path was separated from that transmitted by the acoustic path by enclosing the spacecraft in a sound-proof box and exciting the shroud acoustically. The measured spatial-average response of the spacecraft relative to the spatial-average shroud response is plotted in Figs. 30 and 31. The measured response relative to the external mean-square sound pressure is plotted in Fig. 32.

In Fig. 30 we present two different predictions of the spacecraft response. The first prediction was obtained using the measured values for the energies of the mode groups in the truss, the measured coupling loss factors between truss modes and the spacecraft and the predicted total loss factor of the spacecraft. The agreement between this prediction and the measured values is quite good except at 8000 Hz, which supports the validity of our measured values of the truss to spacecraft coupling loss factors for most of the frequency range. The cause of the deviation between prediction and the measured value at 8000 Hz is probably inaccuracies in our measured value of coupling loss factor at this frequency.

The second prediction of the spacecraft response was obtained using the measured values for the energies of the truss mode groups, the theoretical coupling loss factor between the truss modes and

the spacecraft, and the predicted total loss factor of the spacecraft. This prediction does not agree with the measured values for spacecraft response. We conclude that the assumption made in studying the mechanical path that the spacecraft responds only to moments about the vertical axis, is not valid. However, this assumption does allow us to obtain a rough estimate of the vibration transmission by the mechanical path. Extension of our calculations to include transmission by other forces and moments acting on the spacecraft would require a great deal of additional theoretical work.

The theoretical prediction for the spatial-average spacecraft response to mechanical path transmission relative to the spatial-average shroud response is plotted in Fig. 31. The agreement between measured values and prediction is fair. The prediction is more than 10 dB high at low frequencies and approximately 5 dB low in the range 2000 to 6300 Hz. The major cause of these deviations is inaccuracy in the prediction of the truss-spacecraft vibration transmission. Finally, the prediction and measured values for spacecraft response relative to the external SPL is plotted in Fig. 32. At low frequencies the predicted values are more than 15 dB too high. This inaccuracy is due both to errors in predicting the shroud response and in predicting the transmission from the shroud to the spacecraft.

5.9 Spacecraft Response to Vibration Transmitted by Both Paths

Measurements of the spacecraft response to vibration transmitted by the acoustic and mechanical paths are presented in Figs. 27 and 31. To complete our experiments we measured the spacecraft response to vibration transmitted by both paths. The spacecraft was supported inside the shroud by the mounting trusses, and the

entire spacecraft-shroud assembly was excited acoustically in the reverberant chamber. The measured values for spatial-average spacecraft response levels relative to the exciting sound pressure levels in the chamber are plotted in Fig. 33. The measured values for mean-square response to transmission by both paths is on the average 1-1/2 dB greater than the sum of the mean-square response to acoustic path transmission and the mean-square response to mechanical path transmission. We do not feel that this result occurs because the vibration transmitted by the two paths is correlated. Rather we feel that it occurs because of slight changes in experimental setup for the different measurements, i.e., the trusses were disconnected for the acoustic path measurement while a sound-proof enclosure was added for the mechanical path measurement.

The theoretical prediction for spacecraft response to vibration transmitted by the two paths is plotted in Figs. 34 and 35. In Fig. 34 the theoretical predictions for vibration transmitted by the acoustic path and the mechanical path are compared. Note that the theoretical predictions are comparable throughout the entire frequency range; whereas, the measured values show a clear dominance of one path over the other. However, no real significance is attached to this result. In Fig. 35 the prediction and measured values for transmission by both paths is presented. Comparison of this prediction with the measured values shows reasonable agreement. Deviations between prediction and measured values at low frequencies result because of inaccuracies in predicting the acoustic path transmission. Deviations at high frequencies result because of inaccuracies in predicting the mechanical path transmission. The inaccuracy in predicting mechanical path transmission at low frequencies does not enter into this

final result because the acoustic path transmission is dominant at these frequencies.

5.10 Simulation of the Spacecraft Excitation

The experiments described so far have been to study the vibration transmission in the entire spacecraft-shroud assembly. We are equally interested in techniques to simulate the acoustic and mechanical excitation of the spacecraft so that vibration tests can be conducted more simply.

To simulate the excitation of the spacecraft by the internal acoustic field, we selected a diffuse field of noise. There was no physical reason for selecting this field except that it is relatively easy to obtain. To conduct our measurements we placed the spacecraft in the reverberant chamber and excited the chamber to the sound pressure levels that would exist in the internal space when the external sound pressure levels are 100 dB. The measured spacecraft response levels relative to this hypothetical external field level are plotted in Fig. 36. The measured levels from Fig. 27 are also plotted in Fig. 36. A comparison of these levels indicates that the acoustic excitation of the shroud-enclosed spacecraft can be simulated by a diffuse field. Unfortunately, this result may only be valid for our particular assembly. Further study of this method of simulation is warranted.

The mechanical excitation of the spacecraft was simulated by using a 2 ft section of the shroud as a multimodal fixture. The ring frame connected to the bottom of this section. The top of the section was just above the first ring in the shroud, see Fig. 3. To simulate the mechanical path excitation we excited the multimodal fixture with a point drive shaker at the upper ring and

measured the spatial-average spacecraft response and the spatial-average fixture response. The measured values are plotted in Fig. 37, where they can be compared with the response levels for mechanical path excitation from Fig. 31. The comparison shows good agreement below 5000 Hz. Above this frequency the vibration transmission from the fixture is much larger than from the acoustically excited shroud.

In an attempt to find the cause of this deviation we repeated the measurements while exciting the fixture shell midway between the two ends. For this excitation the vibration transmission from the fixture was equal to that transmitted from the acoustically excited shroud at 8000 Hz but was 5 to 10 dB less at lower frequencies. As a final experiment we excited the fixture acoustically and measured the spacecraft response.* For this type of excitation the vibration transmitted from the fixture was equal to that transmitted from the acoustically excited shroud within ±1 dB. These results are shown in Fig. 38. We conclude that the technique of using a multimodal fixture is valid but that the way in which it is excited is important in obtaining a true simulation of the mechanical path vibration transmission.

*The spacecraft was enclosed in a sound-proof box for this experiment.

6. EXPERIMENTAL STUDY OF CONFIGURATION CHANGES

The configurations of many actual spacecraft assemblies differ slightly from those of the model assembly described in Section 2. For this reason, a number of experiments were conducted to determine the effect of small configuration changes on the vibration transmitted to the model spacecraft. Four such changes were made: a directive acoustic field was used to excite the shroud and the spacecraft; covers were added to the model spacecraft; the absorptive liner was removed from the shroud; and a model spacecraft adaptor was added to the assembly. Data from the above experiments was analyzed in octave bands rather than 1/3 octave bands, since we were interested only in the gross effects of the configuration changes.

6.1 Response to a Directive Acoustic Field

In our theoretical and experimental study of the model spacecraft-shroud assembly, we defined the external acoustic field as a diffuse field of noise. However, a grazing field of noise would probably be a better representation of the actual environment. The shroud response and noise reduction to a grazing field can be calculated with no difficulty using the basic techniques described in Ref. 9. But we have not performed the calculations in this study and have proceeded directly to an experimental evaluation of the shroud response and noise reduction.

In calculating the spacecraft response, we assumed that the acoustic field inside the shroud is diffuse. This assumption is supported for our particular model by the experimental data which showed that the response of the model spacecraft to diffuse field excitation is the same as its response to the acoustic excitation

inside the shroud. It is possible that the internal acoustic field for other spacecraft configurations is not diffuse. Therefore, we conducted an experiment in which the response of the model spacecraft to a grazing sound field was measured.

In setting up the experiments, we placed the test object in a large semi-reverberant space. The walls of this space were covered with absorptive curtains, the floor with a one-inch thick absorptive material, and the ceiling with acoustically absorbant tile. Two sound sources were placed twenty feet from the test object and directed at it. For both experiments, the sound pressure levels on the surface of the test object were surveyed and found to be uniform within plus or minus 1.5 dB.

To measure the response of the model spacecraft to a grazing acoustic field, we suspended the model in the semi-reverberant space so that the vertical axis of the spacecraft and the sound source were aligned. Sound pressure levels over the outside of the model were measured and found to be uniform. However, the levels *inside* the model varied and indicated a reverberant response of the inside cavity. To eliminate this reverberant response, we placed absorptive fiberglass in the cavity and over the openings so that the sound pressure level inside the model was at least 5 dB below the outside levels. The model was then excited with octave bands of noise with center frequencies from 500 Hz to 8,000 Hz. The resulting space-average mean-square response of the spacecraft is plotted in Fig. 39, where it can be compared with the spacecraft response to a diffuse field.

The response to the grazing field is significantly less than the response to a diffuse field in the high frequency bands. We expect the response to the grazing field to be at least 3 dB less because

of the particular experimental setup, where the panels for the grazing field experiment were excited on only one side, while the panels for the diffuse field experiment were excited on both sides. We also expect the model spacecraft to respond less to the grazing field than to the diffuse field at frequencies much higher than the critical frequency because, at these frequencies, the bending wavelength in the panels matches the trace acoustic wavelength on the panels only for sound waves which are near normal incidence. At such high frequencies, no matching occurs between grazing acoustic waves and bending waves, so that the excitation of the panels by the grazing field is well below the excitation by the diffuse field. Since the radiation damping for the two fields is the same, the response to the grazing field is below that to a diffuse field. At frequencies near the critical frequency, matching between the bending waves and the grazing acoustic waves occurs. There, the response to the grazing field should be approximately equal to the response to the diffuse field.

A similar experimental setup was used to measure the response and noise reduction of the model shroud to a grazing field of noise. For this experiment, baffles were placed on each end of the shroud in order to close the internal acoustic space. The space-average mean-square response of the model shroud (shown in Fig. 40) is approximately equal to the response of the shroud to a diffuse field. This result is unlike that found for the model spacecraft, because the frequency bands of excitation are below the critical frequency of the shroud. In such a case, the bending wavelength is less than the acoustic wavelength and matching between the acoustic waves and the bending waves cannot occur. Thus, the shroud is fairly insensitive to the directivity of the exciting acoustic field.

The noise reduction by the model shroud for a grazing field of noise is plotted in Fig. 41. Above 1,000 Hz, the noise reduction for the grazing field is well below that for a diffuse field. This result is expected since the noise reduction over most of the frequency range is governed by transmission by nonresonant mass law modes. Mass law transmission is greatest for grazing incident sound waves (which explains the decrease in noise reduction for the grazing field). Note, however, that the noise reduction is less for the grazing field than for the diffuse field, while the response is unchanged. This result - that the noise reduction does not depend on the response - was predicted theoretically in Ref. 1 and indicates that the transmission is, in fact, due to nonresonant modes.

6.2 Addition of Covers to the Model Spacecraft

The model spacecraft used for our theoretical study consists of an open box of four honeycomb panels. With this configuration, the acoustic field excites both the outside of the panels and the inside. An experiment was conducted to determine the effect of covers on the responsiveness of the model spacecraft to acoustic excitation. The spacecraft covers were constructed from 1/4-inch aluminum plates. Acoustically absorptive fiberglass was placed inside the model - but was not allowed to touch the honeycomb panels. Each cover was connected to the spacecraft frame by 20 screws. The covered spacecraft was then supported in a reverberant chamber and excited with octave bands of diffuse noise. The spatial-average mean-square response of the panels (plotted in Fig. 42) can be compared with the response of the uncovered spacecraft. The response of the covered spacecraft is approximately 3 dB below that of the uncovered spacecraft. This result is

explained by the fact that the covered spacecraft is excited on only one side of each panel.

The addition of covers to the spacecraft would probably also change its responsiveness to excitation by the mounting trusses. Although experiments to determine this effect were not conducted, in one experiment a change in the spacecraft configuration was made and the resulting effect on vibration transmission via the mechanical path was determined. In this experiment, the triangular support plates on the corners of the model spacecraft (see Fig. 8) were replaced with small 1" x 1" plates. No effect on the vibration transmitted via the mechanical path was found.

6.3 Removal of the Absorptive Liner from the Shroud

Most spacecraft shrouds are lined with a thermal blanket that provides acoustic absorption for the internal acoustic space. Since this blanket is not included with every shroud, we conducted three experiments without the liner to determine the change in the vibration transmitted via the acoustic path, the mechanical path, and both paths combined. In each experiment, we measured the noise reduction by the shroud and the spacecraft response.

To measure the noise reduction of the shroud, we suspended it in a reverberant chamber and excited it with octave bands of diffuse sound. The measured noise reduction is plotted in Fig. 43 (where it can be compared with the noise reduction when the liner is in place).

The noise reduction without the liner is significantly less. This result is expected from the theoretical study, since the noise

reduction was directly dependent on the amount of absorption within the shroud. We conclude from this experiment that the use of a thermal blanket in an actual spacecraft configuration has a large effect on the level of vibration transmitted to the enclosed spacecraft.

The level of vibration transmitted to the spacecraft by the acoustic path and the mechanical path is plotted in Figs. 44 and 45. Note that the vibration transmitted by the acoustic path dominates the overall vibration transmitted to the spacecraft. We could expect this result since removal of the liner greatly increases the internal sound pressure levels and, thereby, the vibration transmitted via the acoustic path, but does not increase the vibration transmitted by the mechanical path.

6.4 Addition of a Model Adaptor to the Spacecraft Assembly

In an actual spacecraft assembly, the ring frame connects to an adaptor which, in turn, connects to the booster vehicle. Experiments conducted by the Jet Propulsion Laboratory (see Appendix 3) indicate that this adaptor may have a significant effect on the vibration transmitted to an enclosed spacecraft. To determine this effect, we constructed a model adaptor. This model consisted of a cylindrical shell 30 inches in diameter and two feet long. The walls of the shell were aluminum, 0.060 inch thick. Details of the model adaptor are shown in Fig. 46. We connected one ring of the adaptor to the ring frame by 50 small bolts. A baffle was placed over the end of the adaptor to enclose the internal acoustic space. Experiments were conducted to determine vibration transmitted by the acoustic path, the mechanical path, and both paths combined. In these experiments, the spacecraft-shroud-

adaptor assembly was placed in a reverberant chamber and excited with octave bands of diffuse sound.

The space-average mean-square response of the adaptor, shown in Fig. 47, is higher than the response of the shroud because of the small amount of damping in the model adaptor. The levels of the sound field in the internal acoustic space were found to be non-uniform and were higher in the section surrounded by the adaptor since no liner was included with the adaptor. The average noise reduction of the shroud-adaptor combination is plotted in Fig. 48. It is less than the noise reduction of the lined-shroud alone because of the high sound pressure levels measured in the space surrounded by the adaptor.

The spatial-average mean-square response of the model spacecraft to vibration transmission (by both the acoustic and mechanical paths) is plotted in Fig. 49. The vibration transmitted to the spacecraft with the adaptor connected is somewhat higher than that measured for the original model spacecraft-shroud assembly. In order to find the cause of this increase, we measured the vibration transmitted by the acoustic and the mechanical paths. The procedure was the same as that described in Section 5; results are shown in Fig. 49. Note that the mechanical path vibration transmission is increased by approximately 3 dB. This is due, no doubt, to the high level of excitation of the ring frame by the adaptor. However, vibration transmitted by the acoustic path is not significantly changed. We expected this result, since the sound pressure levels near the spacecraft with the adaptor connected are approximately equal to those without the adaptor.

We conclude, as a result of this experiment, that the addition of an adaptor to a spacecraft-shroud assembly can have a significant effect on the vibration transmitted to the enclosed spacecraft.

7. CONCLUSIONS

The study described in this report has been conducted over the past three years and has involved a substantial expenditure of effort. Most of this effort, however, went into the experimental phase of the study. Effort expended on the theoretical phase was far less than would have been expended if we had used the classical normal mode approach. Thus, the theoretical solution to the problem using Statistical Energy Analysis represents an attractive compromise between the simple, empirical techniques and the tedious, classical techniques. Of course, in using a statistical technique we must be content to ask only for statistics of the response.

The statistical solutions obtained by SEA are for an ensemble of structures which are identical in gross characteristics — modal density, characteristic impedance, dissipation loss factor, etc. but varied in detail — boundary conditions, damping mechanisms, panel aspect ratio, etc. For the calculations of coupling loss factors presented in this report we have assumed that the resonances frequencies of the modes of each element are random variables with a uniform probability distribution in frequency space and an average density given by the modal density for the element. This assumption allows us to use the wave (impedance) approach to calculate the coupling loss factors.[10]

The deviations between the theoretical predictions presented in this report and the experimental model study results are a result of two factors. First, the predictions are for the ensemble average vibration and sound pressure levels, where the average is over an ensemble of structures. The experimental results are for one member of the ensemble. Therefore, deviations between the

ensemble average and the data from one member of the ensemble are expected. The extent of these expected variations is governed by the distribution of results across the ensemble. Unfortunately, we cannot calculate this distribution within the present state-of-the-art of SEA, although progress is being made toward this goal.[11]

The second cause of the deviations between theory and experimental results is errors in the mathematical model which we have selected to represent the structure used for the experiments. The most significant of these errors is discussed in Sec. 5.8. In studying a complex structure it is difficult to avoid such modelling errors.

There are no set rules for modelling and often a compromise is dictated by our limited ability to analyze the model selected. The use of SEA does not solve the modelling problem. But it helps by allowing the analyst to focus his attention on those parameters which have the greatest effect on the vibratory response and transmission.

REFERENCES

1. Manning, J.E., Lyon, R.H., and Scharton, T.D., "Transmission of Sound and Vibration to a Shroud-Enclosed Spacecraft," NASA Rept. CR-81688, BBN Rept. 1431, October, 1966.

2. Manning, J.E., Koronaios, N., "Experimental Study of Sound and Vibration Transmission to a Shroud-Enclosed Spacecraft," NASA Rept. CR-96144, BBN Rept. 1592, August, 1968.

3. An excellent review of statistical energy analysis is given by Lyon, R.H., "What Good is Statistical Energy Analysis Anyway?" to appear in *Shock and Vibration Digest*, 1970.

4. Scharton, T.D. and Lyon, R.H., "Power Flow and Energy Sharing in Random Vibration," *J. Acoust. Soc. Amer.* 43 (6) pp. 1332–1343, 1968.

5. Lyon, R.H. and Maidanik, G., "Power Flow Between Linearly Coupled Oscillators," *J. Acoust. Soc. Amer.* 34 (5), 623 1962.

6. See, for example, Ungar, E.E. and Manning, J.E., "Analysis of Vibratory Energy Distributions in Composite Structure," in *Dynamics of Structural Solids* published by ASME, December, 1968.

7. See, for example, *Noise Reduction* edited by L.L. Beranek, published by McGraw-Hill Book Co., New York, 1960, pp. 295–297.

8. See, for example, *Random Vibration* edited by S.N. Crandall, published by MIT Press, Cambridge, Mass, 1963, p. 14.

9. Smith, P.W. and Lyon, R.H., "Sound and Structural Vibration," NASA Rept. CR-160, 1964.

10. Manning, J.E. and Remington, P.J., "A Review of Statistical Energy Analysis," BBN Rept. 1943, June 1970.

11. Lyon, R.H., "Statistical Analysis of Power Injection and Response in Structures and Rooms," *J. Acoust. Soc. Amer.* 45 (3), pp. 545–565, March 1969.

APPENDIX 1

REVIEW OF DATA IN BBN REPORT NO. 1592

Some of the data presented in Report No. 1592 are incorrect because of errors in calculating the accelerometer loading correction for the shroud, errors in measuring the damping by the decay-rate technique, and errors in the basic structural parameters of the shroud. Correct data are presented in Figs. 14, 15, 16, 19, 23, 24, 25, 27, 30, 31, 32, 34, and 46. Data in Figs. 20, 21, 26, 28, 29, 35, 38, and 42 are incorrect because the loading correction is wrong. Data presented in Figs. 18, 22, 33, and 36 are incorrect because of uncertainties in using the decay-rate technique. And finally, data presented in Figs. 17, 33, 35, 37, 38, 39, 40, 41, 43, 44 and 45 are incorrect because of errors in the basic structural parameters used in the calculations.

APPENDIX 2

STRONG MODAL COUPLING

In the case of strong modal coupling between AF and AS modes we assume that

$$\eta_{ASAF} \approx \eta_{AStot} \tag{A.1}$$

and

$$\eta_{AFAS} \approx \eta_{AFtot} \tag{A.2}$$

with these conditions Eqs. 12 can be solved to give

$$\frac{E_{AF}}{n_{AF}} \approx \frac{E_{AS}}{n_{AS}} \tag{A.3}$$

If in addition we assume that

$$\frac{E_i}{n_i} << \frac{E_e}{n_e} . \tag{A.4}$$

Equations 12 give

$$\frac{E_{AF}}{n_{AF}} \approx \frac{E_{AS}}{n_{AS}} \approx \frac{n_{AF}\eta_{AFe}+n_{AS}\eta_{ASe}}{n_{AF}\eta_{AFt}+n_{AS}\eta_{ASt}} \frac{E_e}{n_e} \tag{A.5}$$

where

$$\eta_{AFt} = \eta_{AFtot} - \eta_{AFAS} \tag{A.6}$$

and

$$\eta_{ASt} = \eta_{AStot} - \eta_{ASAF} \cdot \tag{A.7}$$

For strong coupling the internal modal energy levels are given by

$$\frac{E_i}{n_i} = \frac{\eta_{iAS}+\eta_{iAF}}{\eta_{itot}} \frac{E_{AF}}{n_{AF}} + \frac{\eta_{ie}}{\eta_{itot}} \frac{E_e}{n_e} \cdot \tag{A.8}$$

Since the AF modes and AS modes are strongly coupled they will have the same modal energy and can be treated as one modal group if we use the equivalent coupling loss factor

$$\eta_{ce} = \frac{n_{AF}}{n_c} \eta_{AFe} + \frac{n_{AS}}{n_c} \eta_{ASe} \tag{A.9}$$

where η_{ce} is an equivalent coupling loss factor between the cylindrical shell and the acoustic space, and n_c is the density of AF *and* AS modes of the cylinder.

APPENDIX 3

RANGER ACOUSTIC TEST ANOMALIES

In the JPL Ranger acoustic tests, several unexplained anomalies were encountered. Three tests were performed:

1. Agena adaptor and shroud hard-mounted,
2. Adapter isolated from Agena section,
3. Adapter isolated from Agena section and shroud.

In all three tests the acceleration power spectral density (PSD) at the Ranger spacecraft were found to be about the same. There was, however, a 5 dB drop in sound pressure level (SPL) internal to the shroud in tests 2 and 3, which appears inconsistent with the constant acceleration PSD at the spacecraft.

From three other tests performed on the Ranger spacecraft, one can come to several tentative conclusions.

The *ground simulation lift-off test*, in which the Agena-adapter-shroud enclosed spacecraft is excited acoustically, gives the same acceleration PSD at the spacecraft as the *ground simulation transonic tests* in which only the adapter is excited acoustically. These tests eliminate the shroud acoustic path as an important energy transmission path to the spacecraft and suggest that the acoustic excitation of the adapter is the major means of admitting energy to the spacecraft.

In the *Ranger Block III PTM acoustic test* the Ranger spacecraft *alone* is excited acoustically. It is found that the acceleration PSD of the spacecraft is 10 dB to 15 dB below that found in the *ground simulation liftoff test* for the same exciting SPL. Thus,

we conclude that the Ranger spacecraft is relatively insensitive to acoustic excitation and that the major path of energy transmission is acoustic coupling to the adapter and then mechanical coupling to the spacecraft through the spacecraft feet.

With the above conclusion the isolation test results begin to make sense, and though the 5 dB internal SPL drop is not explained, the result that a change in the internal SPL does not change the acceleration PSD of the spacecraft is expected. In addition, the result that isolating the shroud from the adapter makes no change in the PSD of the spacecraft is expected.

We conclude that the Agena adapter vibration levels are induced by the acoustic excitation and that the path of energy transmission to the spacecraft is mechanical from the adapter through the mounting feet.

TABLE I. PARAMETERS FOR THE MODEL ASSEMBLY

V_1	2900 ft^3	Test chamber volume
ρ_o	1/13.45 lbs/ft^3	Air density
c_o	1130 ft/sec	Speed of sound in air
A_2	51.2 ft^2	Surface area of shroud
ρ_{s2}	0.775 lbs/ft^2	Surface density of shroud wall
ρ_{m2}	107 lbs/ft^3	Volume density of shroud material
$c_{\ell 2}$	11800 ft/sec	Speed of sound in shroud material
t_2	0.087 in	Shell wall thickness
κ_2	0.025 in	Shell wall radius of gyration
D_2	32 in	Diameter of the shroud
E_2	$3.24 \times 10^6 lbs/in^2$	Young's Modulus for shroud material
V_3	34.1 ft^3	Internal acoustic space volume
A_4	14.6 ft^2	Surface area of spacecraft — all 4 panels
ρ_{s4}	0.38 lbs/ft^2	Surface density of spacecraft panels
I_4	5.5×10^{-4} in^3	Bending moment of inertia of spacecraft panels
$\kappa_4 c_{\ell 4}$	197 ft^2/sec	Product of radius of gyration and longitudinal wavespeed in the spacecraft
L_5	94 in	Ring frame length
$\rho_{\ell 5}$	0.875 lbs/ft	Ring frame density per unit length
κ_{fv5}	0.435 in	Radius of gyration for flexure in the vertical plane for the ring frame

TABLE I. PARAMETERS FOR THE MODEL ASSEMBLY *(cont'd.)*

κ_{fh}	0.500 in	Radius of gyration for flexure in the horizontal plane for the ring frame
κ_t	0.662 in	Radius of gyration for torsion of the ring frame
J_{t_5}	0.329 in^4	Polar moment of inertia for the ring frame
K_{t_5}	0.0268 in^4	Torsional stiffness constant for ring frame
c_{ℓ_5}	17000 ft/sec	Longitudinal wavespeed in the ring frame
c_{s_5}	10000 ft/sec	Shear wavespeed in the ring frame
L_6	40 in	Length of all four trusses
ρ_{ℓ_6}	0.328 lb/ft	Density per unit length for the mounting trusses
κ_{fv_6}	0.50 in	Radius of gyration for flexure in the vertical plane for the truss
κ_{fh_6}	0.66 in	Radius of gyration for flexure in the horizontal plane for the truss
κ_{t_6}	0.83 in	Radius of gyration for torsion of the truss
J_{t_6}	0.193 in^4	Polar moment of inertia
K_{t_6}	3.66 x 10^{-4} in^4	Torsional stiffness constant for the truss
c_{ℓ_6}	17000 ft/sec	Longitudinal wavespeed in the truss
c_{s_6}	10000 ft/sec	Shear wavespeed in the truss
K_6	1.02 lb.ft.	Static stiffness of the truss
θ	20°	Angle between mounting truss and an axis parallel to axis of revolution of the cylindrical shell

TABLE II. THEORETICAL MODAL DENSITIES

Acoustic Space	$n(f) = \frac{4\pi f^2 V}{c_o^3}$
Interior Acoustic Space	$n_3(f) = 0.3\left(\frac{f}{1000}\right)^2$
Flat Plate	$n(f) = \frac{A}{2\kappa c_\ell}$
Spacecraft - All Four Panels*	$n_4(f) = 1/27$
Cylindrical Shell	See Fig. A with $f_R = \frac{c_\ell}{\pi D}$ and $f_c = \frac{1}{2\pi}\frac{c_o^2}{\kappa c_\ell}$
Shroud	See Fig. A with $f_R = 1400$ Hz and $f_c = 8000$ Hz
Beam in Flexure	$n(f) = \frac{L}{\sqrt{\omega\kappa c_\ell}}$
Ring Frame - Flexure in the Vertical Plane	$n_{fv5}(f) = \frac{0.126}{\sqrt{f}}$
Ring Frame - Flexure in the Horizontal Plane	$n_{fh5}(f) = \frac{0.118}{\sqrt{f}}$
One Mounting Truss** - Flexure in the Vertical Plane	$n_{fv6}(f) = \frac{1}{80\sqrt{f}}$
One Mounting Truss** - Flexure in the Horizontal Plane	$n_{fh6}(f) = \frac{1}{92\sqrt{f}}$

TABLE II. THEORETICAL MODAL DENSITIES *(cont'd.)*

Beam in Torsion	$n(f) = \frac{2L}{c_s}\sqrt{\frac{J}{K_t}}$
Ring Frame	$n_{t_5} = 5.5 \times 10^{-3}$
One Mounting Truss**	$n_{t_6} = 3.84 \times 10^{-3}$

*Note: The modal density of the spacecraft is the sum of the modal densities of the four panels.

**Note: The modal density of four trusses is four times the modal density of one truss.

TABLE III. THEORETICAL COUPLING LOSS FACTORS

Acoustically Fast (AF) Mode to Acoustic Space

$$\eta = \frac{\rho_o c_o^*}{\omega \rho_s}$$

Shroud AF Mode to Acoustic Space

$$\eta_{2AF,1} = \frac{17.3}{f}$$

$$\eta_{2AF,3} = \frac{17.3}{f}$$

Spacecraft AF Mode to Acoustic Space

$$\eta_{4AF,3} = \frac{70.4}{f}$$

Acoustically Slow (AS) Mode to Acoustic Space

$$\eta = \frac{\rho_o c_o}{\omega \rho_s} \frac{P_r}{A} \frac{c_o}{f_c} g_2(f/f_c)^*$$

g_2 is plotted in Fig. B

Shroud AS Mode to Acoustic Space

$$\eta_{2AS,1} = \frac{3.89}{f} g_2$$

$$\eta_{2AS,3} = \frac{3.89}{f} g_2$$

Spacecraft AS Mode to Acoustic Space

$$\eta_{4AS,3} = \frac{61.5}{f} g_2$$

Acoustic Space i to Acoustic Space j Through Nonresonant "Mass Law" Motion of a Dividing Structure

$$\eta_{ij} = \frac{c_o A}{4\omega V_i} \bar{\tau}$$

TABLE III. THEORETICAL COUPLING LOSS FACTORS *(cont'd.)*

$$\bar{\tau} = \left(\frac{4\rho_o c_o}{\omega \rho_s}\right)^2 \text{ for field incidence}^7$$

Interior Acoustic Space to Exterior Acoustic Space

$$\eta_{31} = \frac{67.5}{f}\left(\frac{69.2}{f}\right)^2$$

Ring Frame Horizontal Flexure to Truss Torsion

$$\eta_{fh_5, t_6} = \frac{.8\ Re\{Z_6\}}{\rho_{\ell_5} L_5 \kappa_{fh_5} c_{\ell_5}} \left| \frac{Z_5}{Z_5 + Z_6} \right|^{2} **$$

$$Z_5 = 2(1-i)\ \rho_{\ell_5}\ \kappa_{fh_5}^2\ c_{\ell_5}^2 \left(\omega \kappa_{fh_5} c_{\ell_5}\right)^{-\frac{1}{2}}$$

$$Z_6 = \rho_{\ell_6}\ \kappa_{t_6}^2\ c_{s_6} \sqrt{\frac{K_{t_6}}{J_{t_6}}}\ (1 + \tan^2\theta)^{-1}$$

Truss Torsion to Spacecraft Flexure

$$\eta_{t_6, 4} = \frac{8\ \cos^2\theta}{\omega \rho_{\ell_6} L_6\ \kappa_{t_6}^2}\ Re\{Z_4\} \left| \frac{Z_6}{Z_6 + Z_4} \right|^{2} **$$

$$Z_4 = \frac{\rho_{s_4} \kappa_4^2 c_{\ell_4}^2}{\omega} \frac{A - iB}{A^2 + B^2}$$

$$A = 0.189$$

$$B = 0.275\ \ell n_e \left[\frac{w}{5}\left(\frac{\omega}{\kappa_4 c_{\ell_4}}\right)^{\frac{1}{2}}\right]$$

$$w = \text{truss width} - 1.5 \text{ inches}$$

---

*This expression applies when the mode can radiate to the acoustic space from one side. Multiply by two when the mode can radiate from both sides.

**These expressions were evaluated by use of a computer.

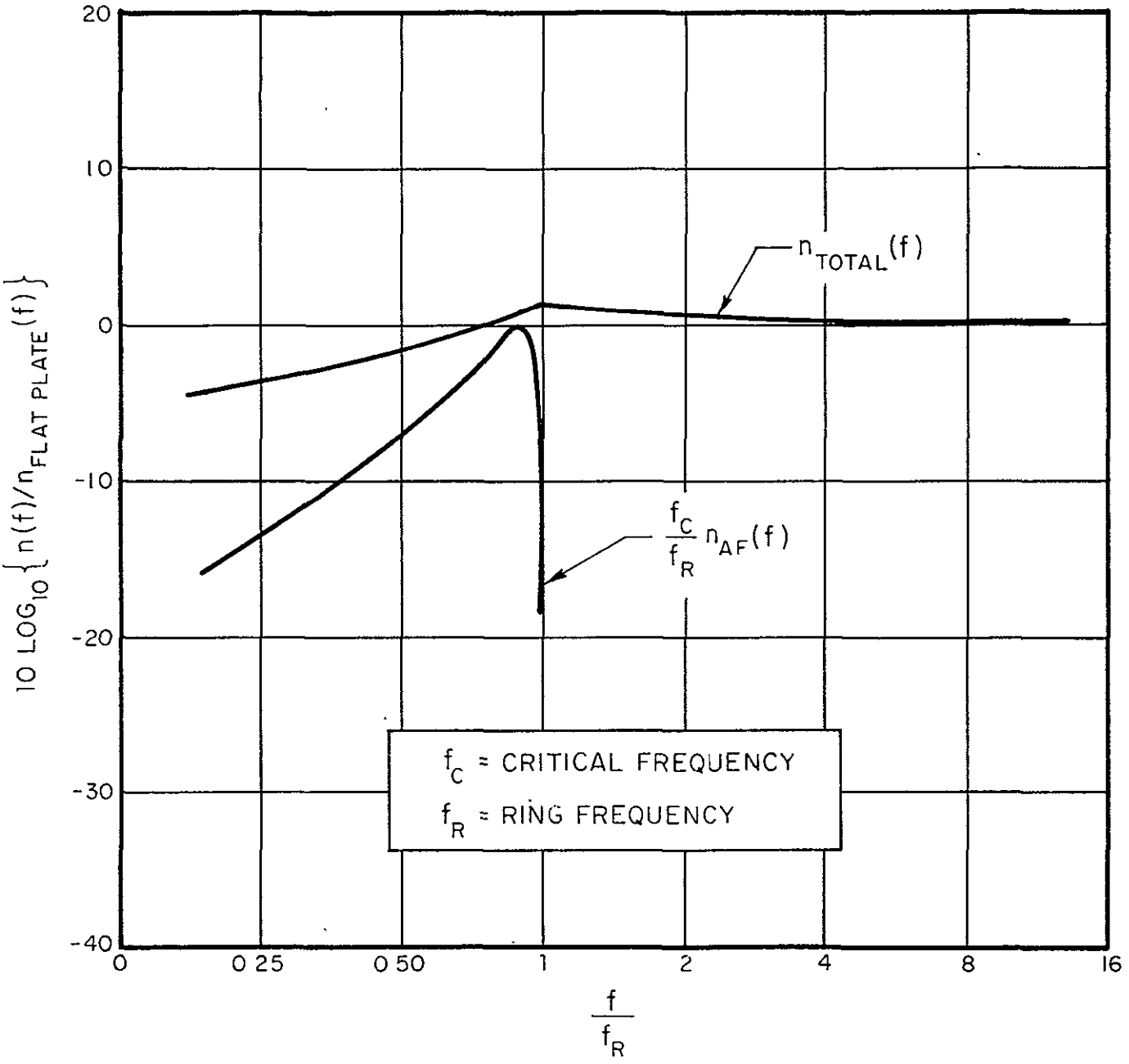

FIGURE A. MODEL DENSITIES FOR A CYLINDRICAL SHELL — AVERAGED IN ONE-THIRD OCTAVE BANDS

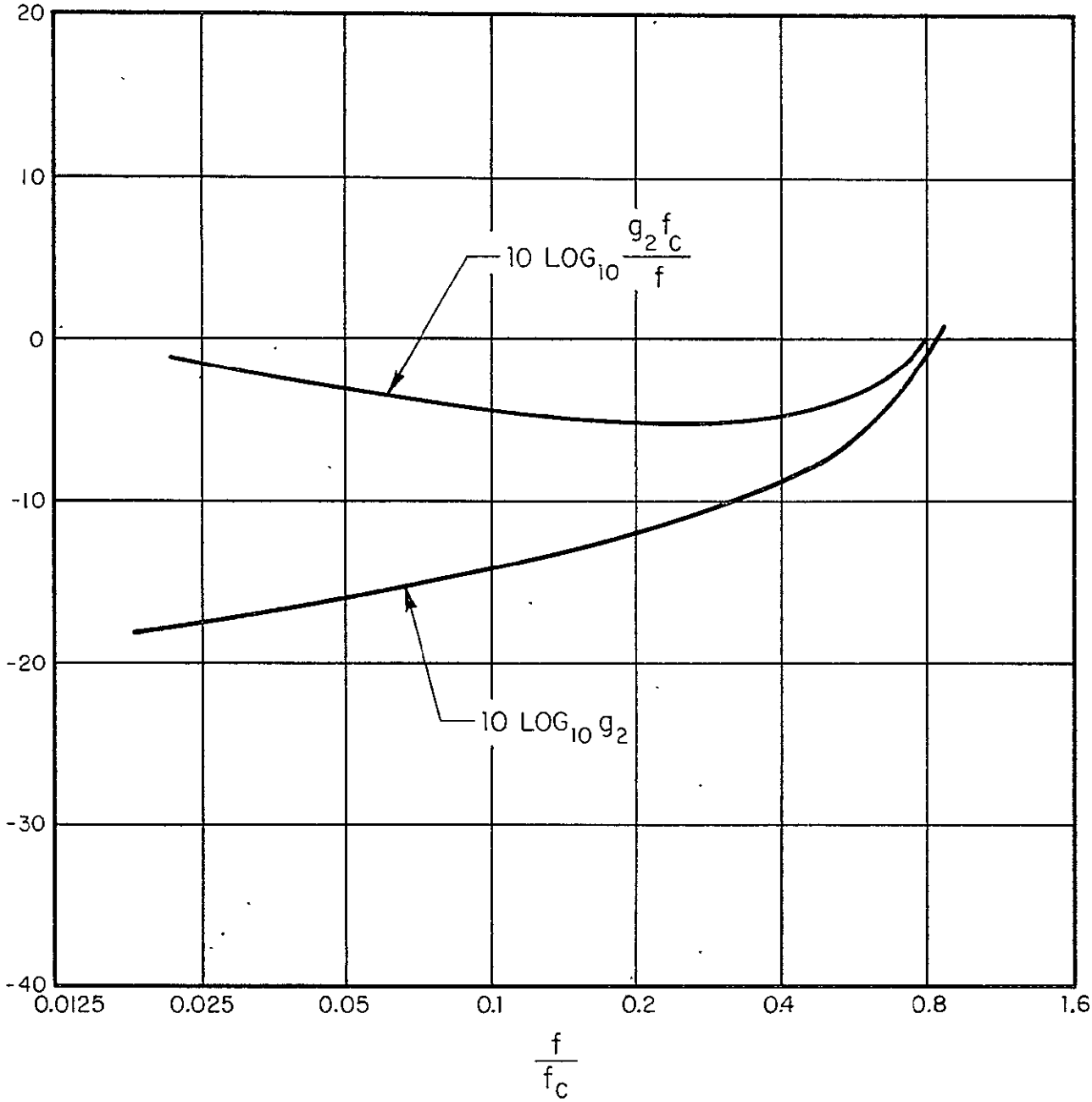

FIGURE B. THE FUNCTIONS g_2 and $\frac{g_2 f_c}{f}$

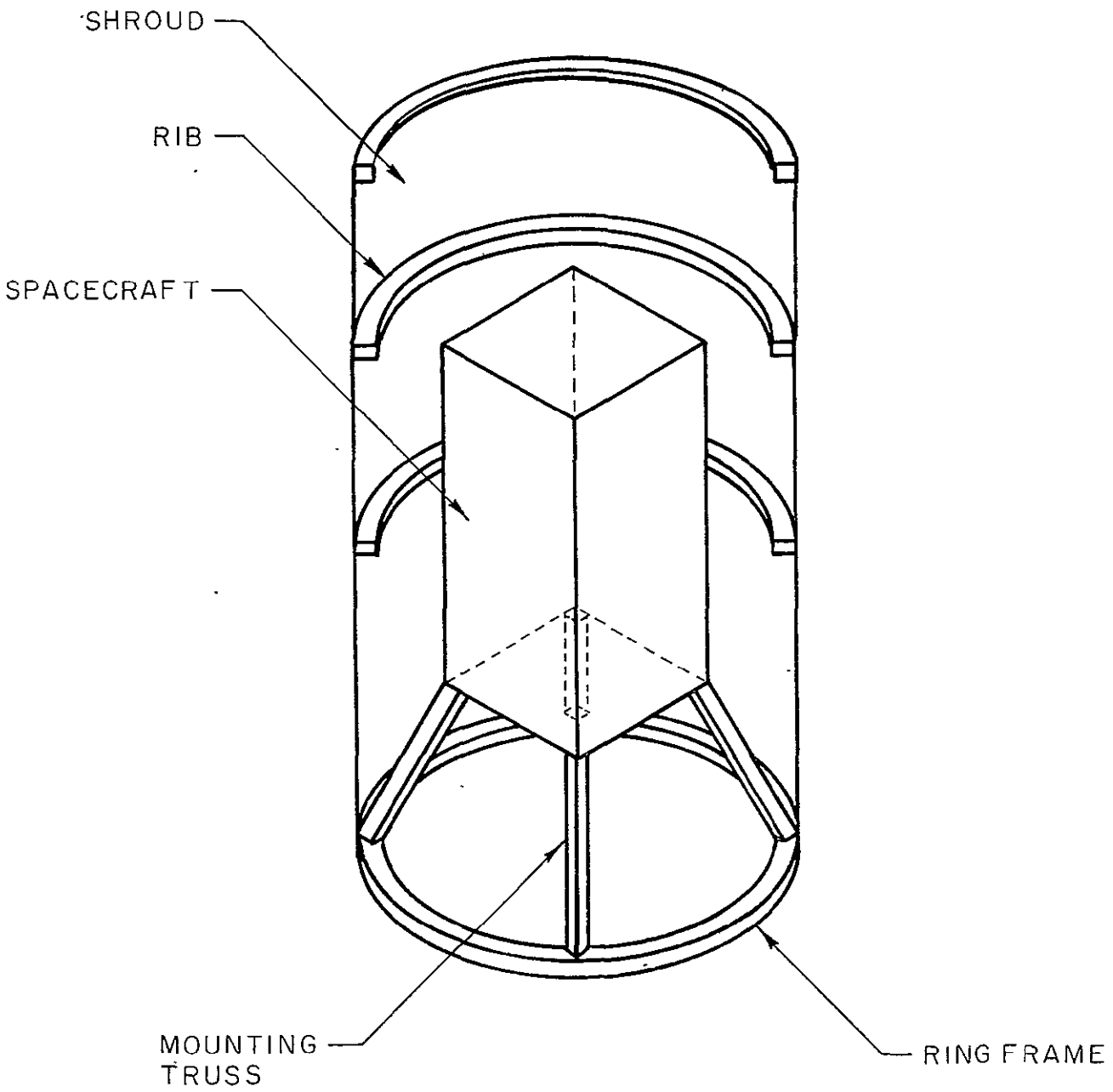

FIGURE 1. MODEL SPACECRAFT-SHROUD ASSEMBLY

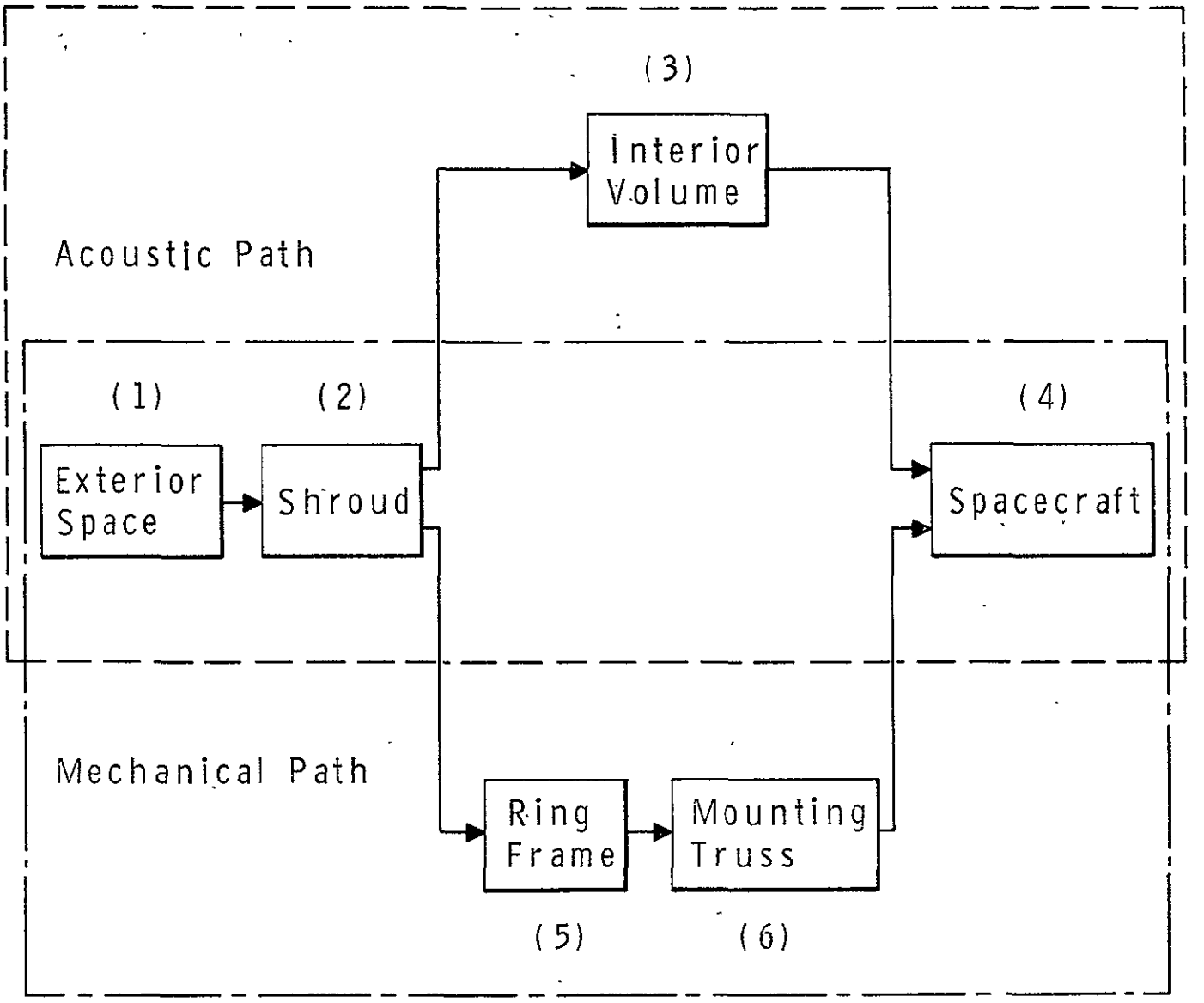

FIGURE 2. ELEMENTS OF THE MODEL ASSEMBLY

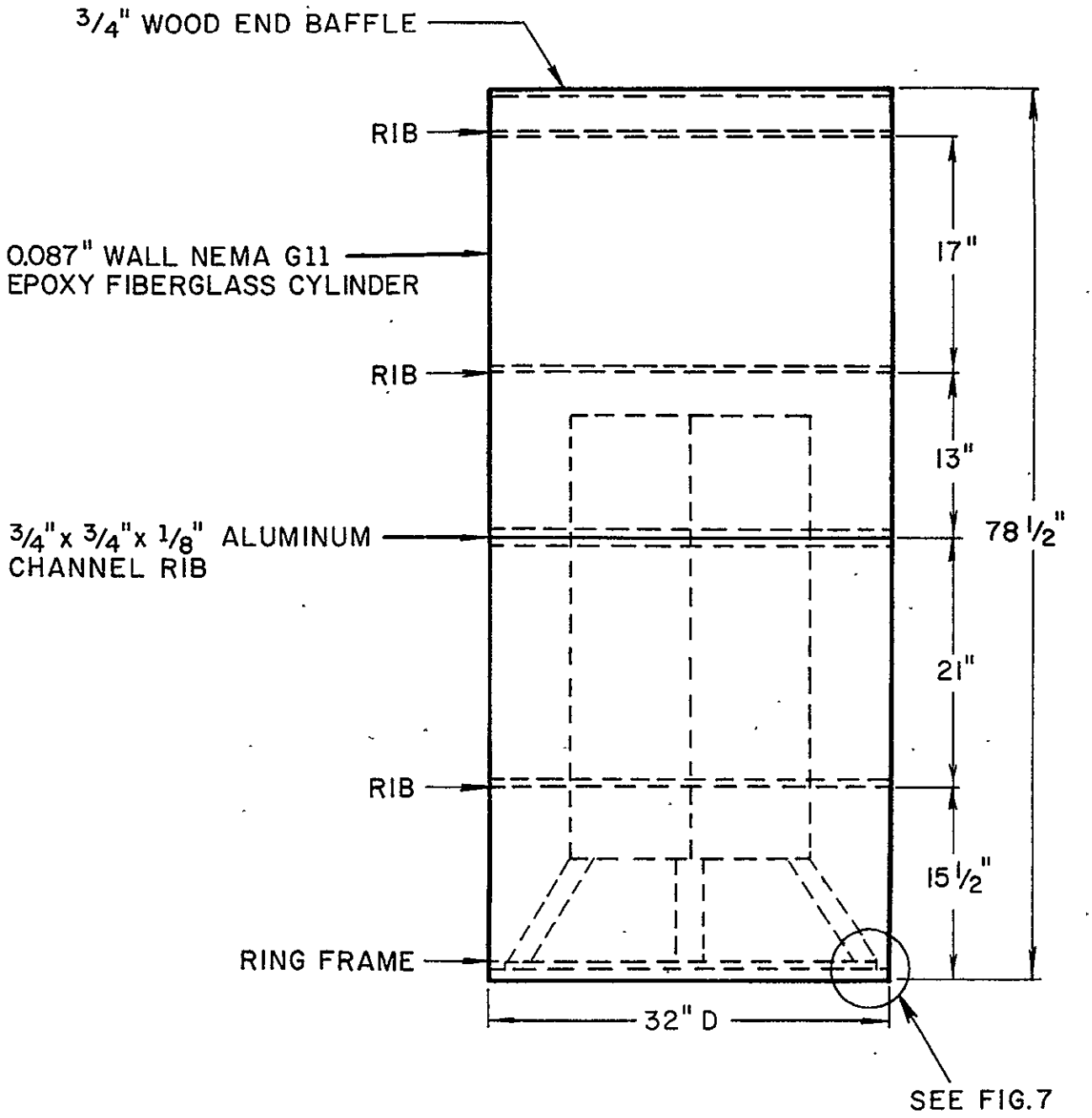

FIGURE 3. MODEL SHROUD

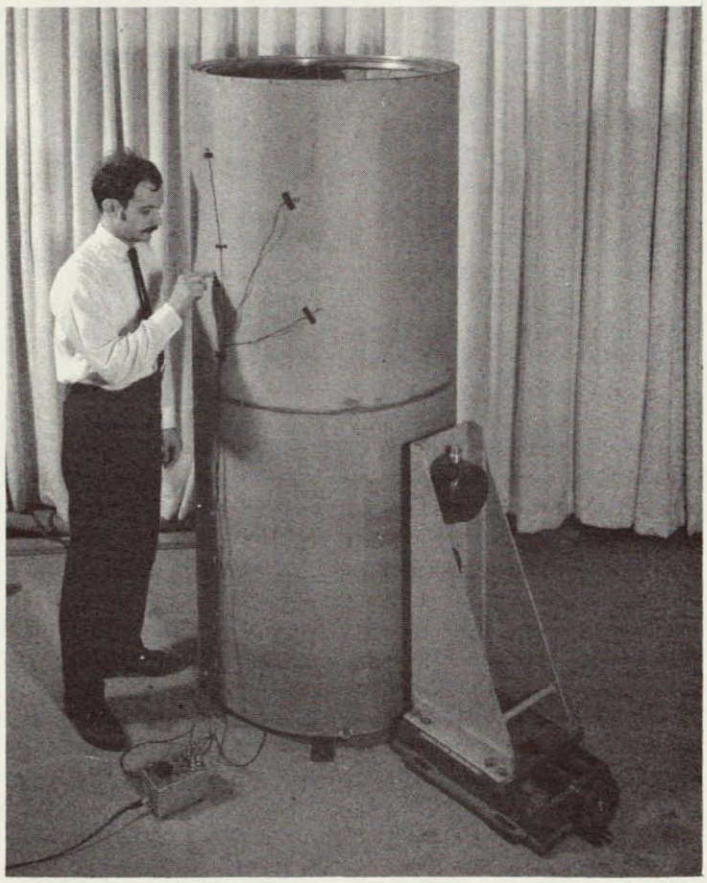

FIGURE 4. PHOTO OF THE MODEL SHROUD

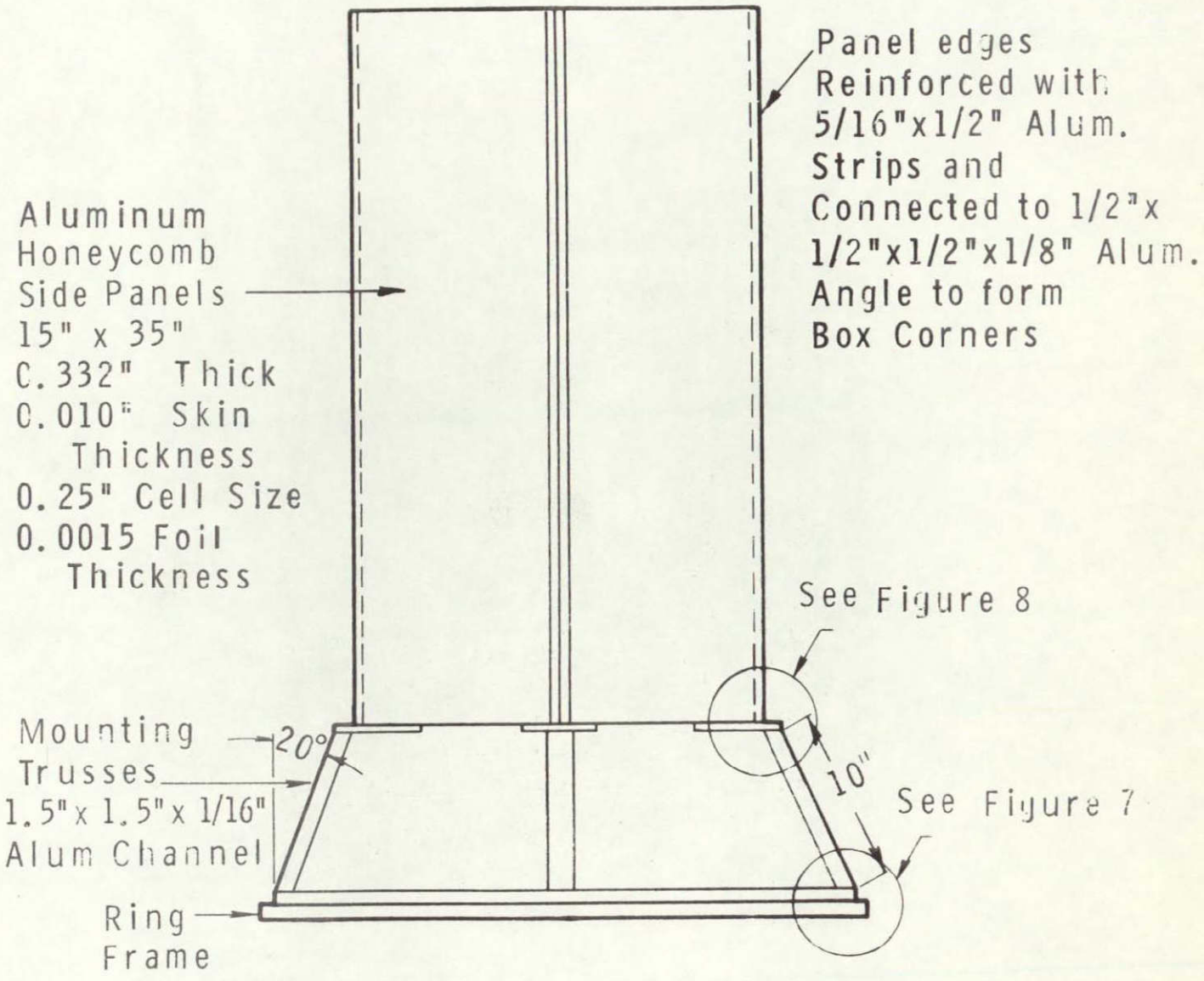

FIGURE 5. MODEL SPACECRAFT AND MOUNTING TRUSSES

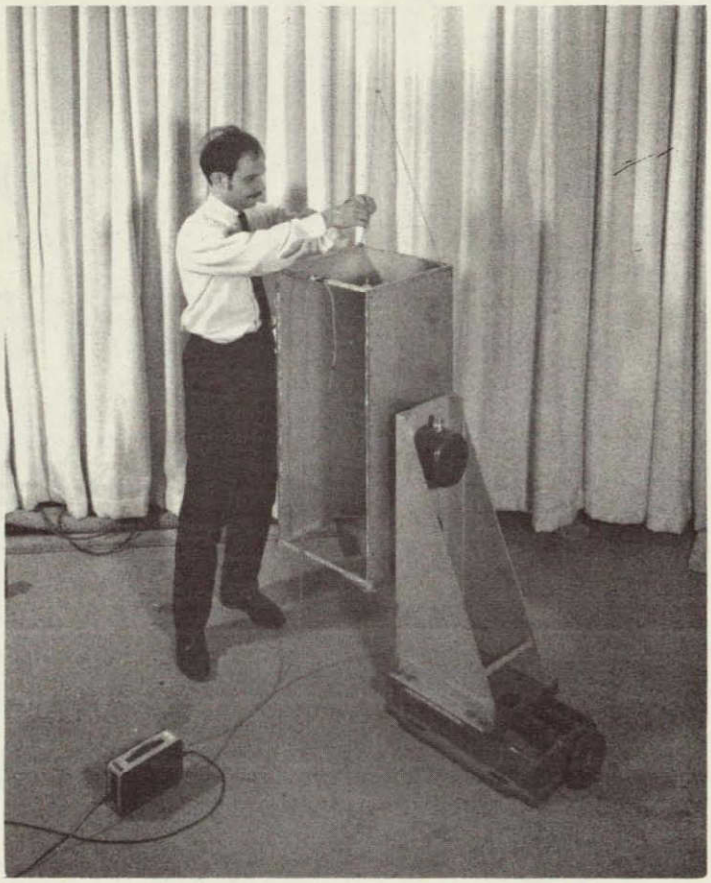

FIGURE 6. PHOTO OF MODEL SPACECRAFT — ONE PANEL REMOVED

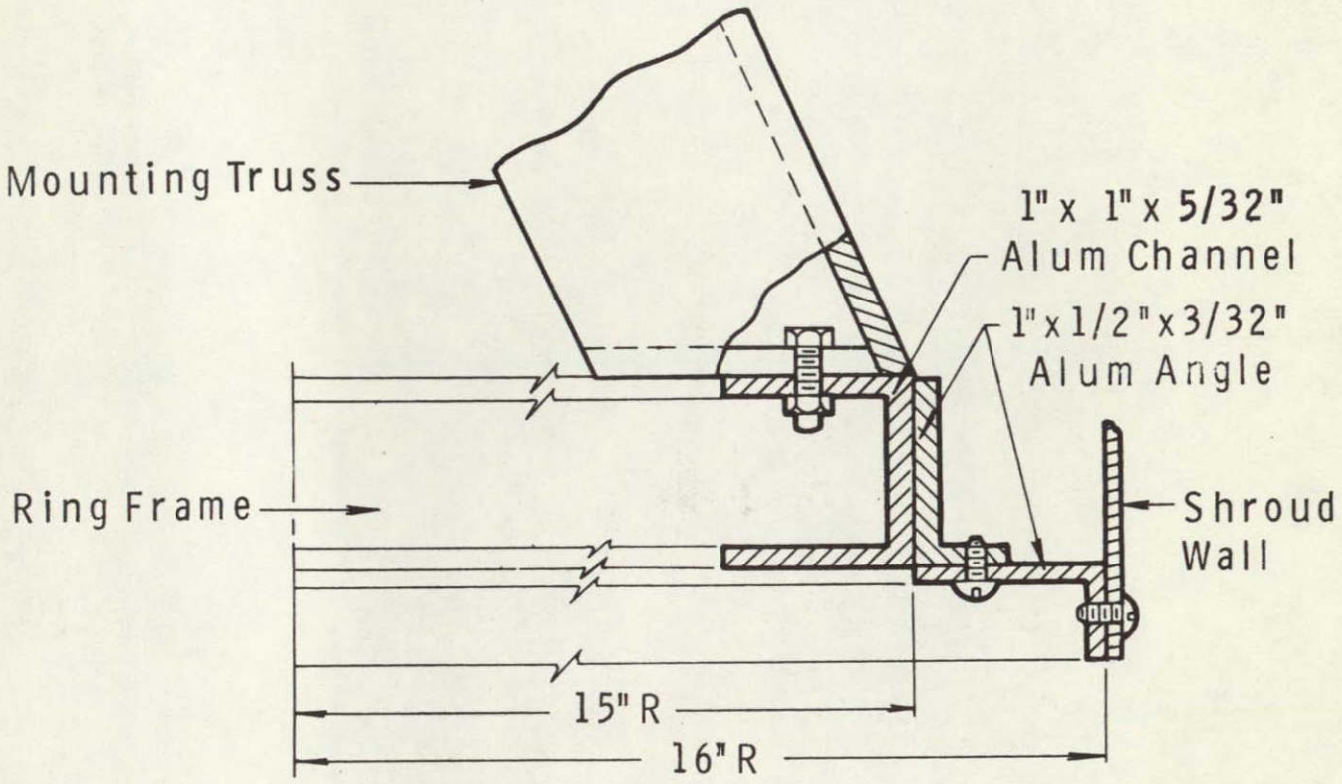

FIGURE 7. MODEL RING FRAME TO MOUNTING TRUSS CONNECTION

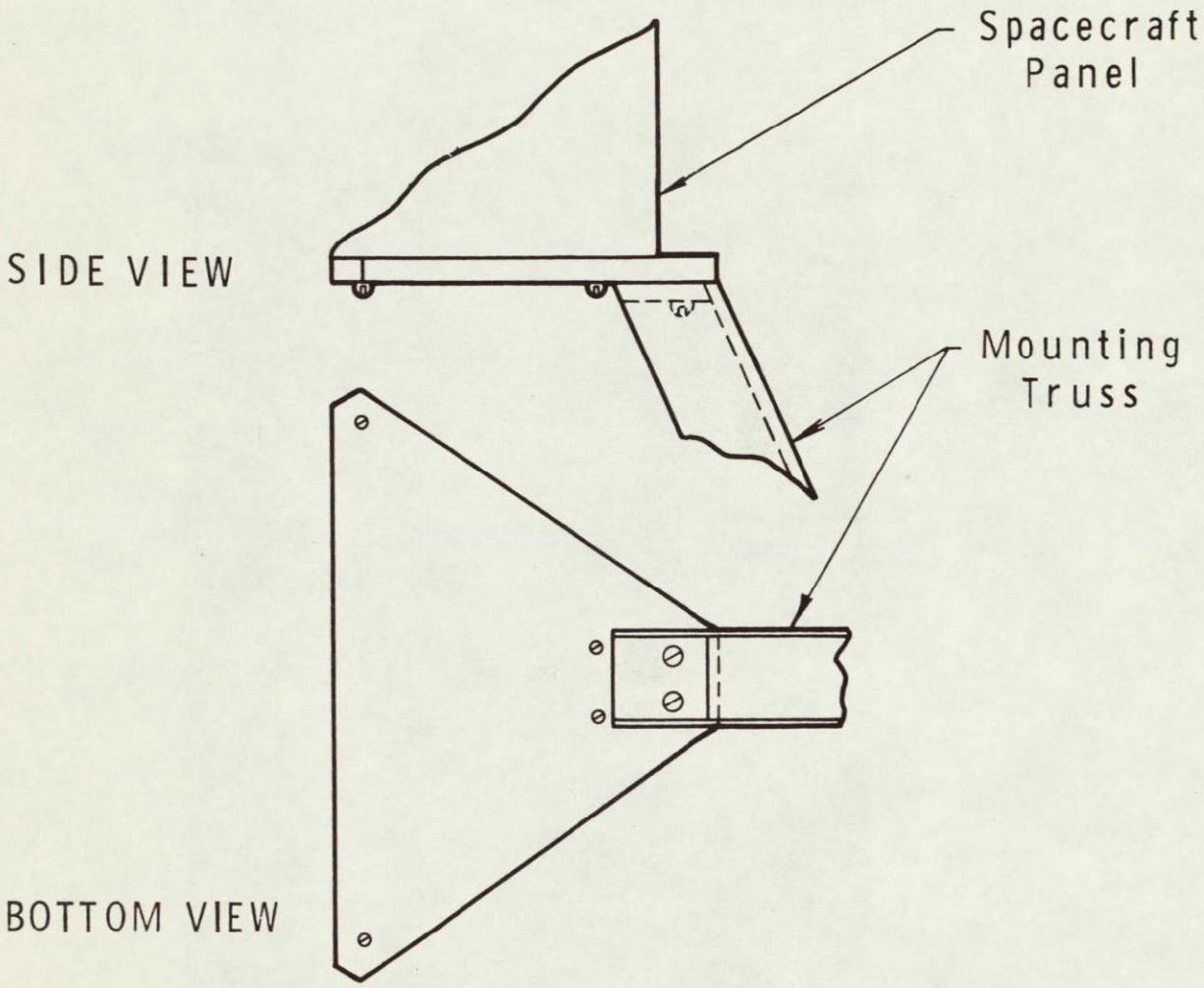

FIGURE 8. MODEL MOUNTING TRUSS TO SPACECRAFT CONNECTION

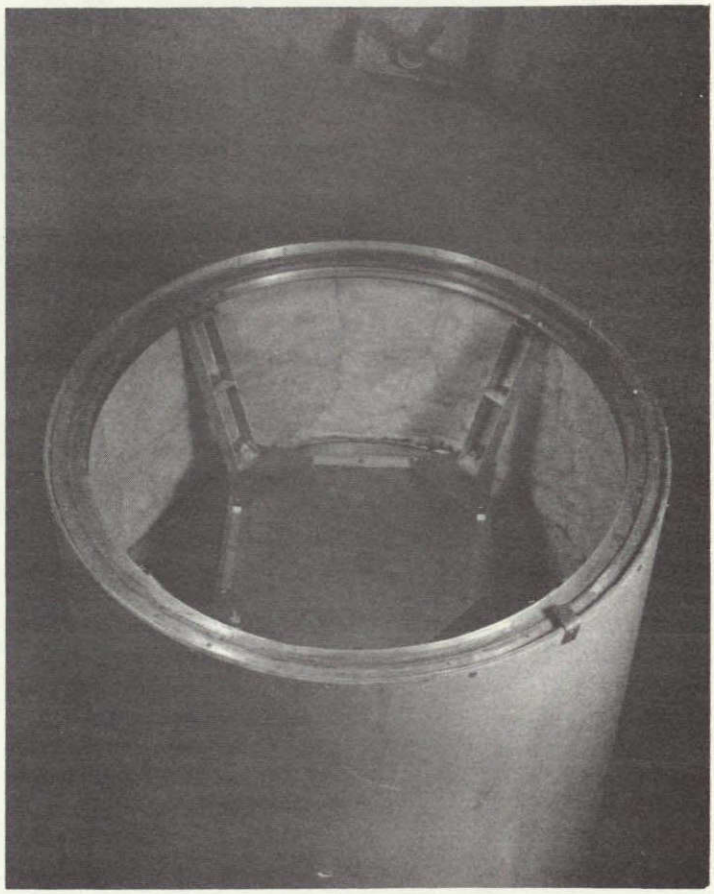

FIGURE 9. PHOTO OF MODEL MOUNTING TRUSSES

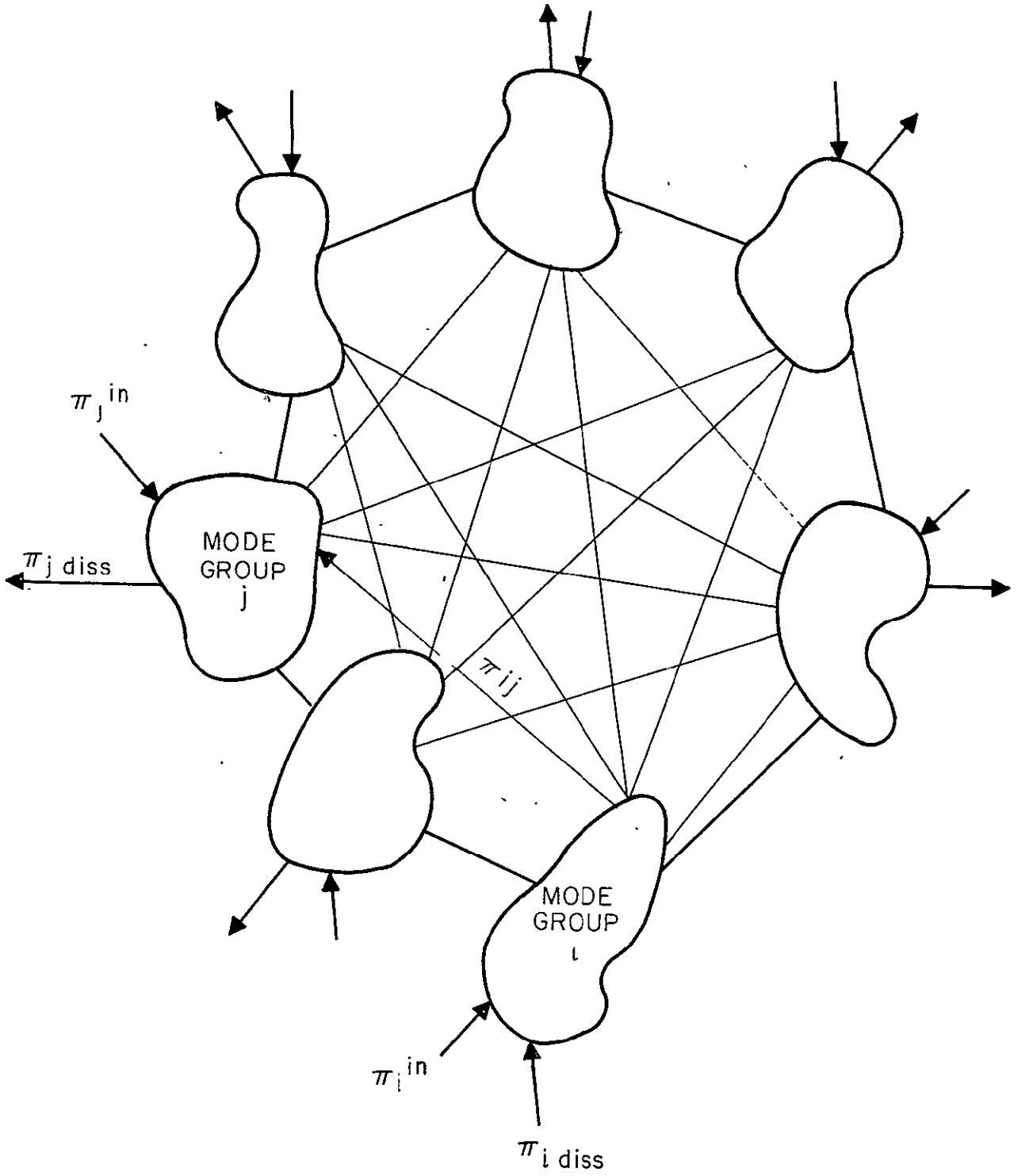

FIGURE 10. INTER-CONNECTED MODE GROUPS

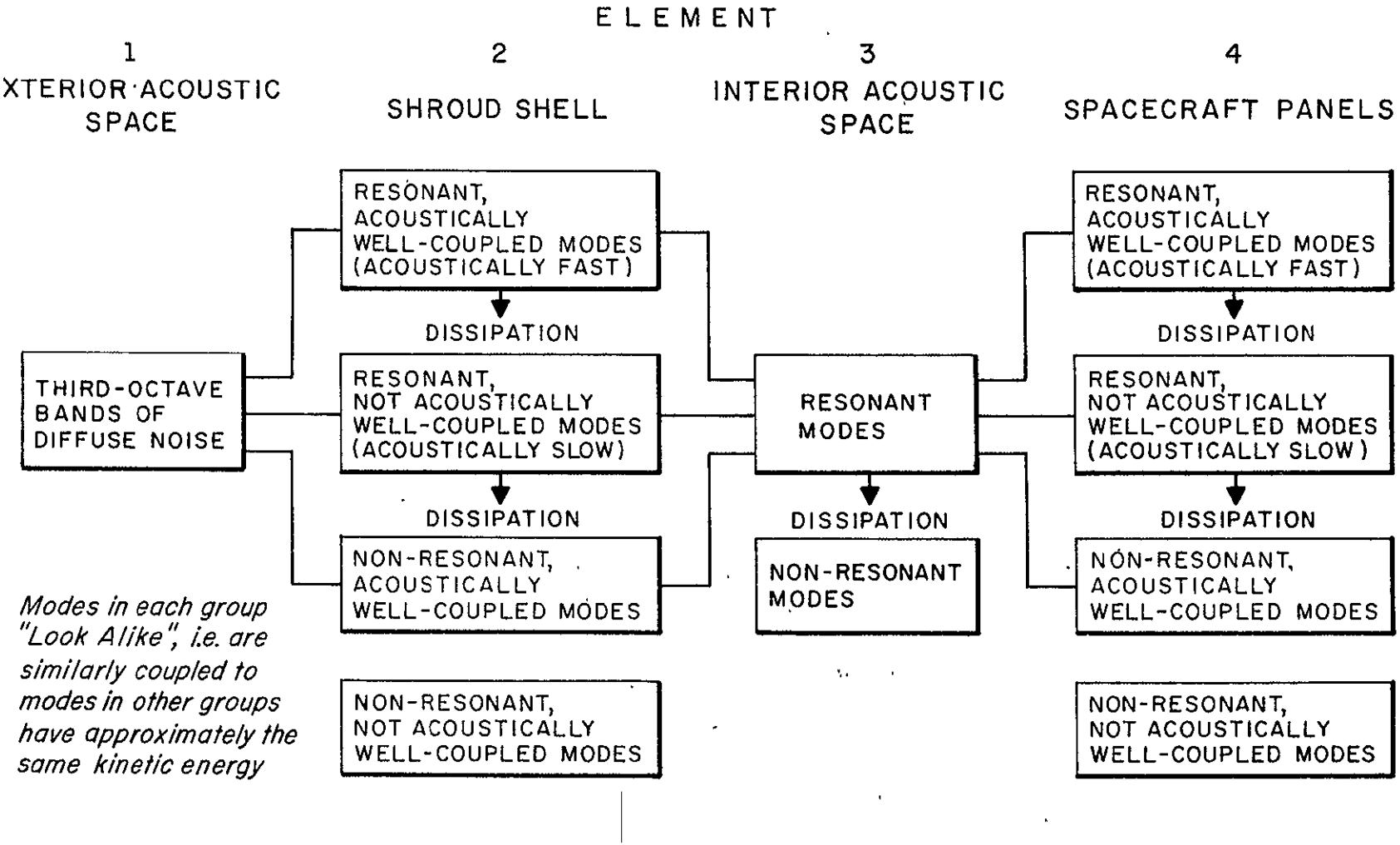

FIGURE 11. MODAL GROUPINGS FOR THEORETICAL TREATMENT OF THE ACOUSTIC PATH

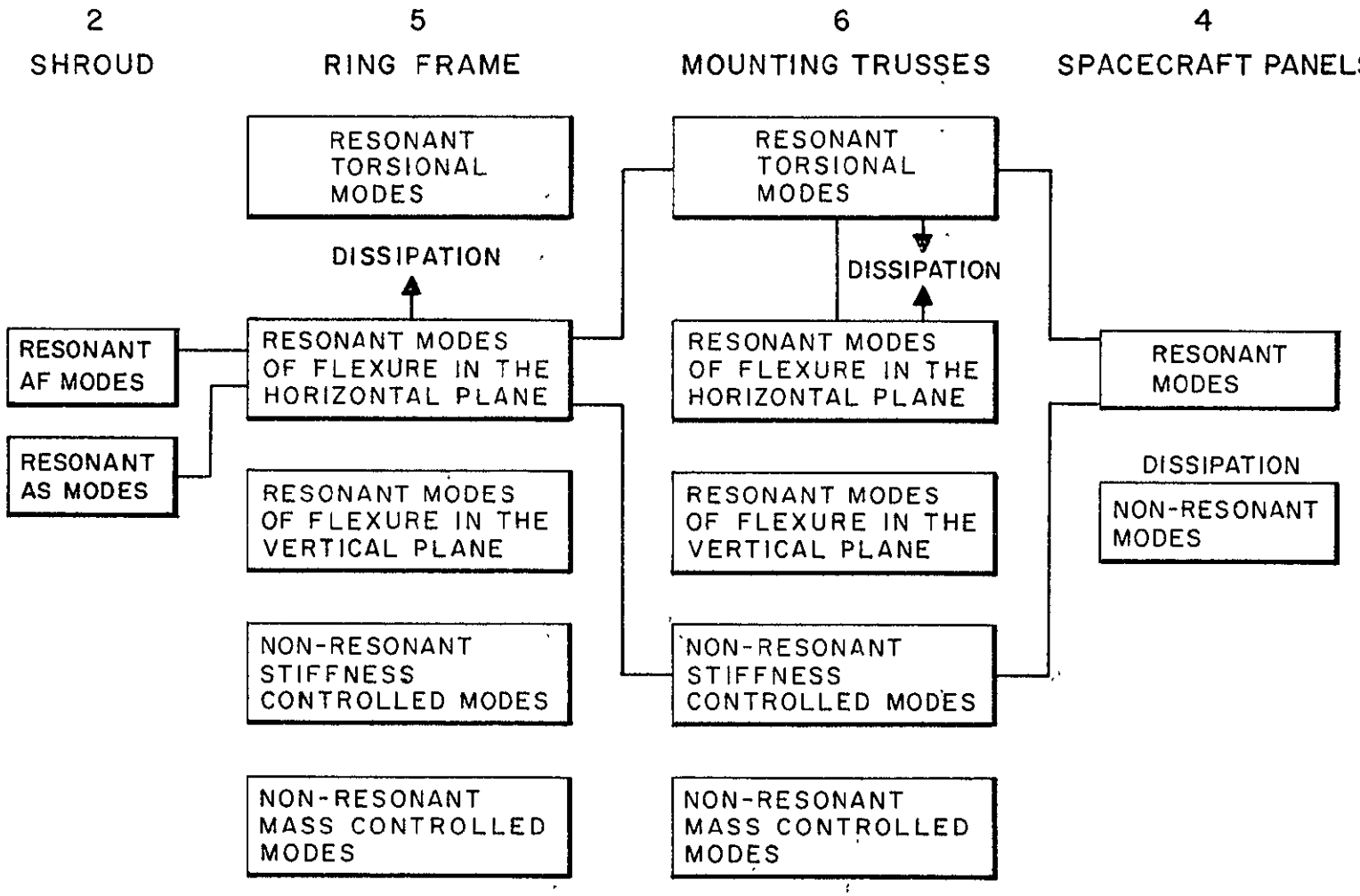

FIGURE 12. MODAL GROUPINGS FOR THE THEORETICAL TREATMENT OF THE MECHANICAL PATH

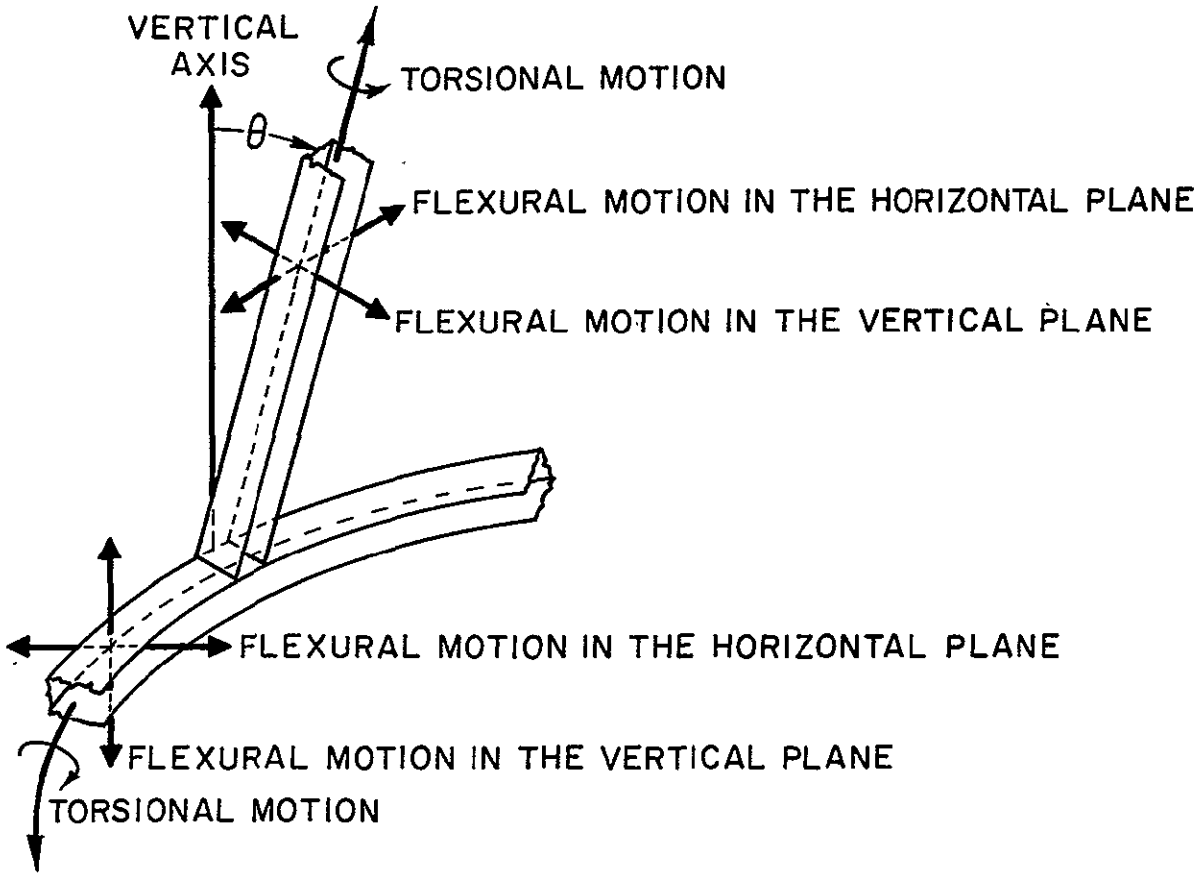

FIGURE 13. MOTION OF THE RING FRAME AND MOUNTING TRUSSES

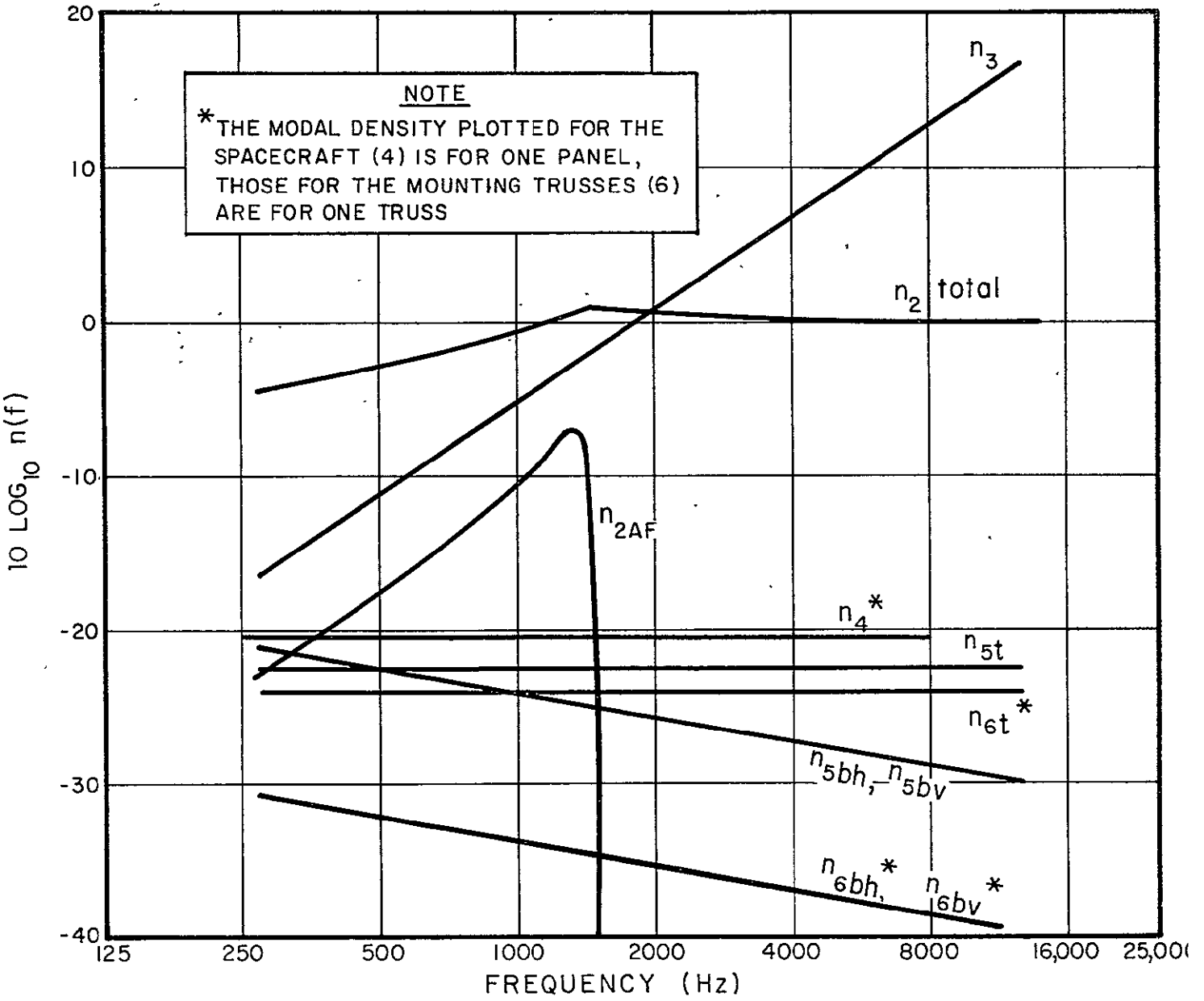

FIGURE 14. THEORETICAL MODAL DENSITIES

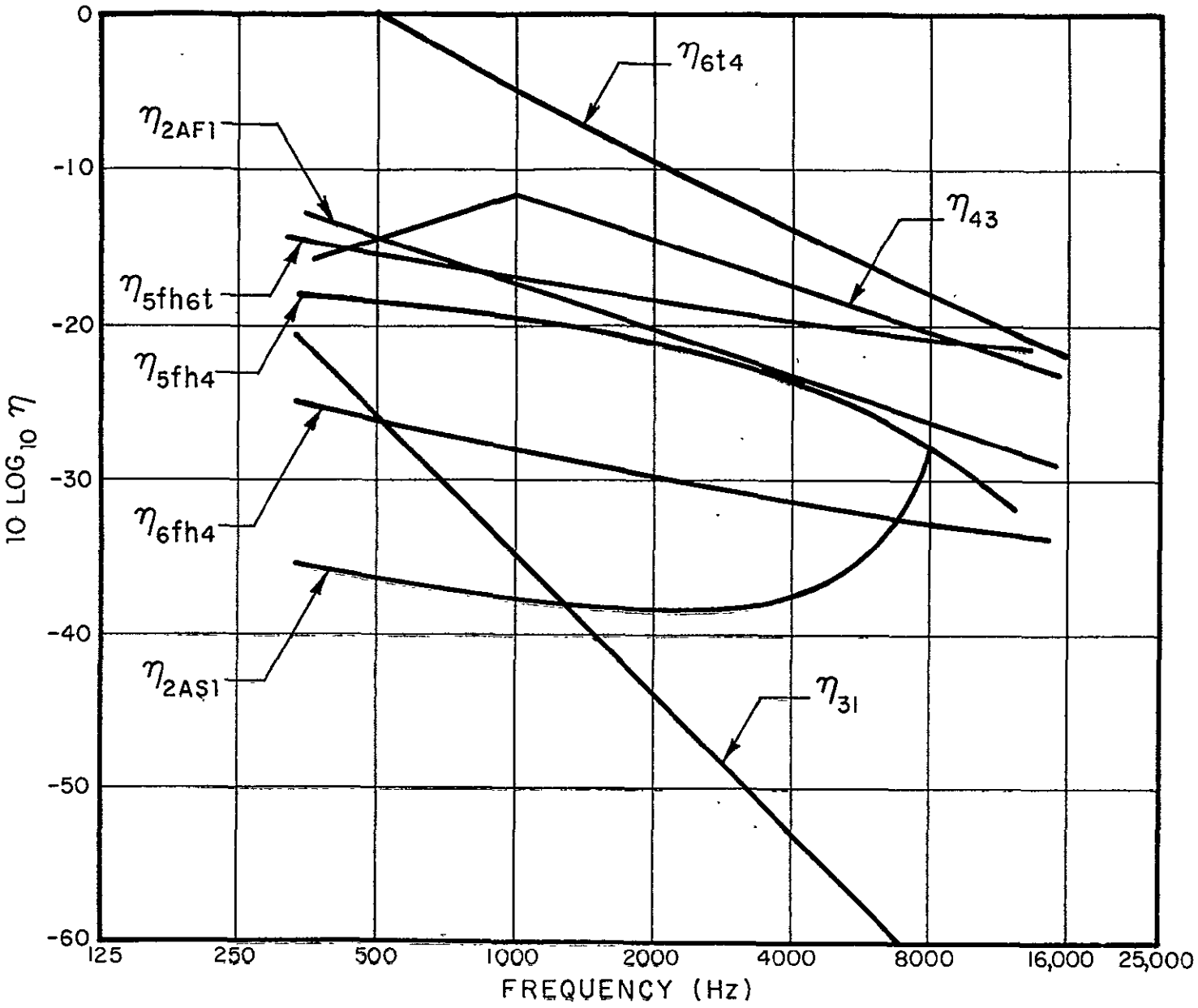

FIGURE 15. THEORETICAL COUPLING LOSS FACTORS

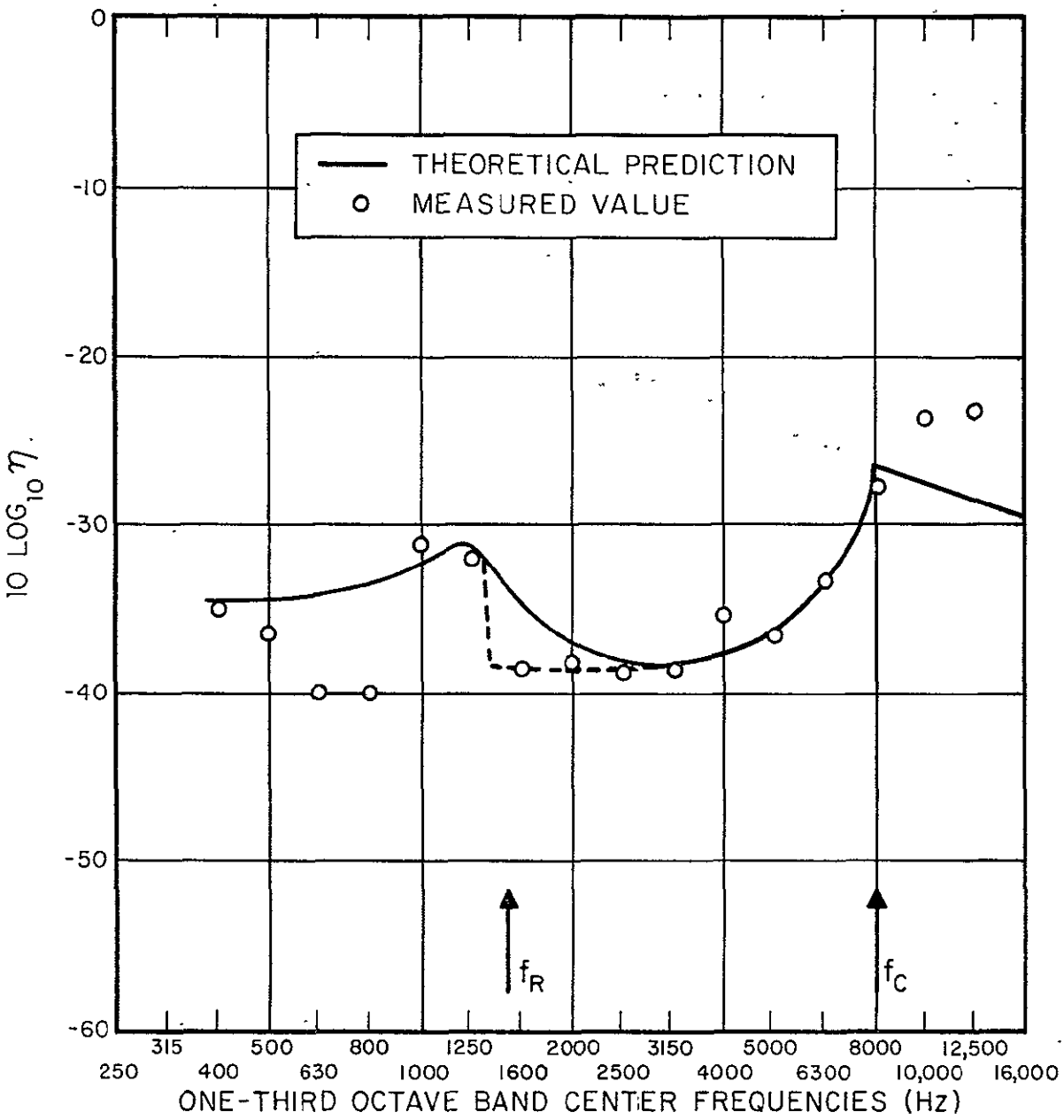

FIGURE 16. SHROUD-ACOUSTIC SPACE COUPLING LOSS FACTOR

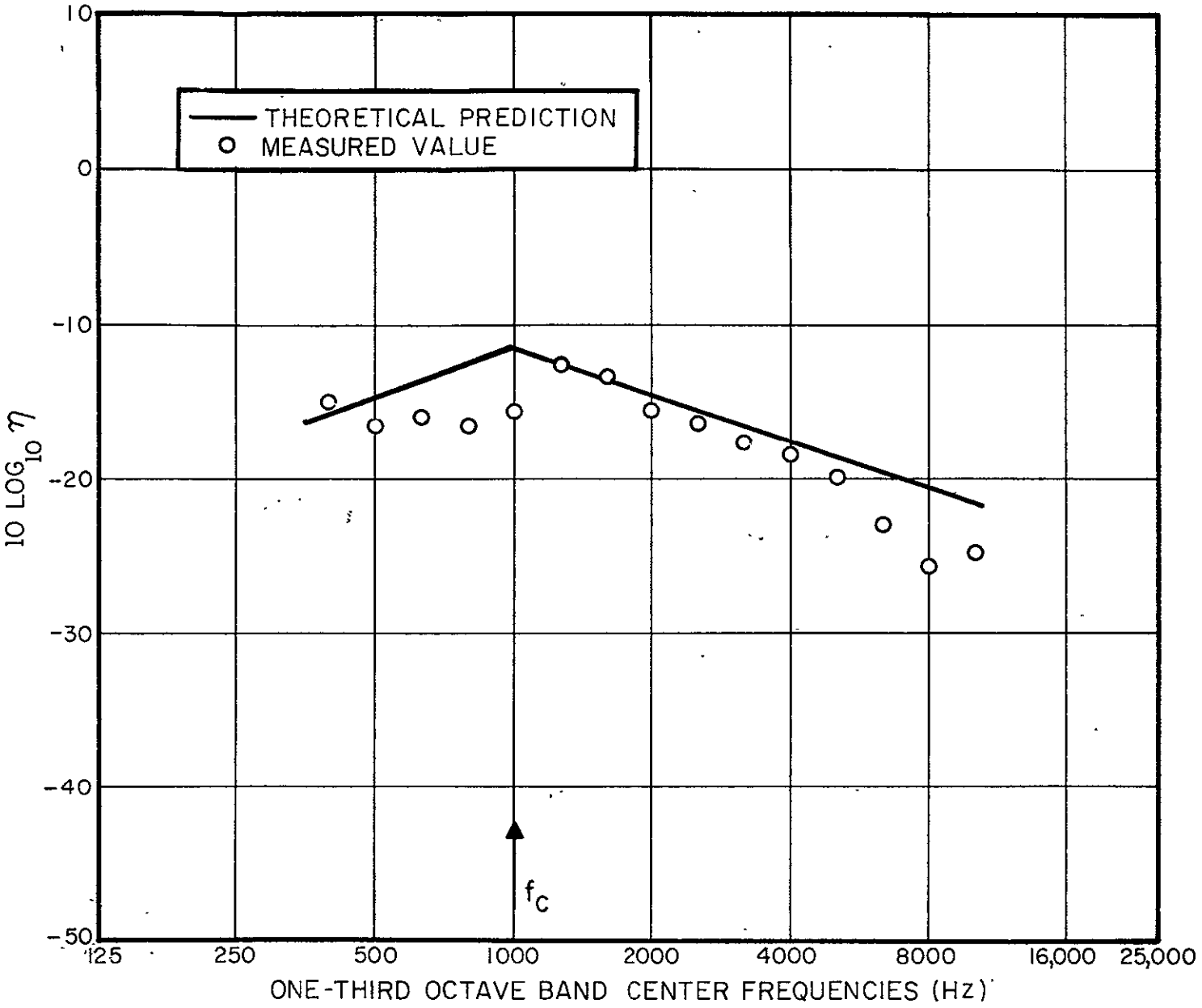

FIGURE 17. SPACECRAFT-ACOUSTIC SPACE COUPLING LOSS FACTOR

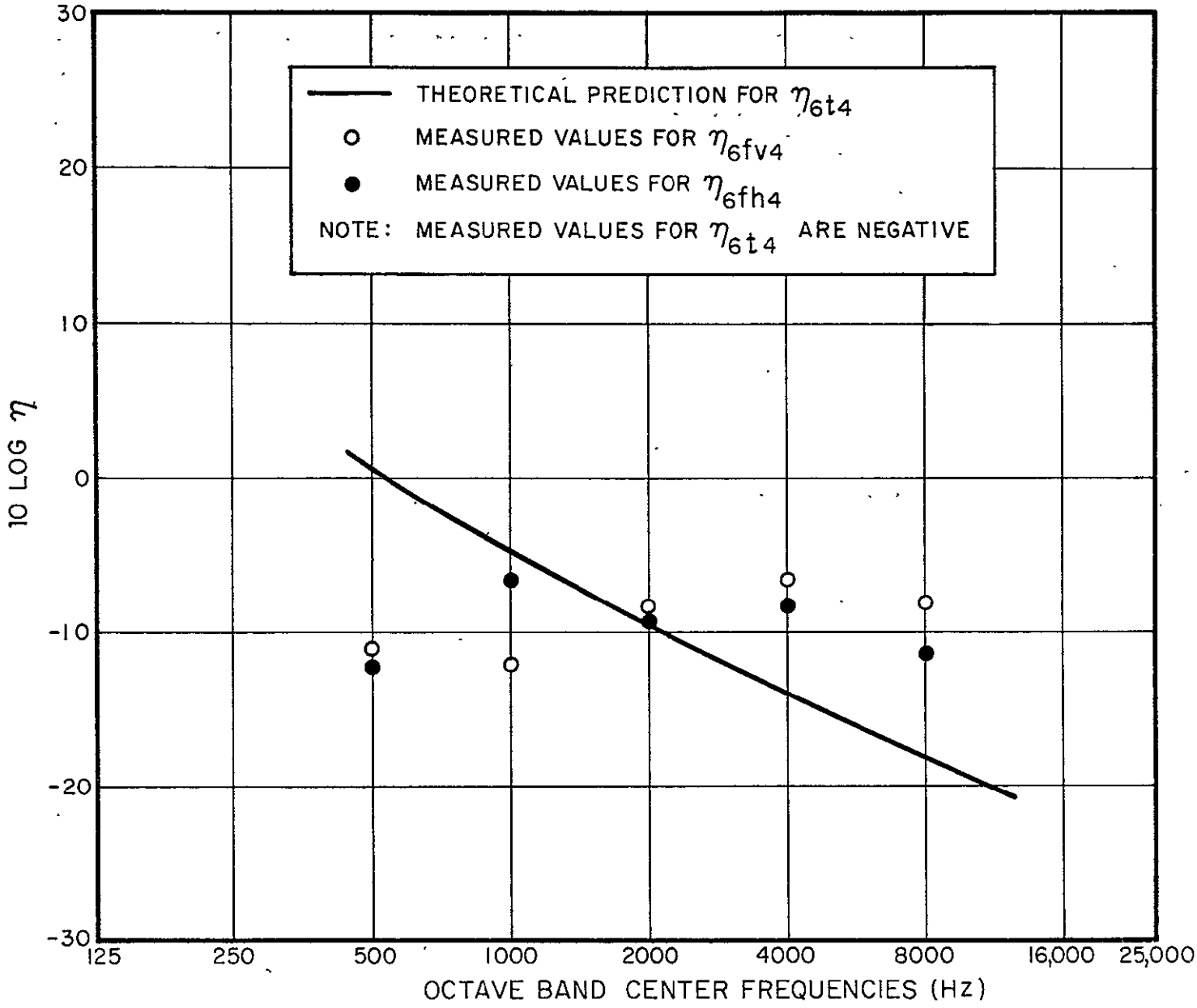

FIGURE 18. TRUSS-SPACECRAFT COUPLING LOSS FACTORS

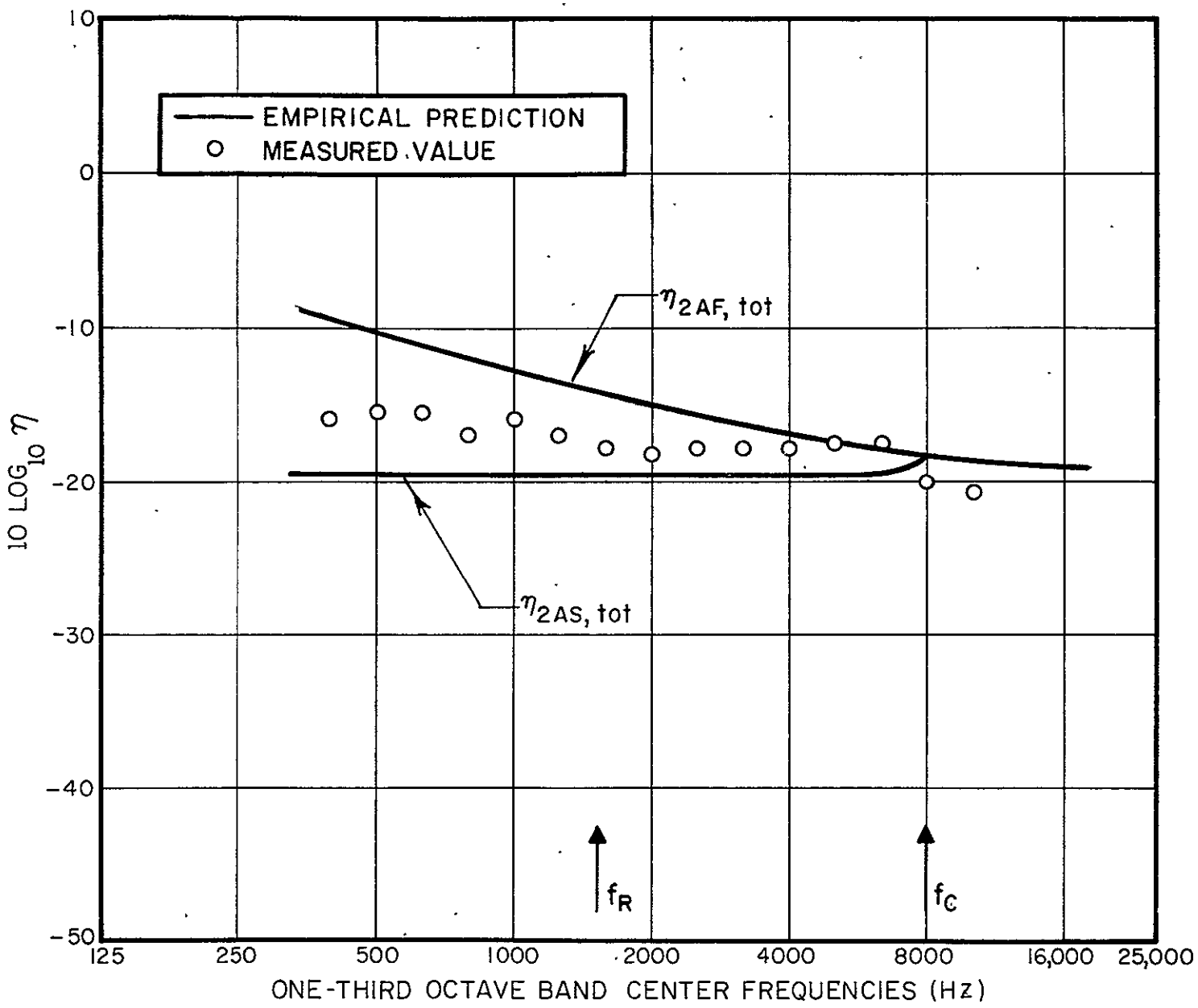

FIGURE 19. SHROUD TOTAL LOSS FACTOR

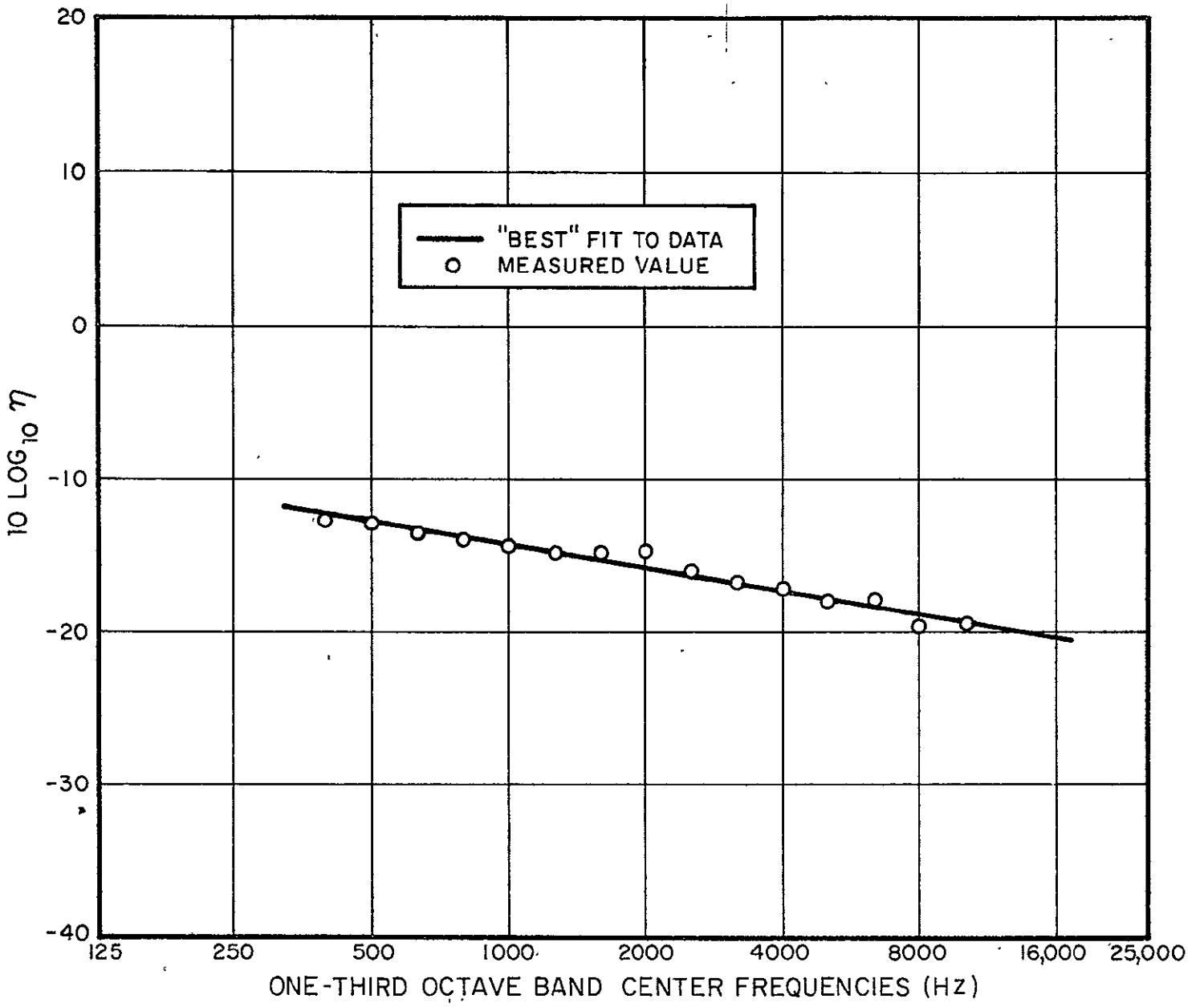

FIGURE 20. INTERNAL ACOUSTIC SPACE COUPLING LOSS FACTOR

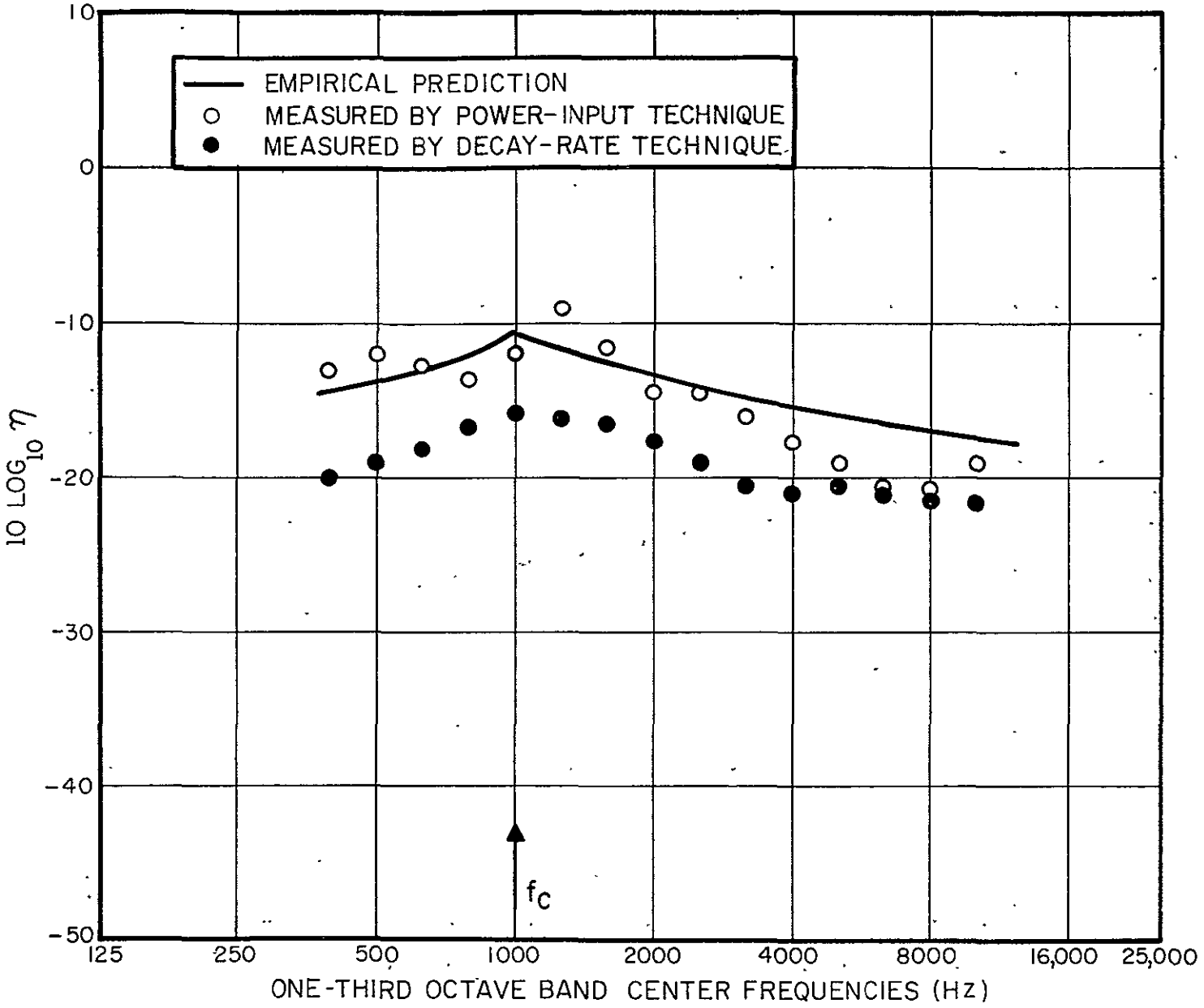

FIGURE 21. SPACECRAFT TOTAL LOSS FACTOR

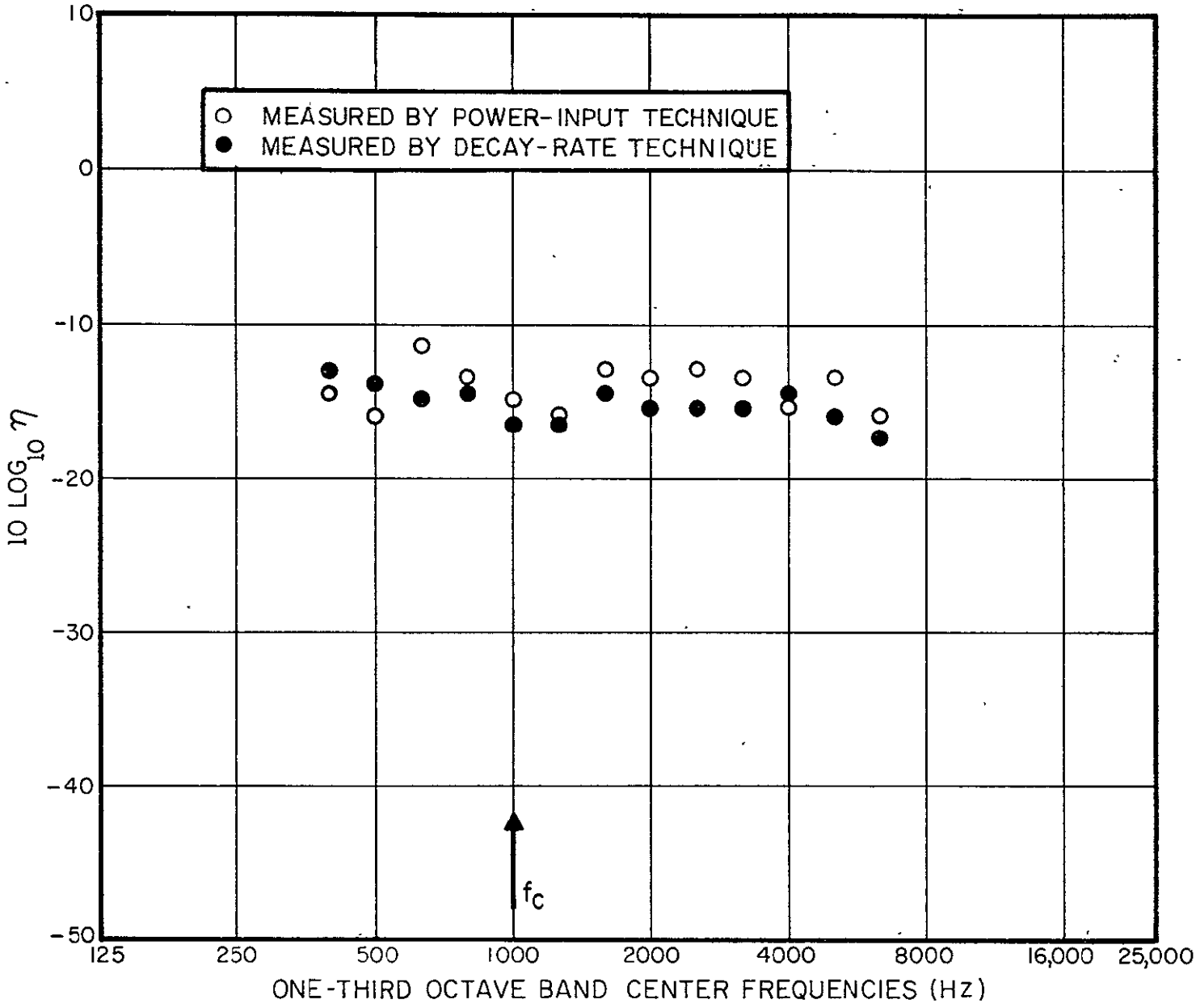

FIGURE 22. SINGLE PANEL TOTAL LOSS FACTOR — PANEL EDGES SIMPLY SUPPORTED

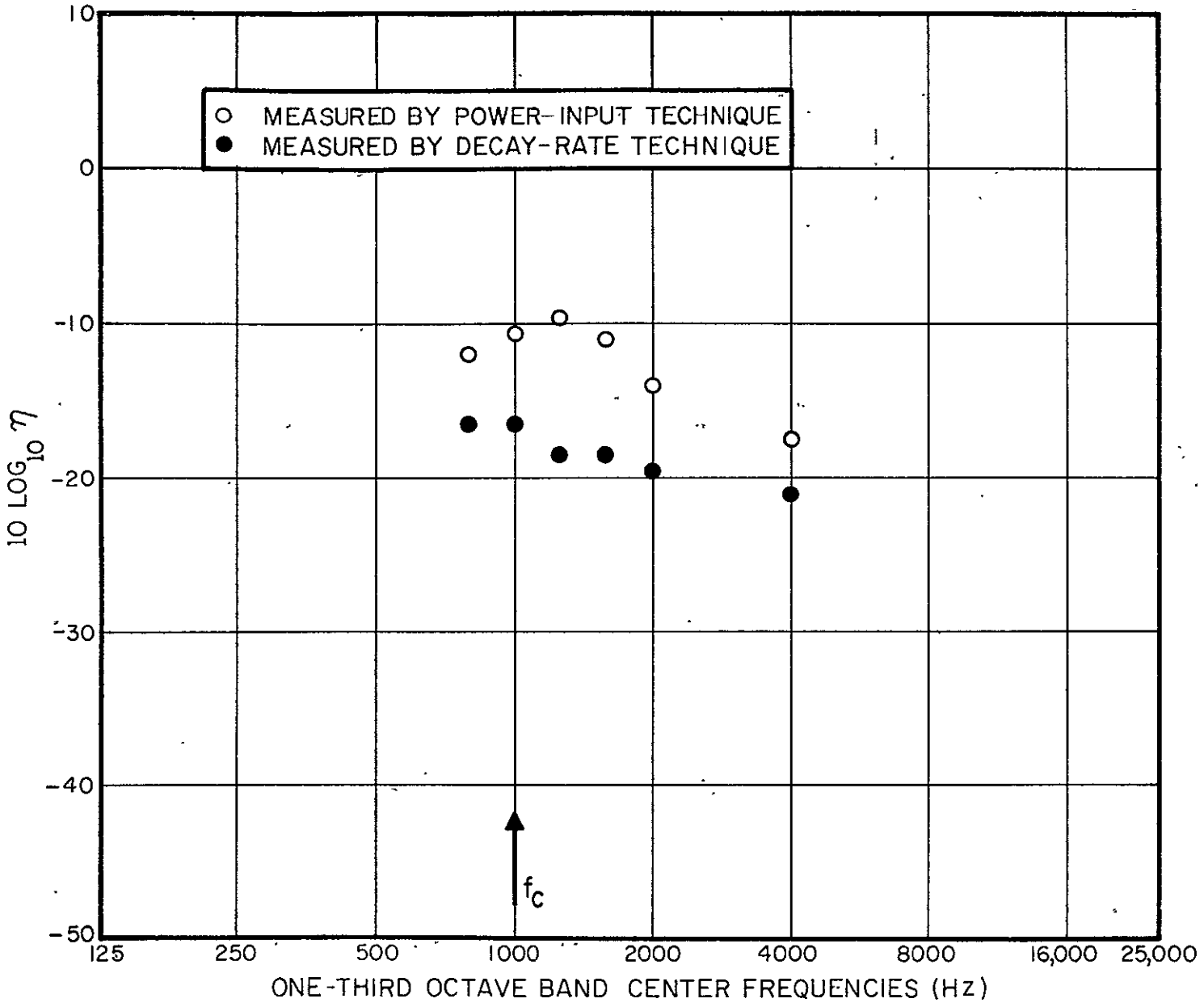

FIGURE 23. SINGLE PANEL TOTAL LOSS-FACTOR — PANEL EDGES UNSUPPORTED

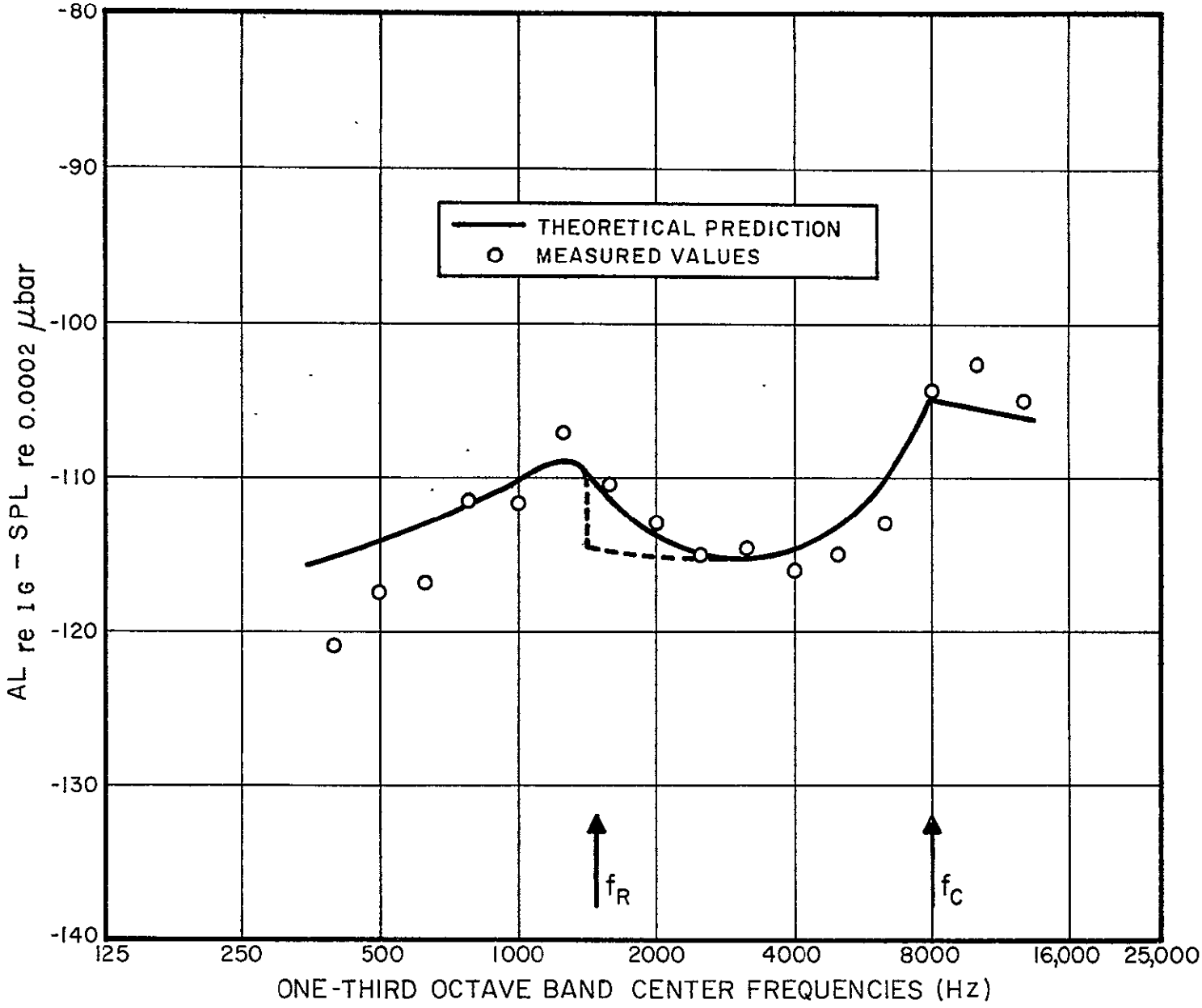

FIGURE 24. SHROUD RESPONSE TO ACOUSTIC EXCITATION

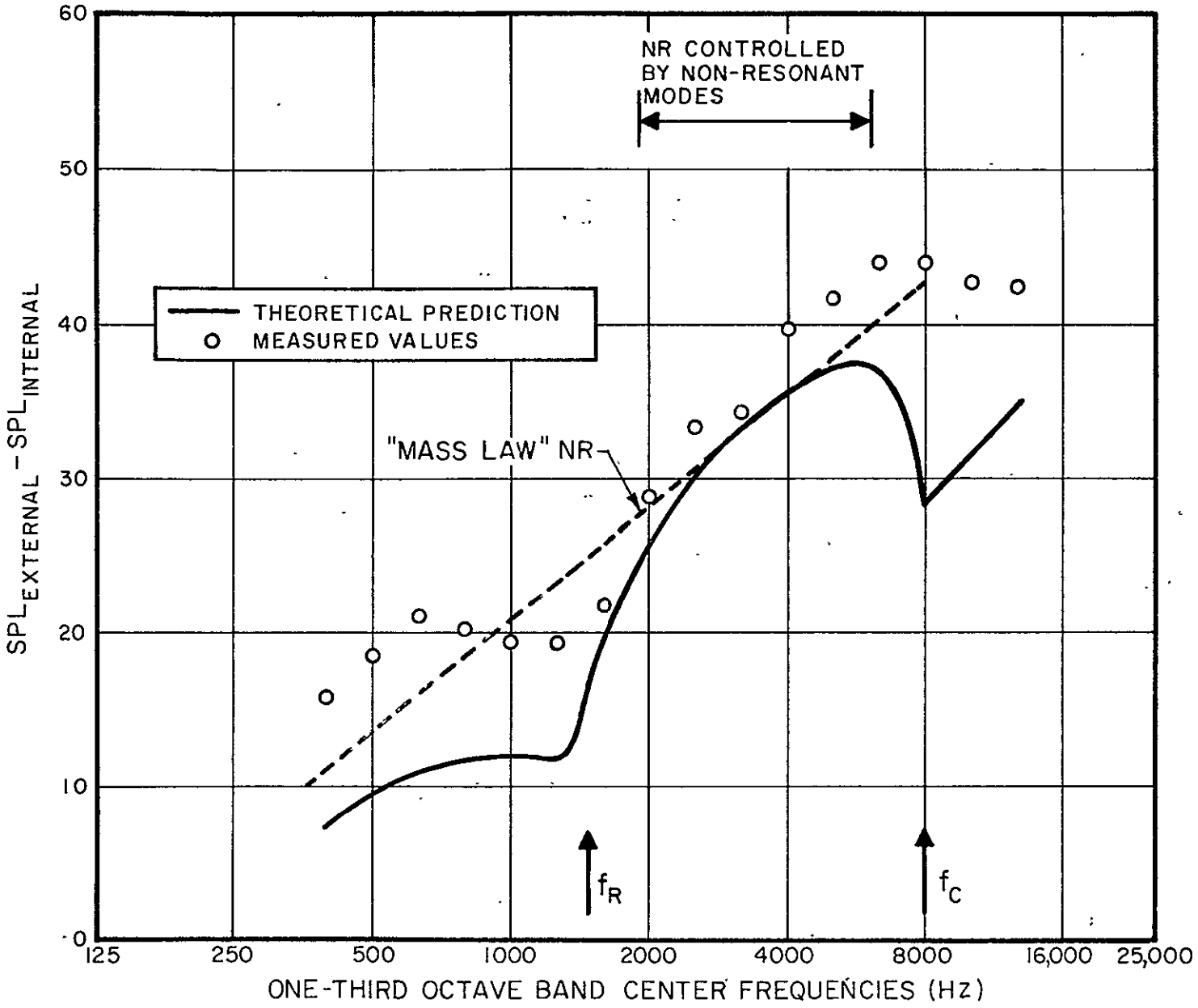

FIGURE 25. SHROUD NOISE REDUCTION

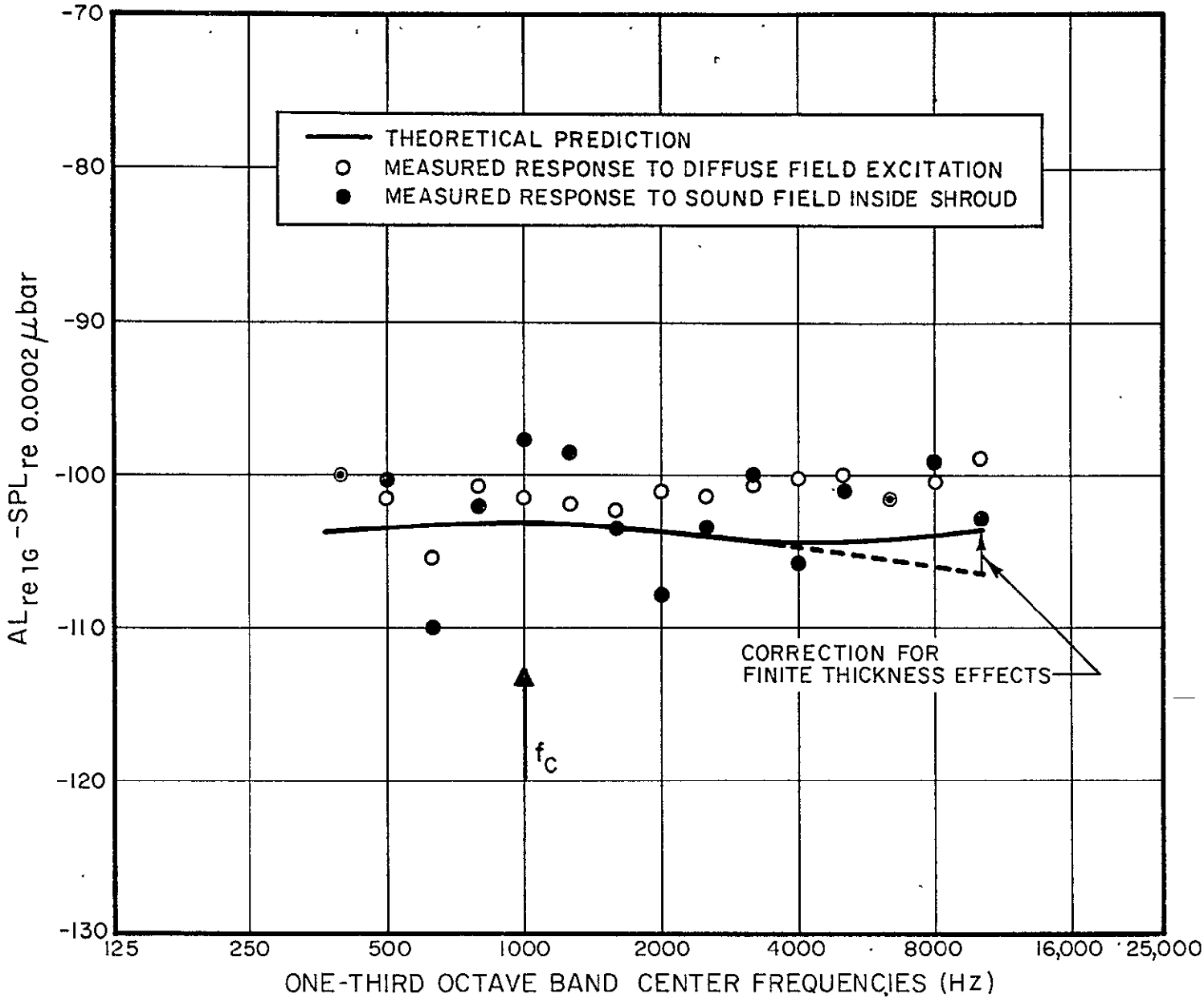

FIGURE 26. SPACECRAFT RESPONSE TO ACOUSTIC EXCITATION

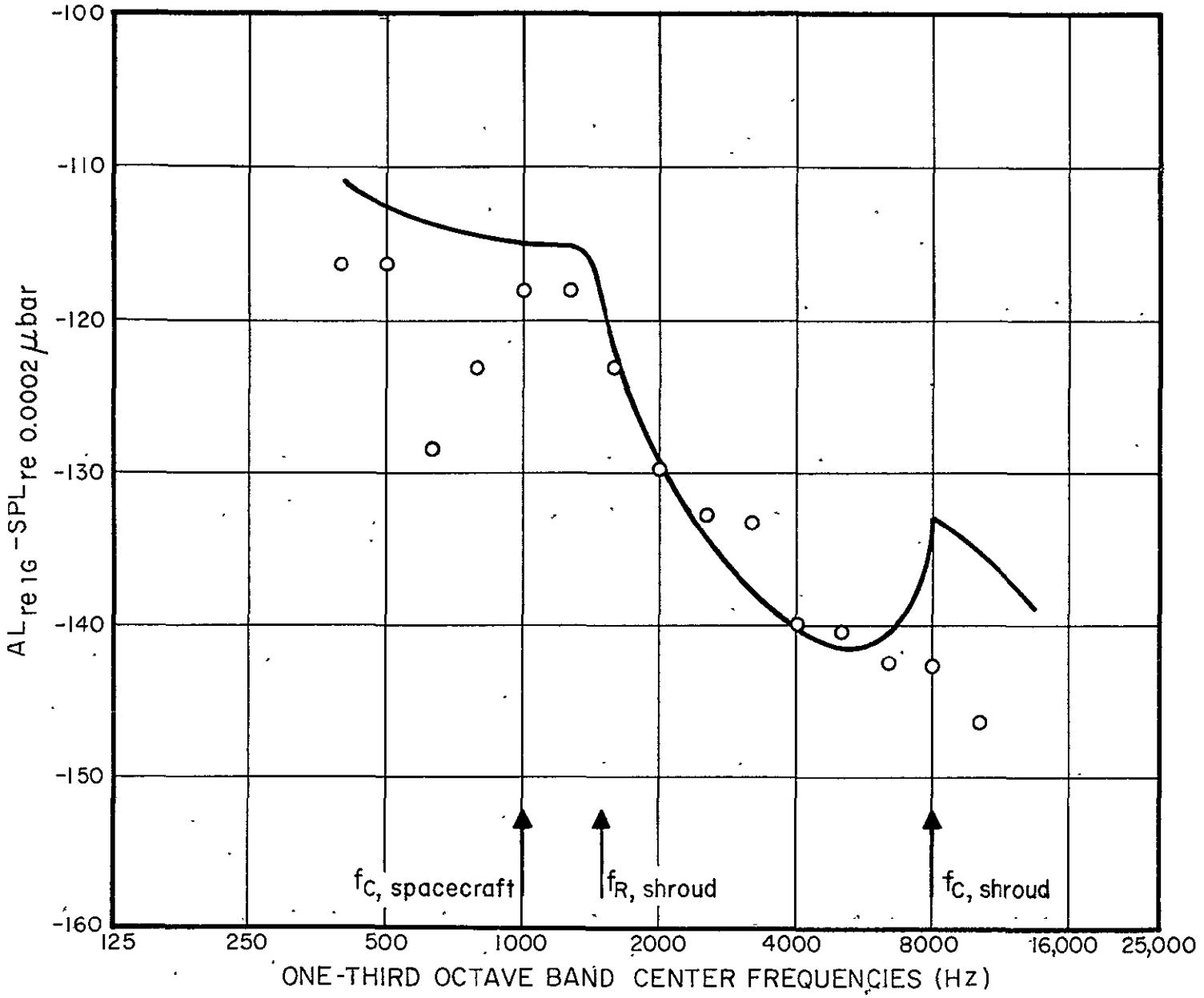

FIGURE 27. SPACECRAFT RESPONSE TO VIBRATION TRANSMITTED BY THE ACOUSTIC PATH

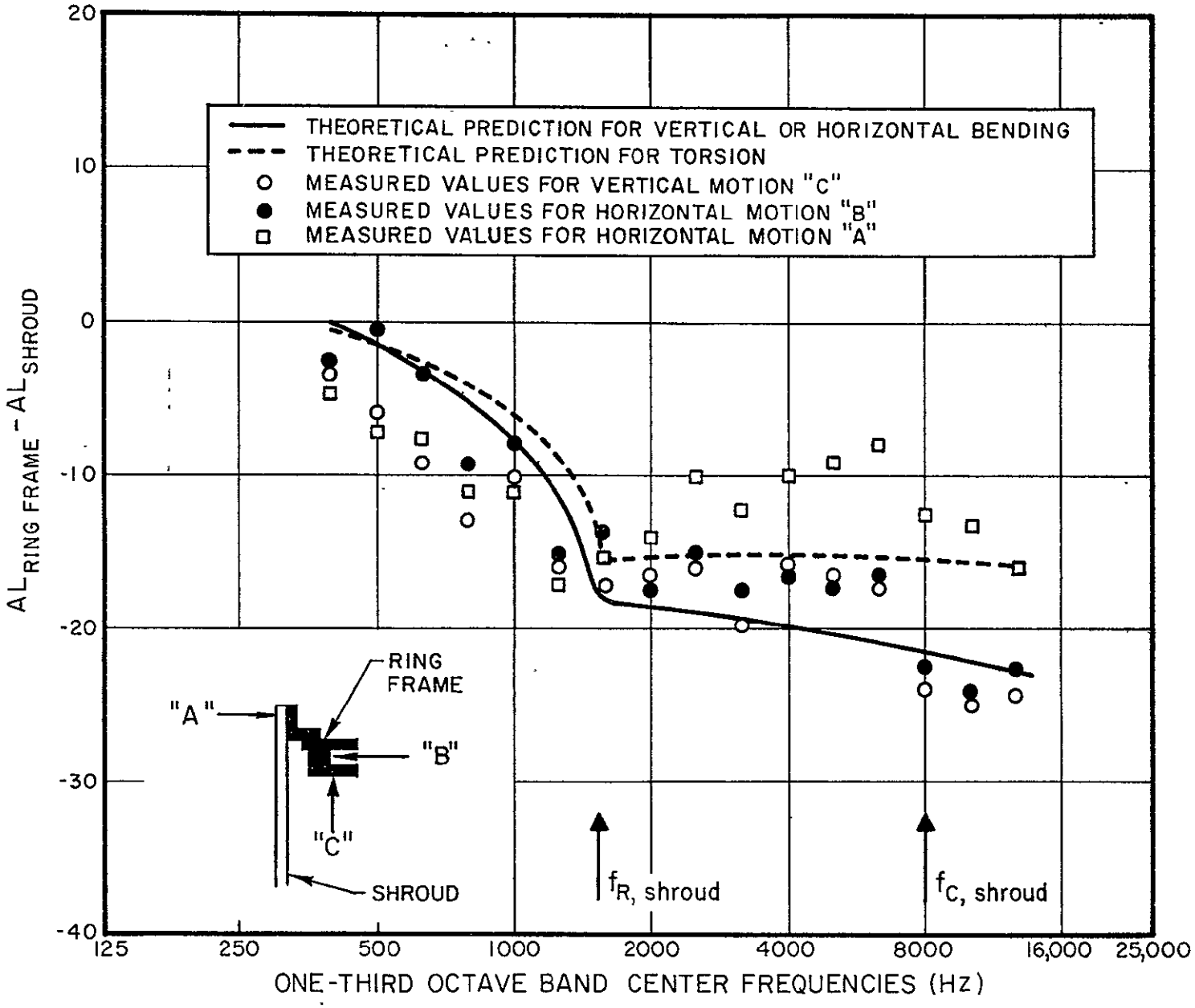

FIGURE 28. RING FRAME RESPONSE

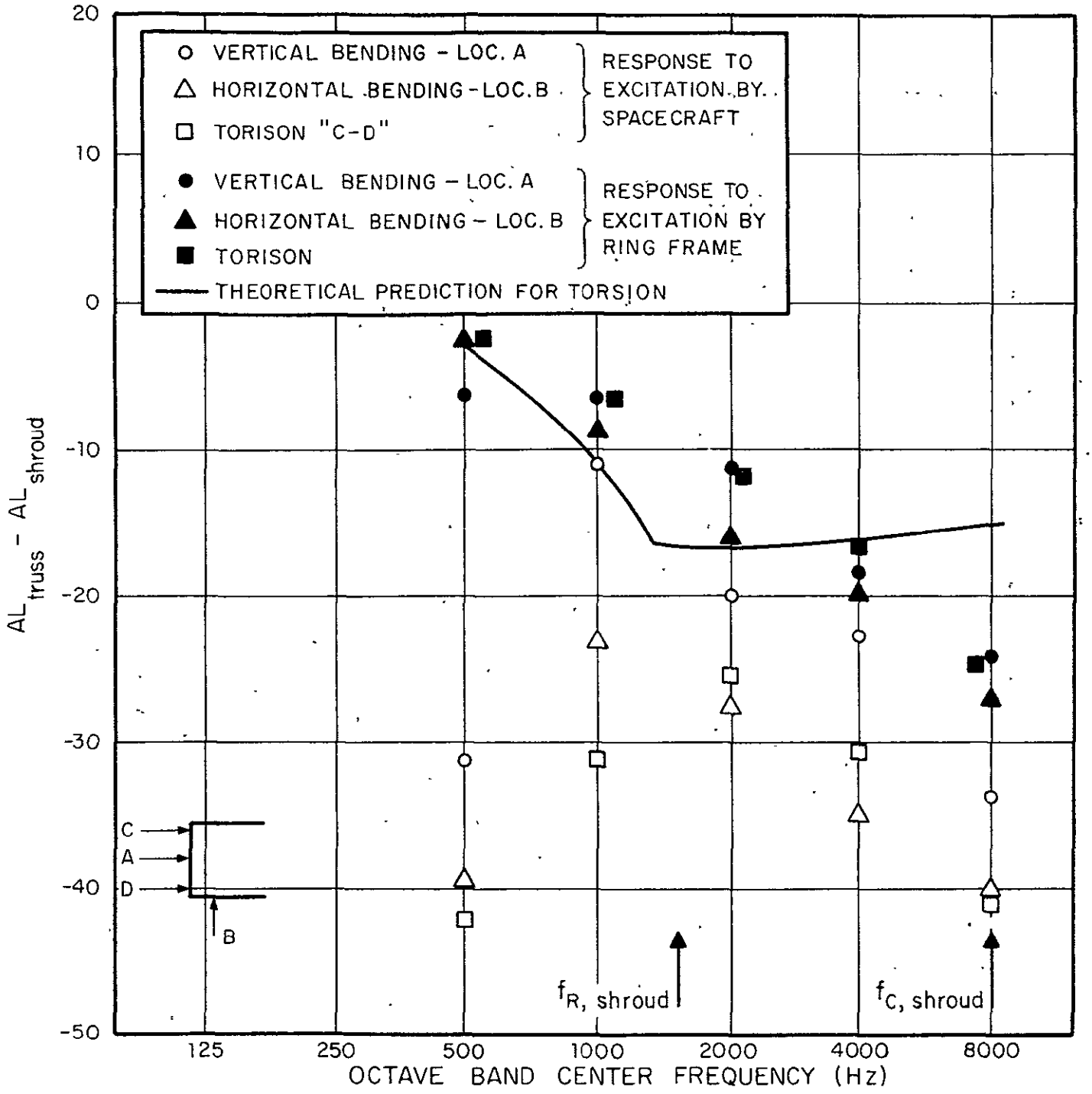

FIGURE 29. TRUSS RESPONSE

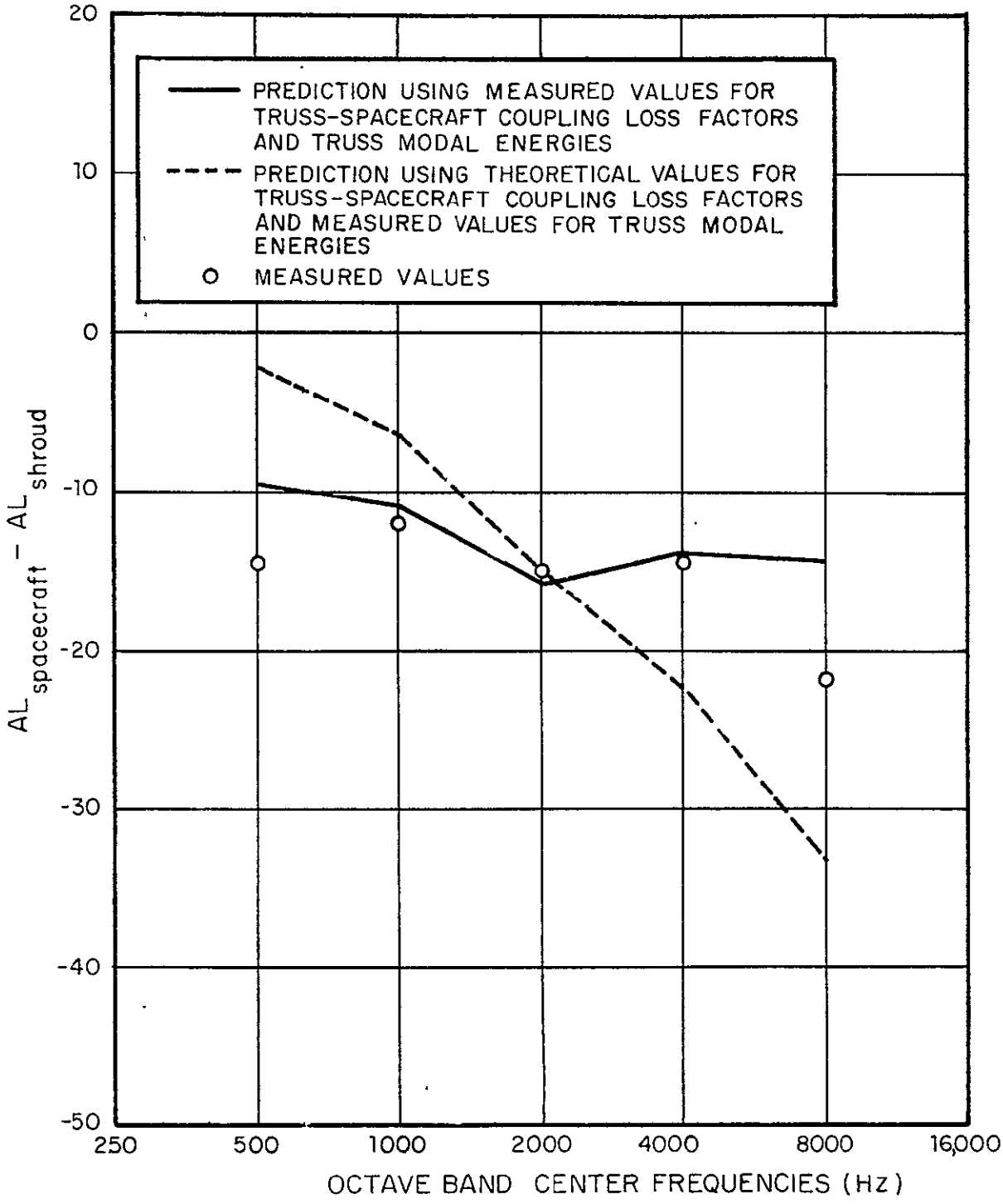

FIGURE 30. SPACECRAFT RESPONSE TO EXCITATION BY THE TRUSSES

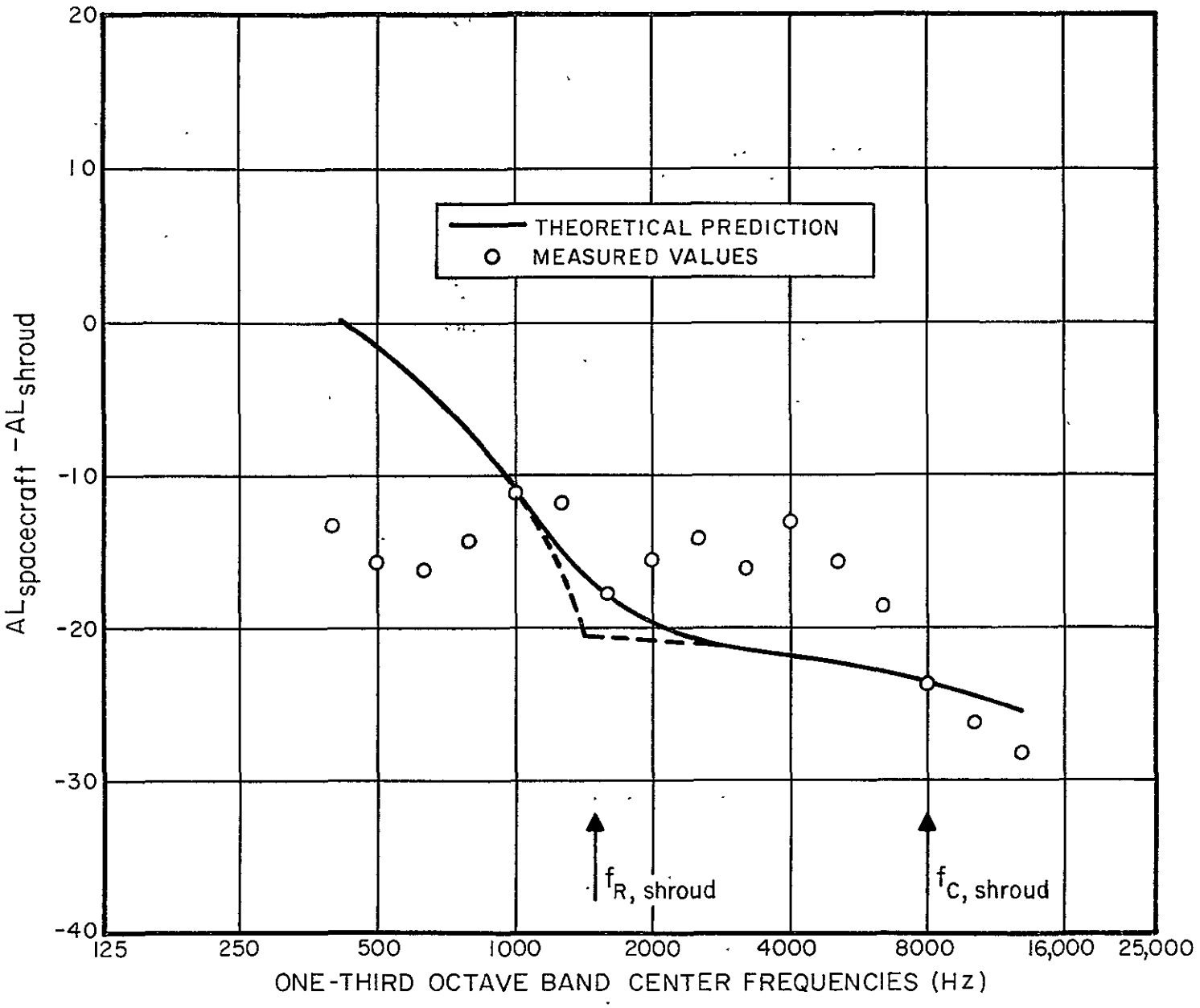

FIGURE 31. SPACECRAFT RESPONSE TO VIBRATION TRANSMITTED BY THE MECHANICAL PATH

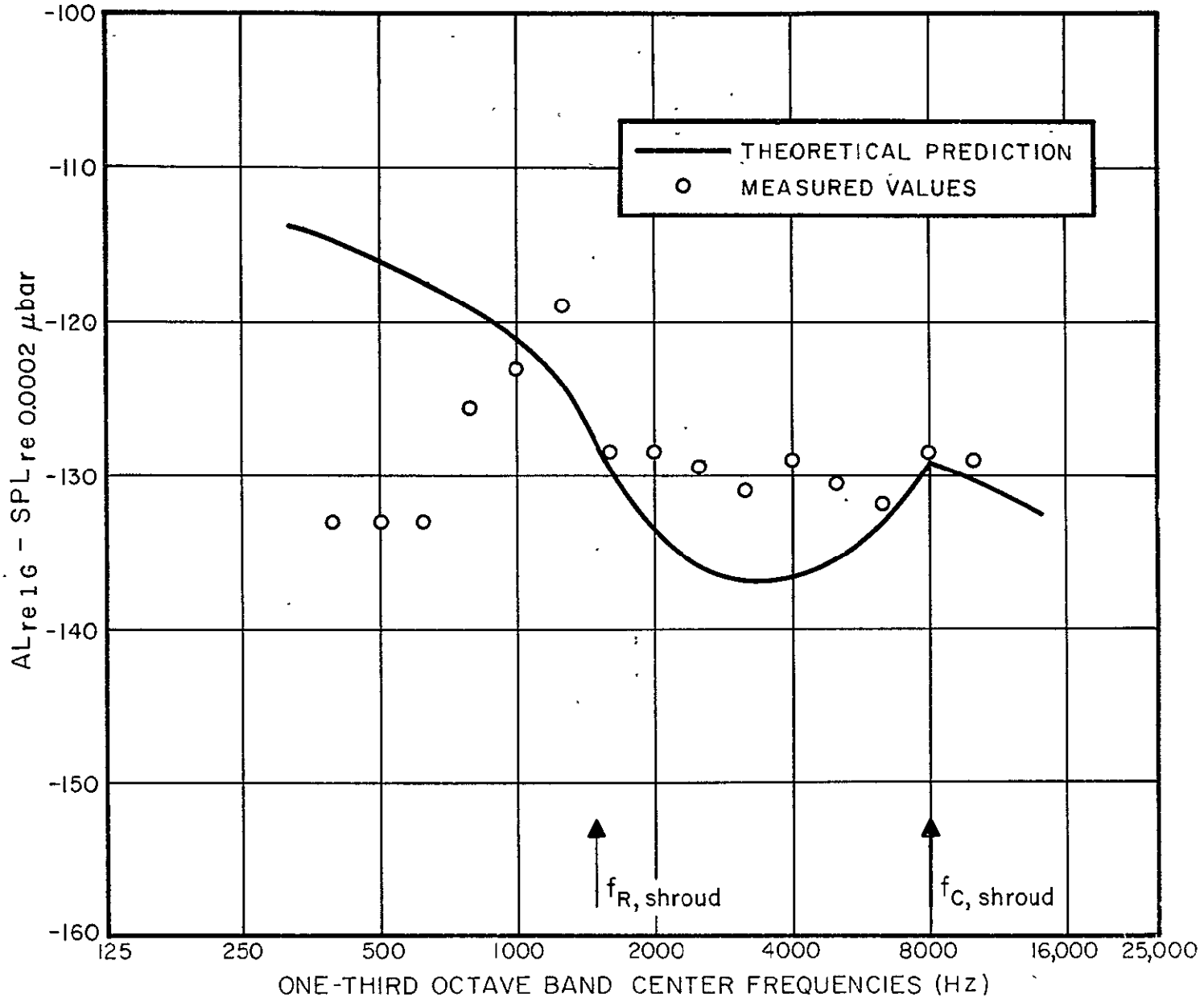

FIGURE 32. SPACECRAFT RESPONSE TO VIBRATION TRANSMITTED BY THE MECHANICAL PATH

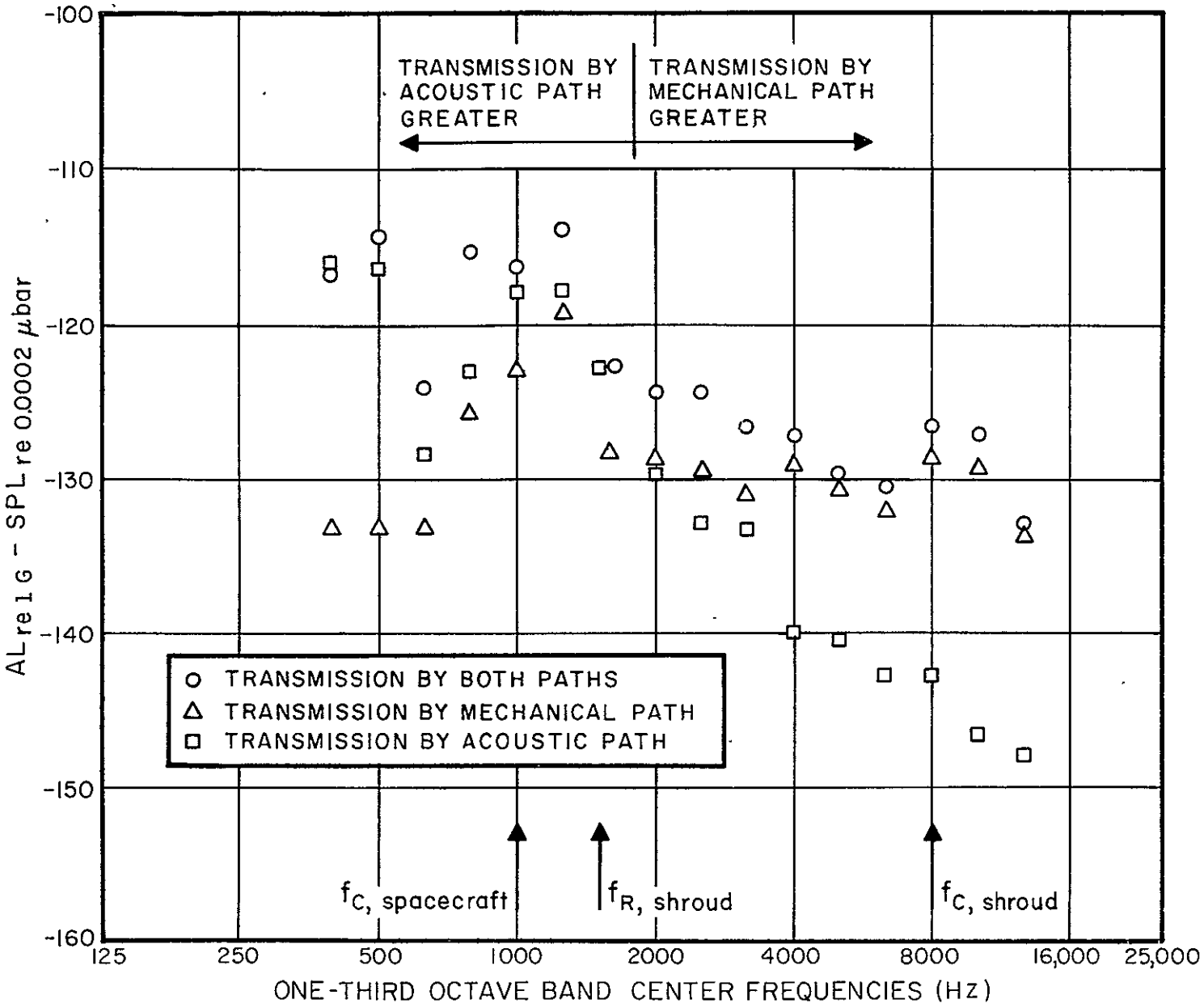

FIGURE 33. MEASURED VALUES OF SPACECRAFT RESPONSE TO VIBRATION TRANSMITTED BY THE DIFFERENT PATHS

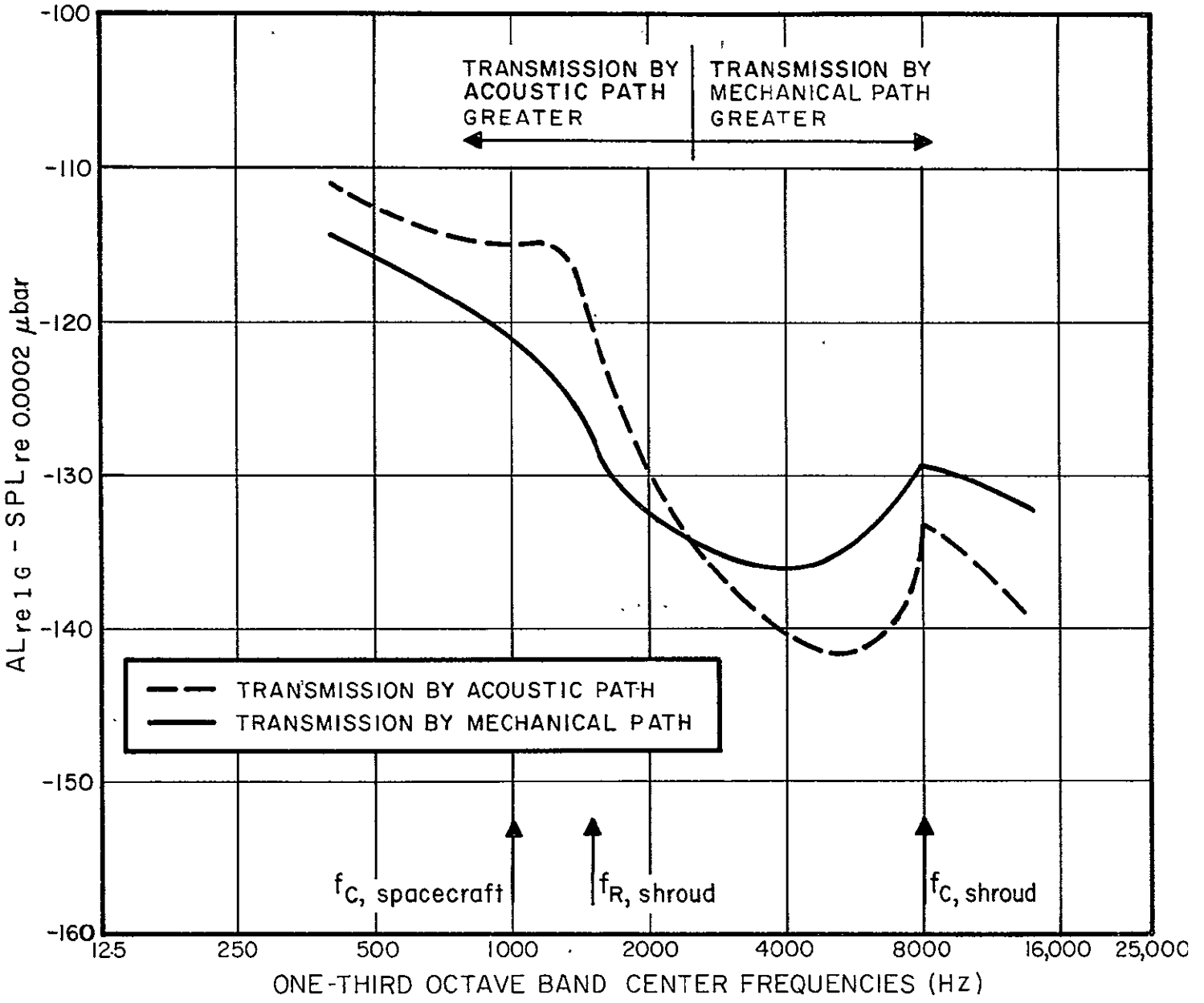

FIGURE 34. PREDICTED VALUES OF SPACECRAFT RESPONSE TO VIBRATION TRANSMITTED BY THE DIFFERENT PATHS

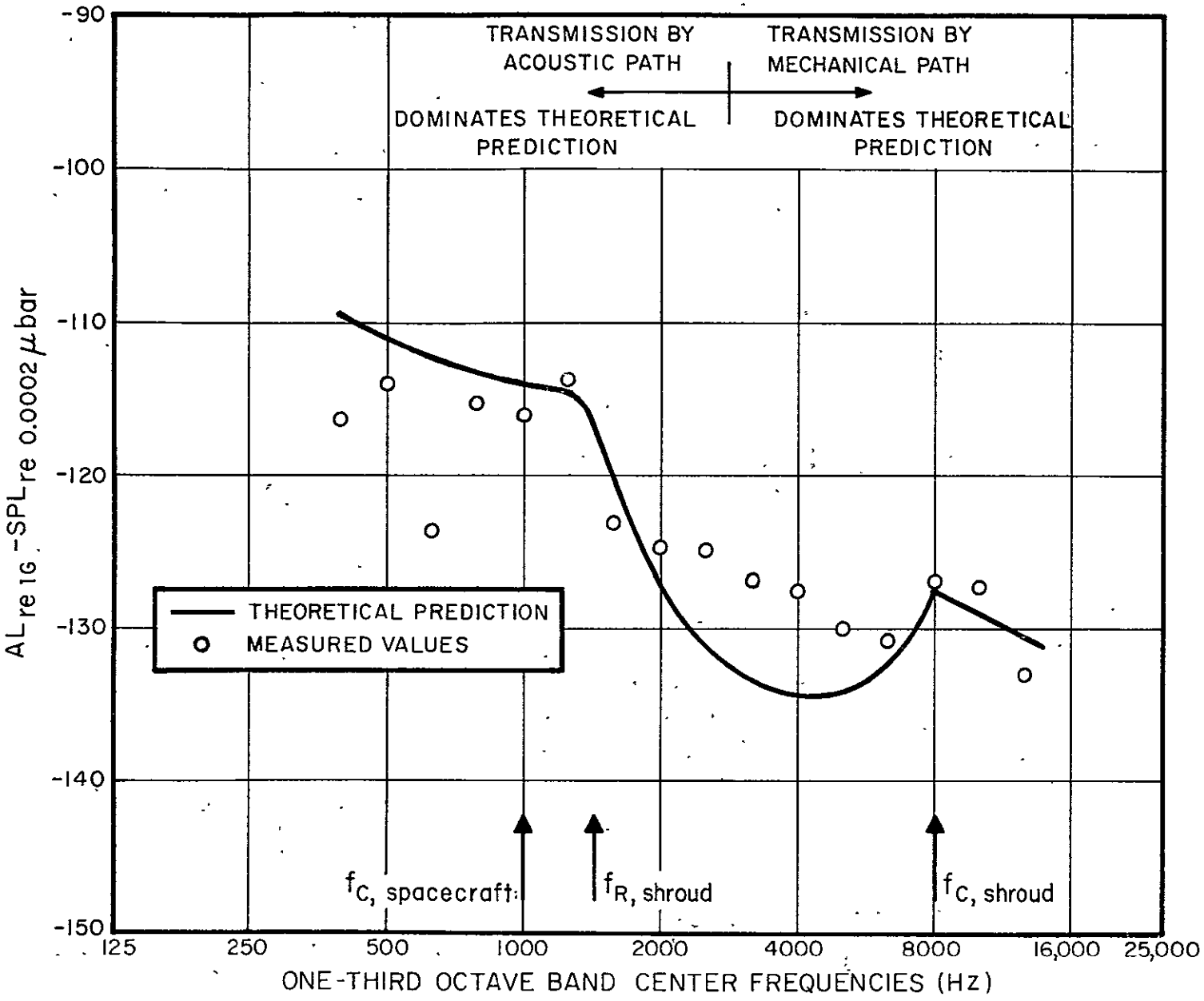

FIGURE 35. SPACECRAFT RESPONSE TO VIBRATION TRANSMITTED BY BOTH PATHS

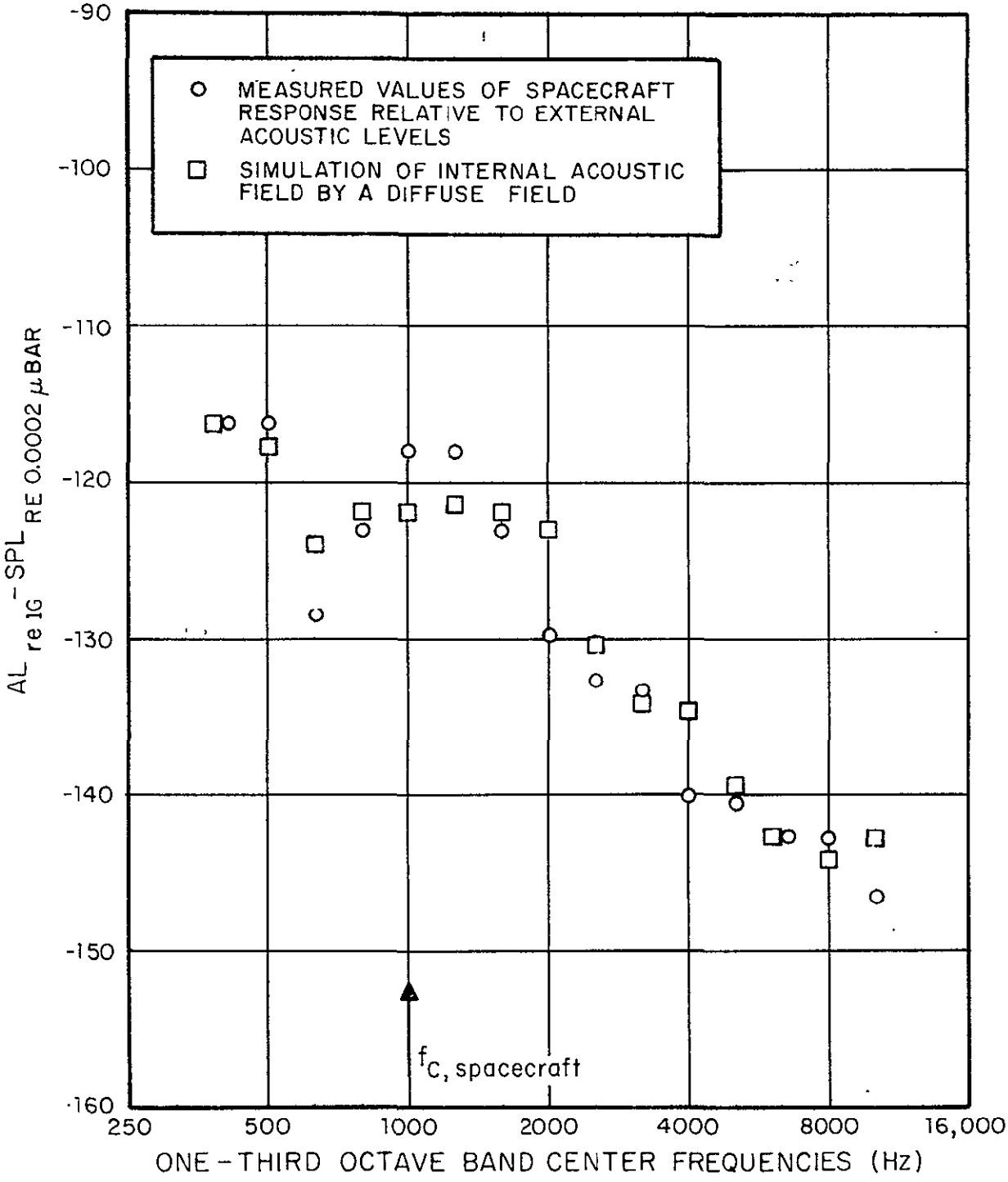

FIGURE 36. SIMULATION OF THE ACOUSTIC PATH EXCITATION

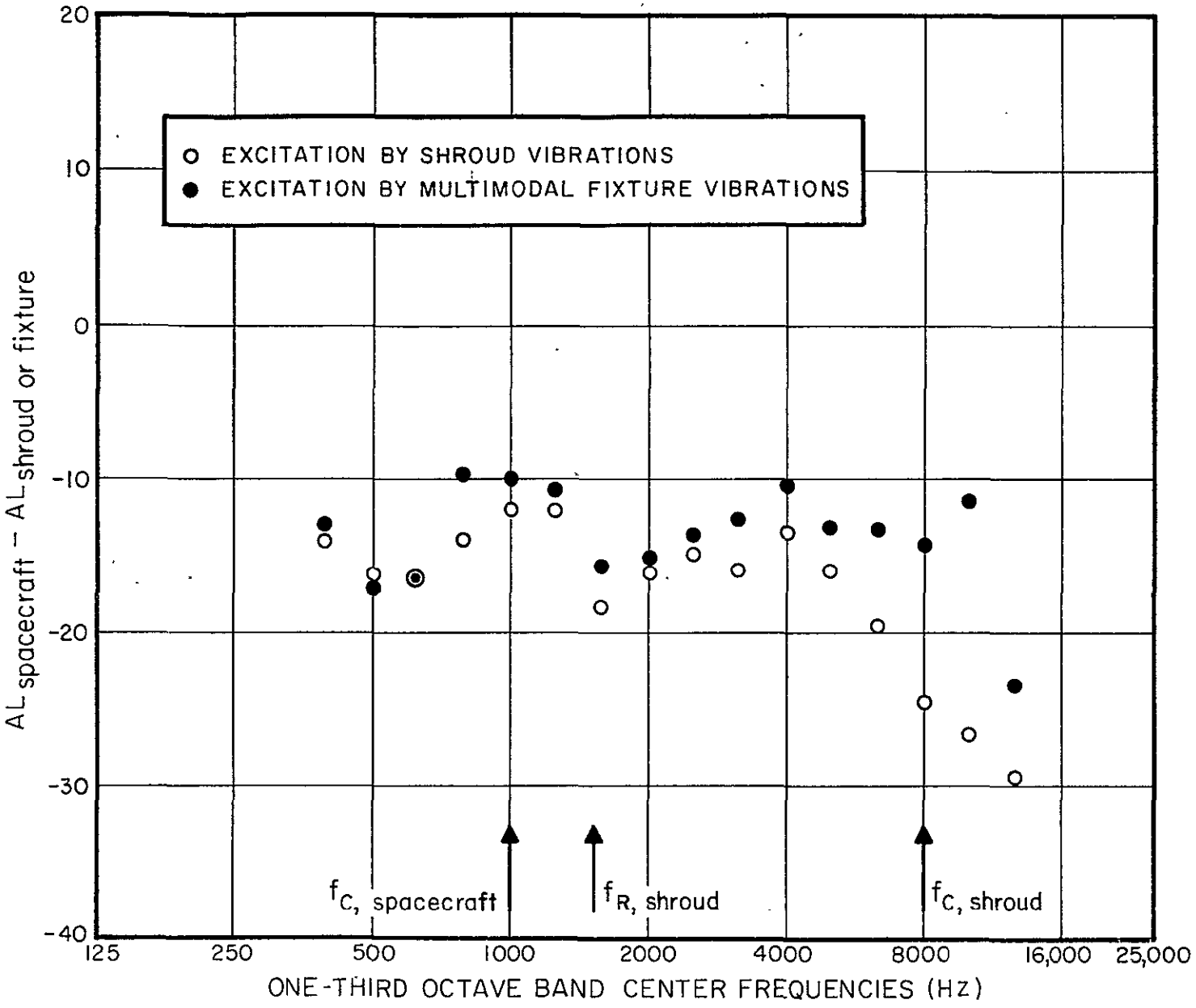

FIGURE 37. SIMULATION OF THE MECHANICAL PATH EXCITATION

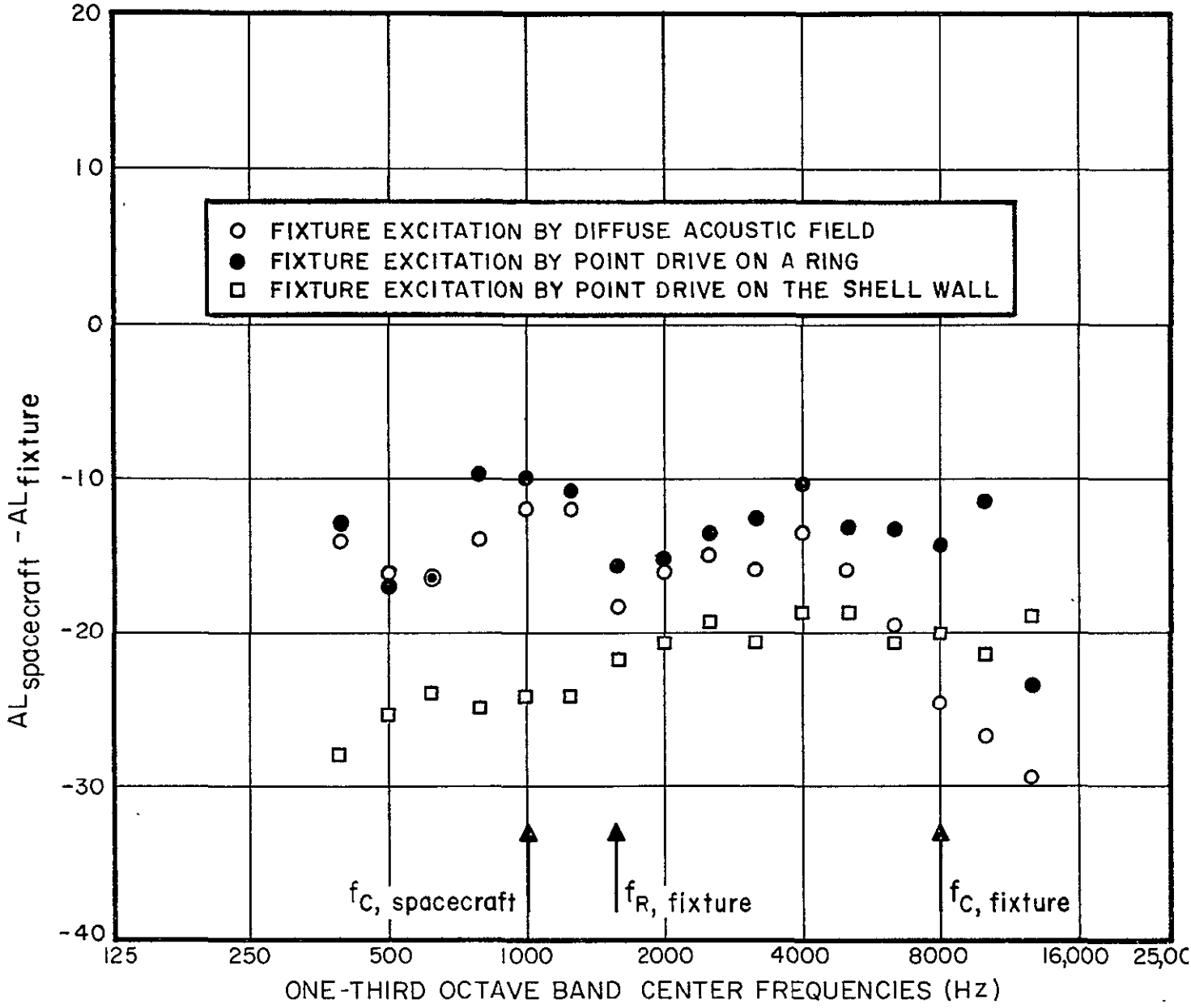

FIGURE 38. VIBRATION TRANSMISSION FOR DIFFERENT TYPES OF EXCITATION

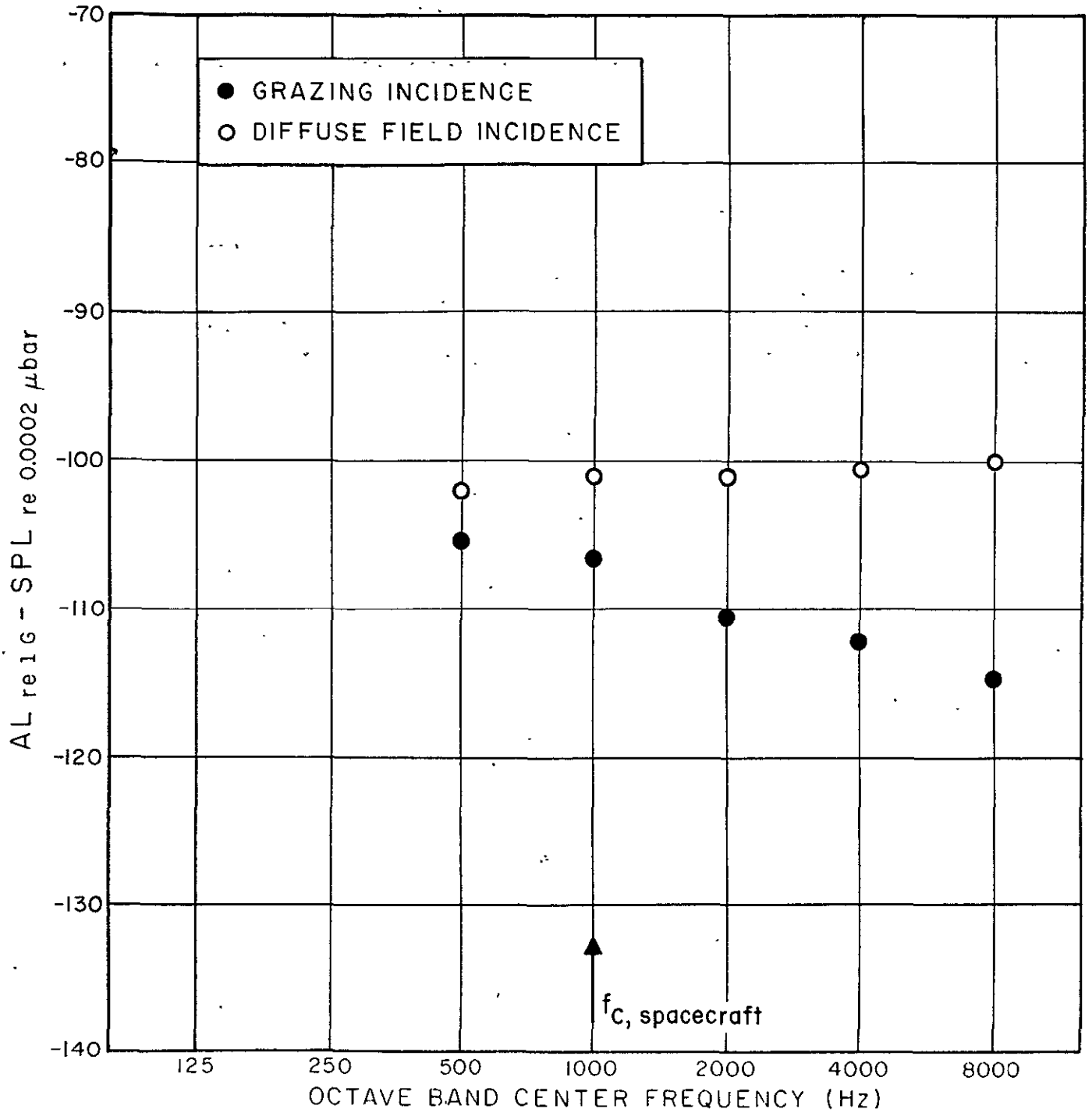

FIGURE 39. SPACECRAFT RESPONSE TO GRAZING ACOUSTIC EXCITATION

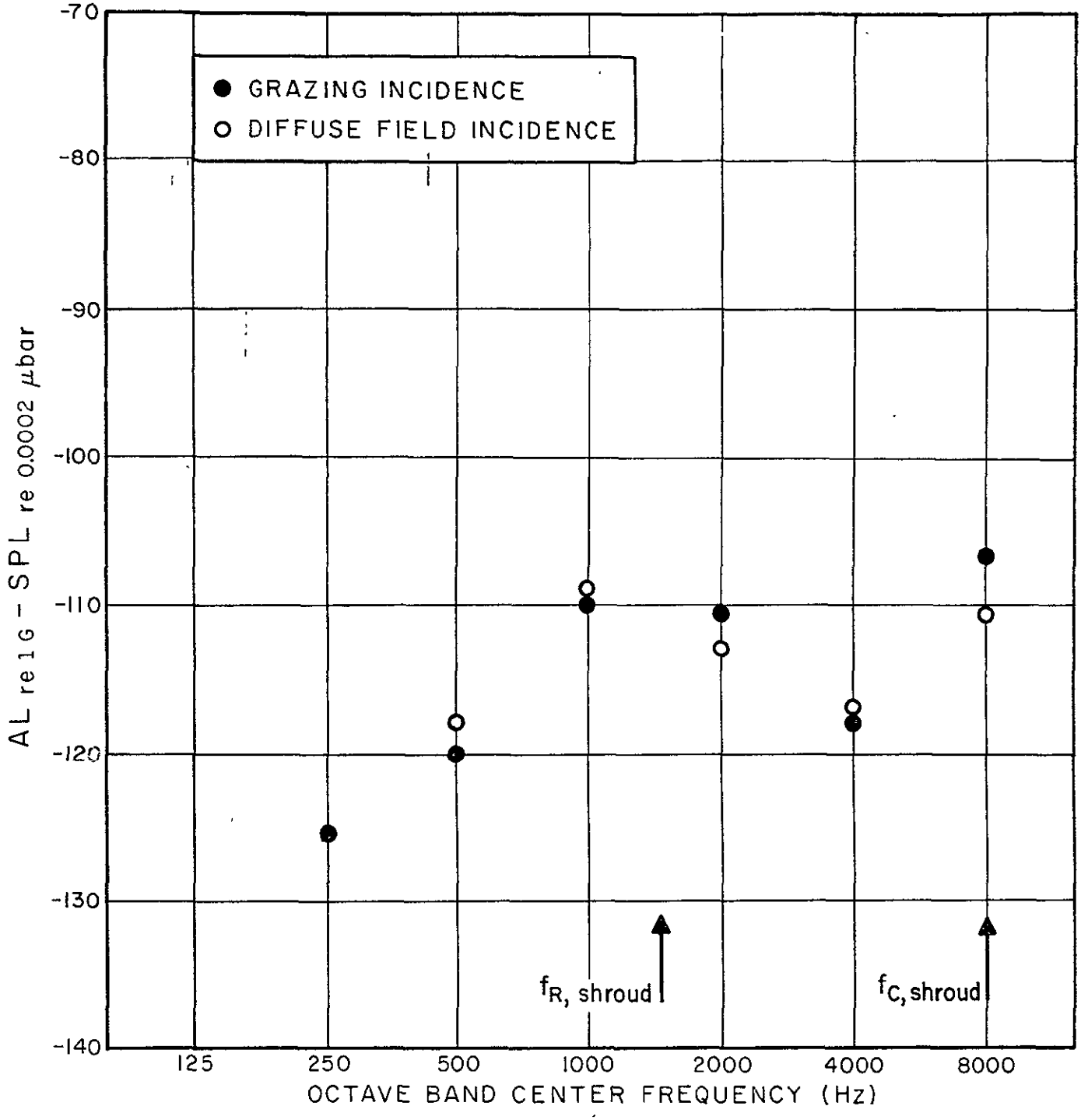

FIGURE 40. SHROUD RESPONSE TO GRAZING ACOUSTIC EXCITATION

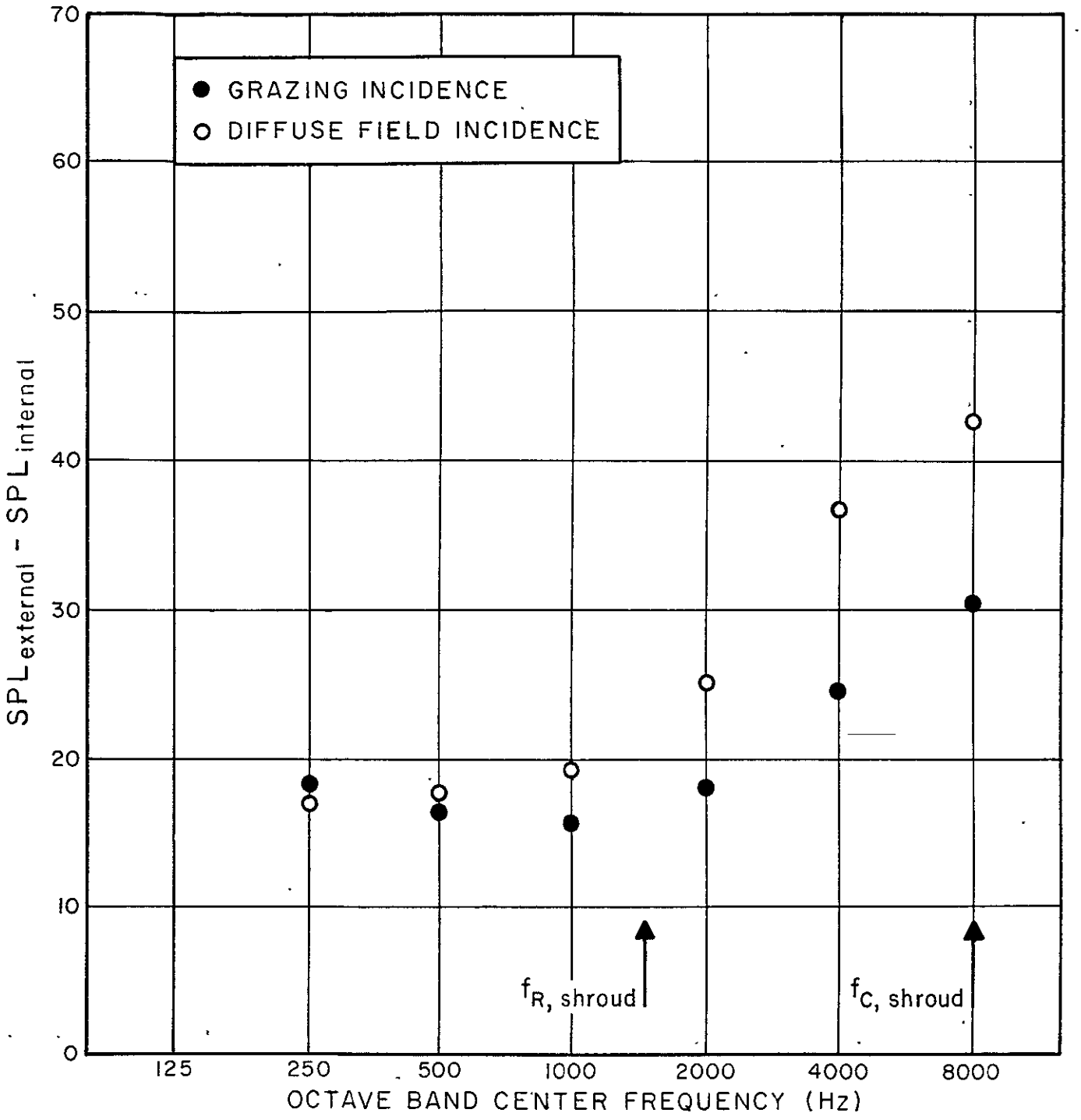

FIGURE 41. SHROUD NOISE REDUCTION FOR GRAZING ACOUSTIC EXCITATION

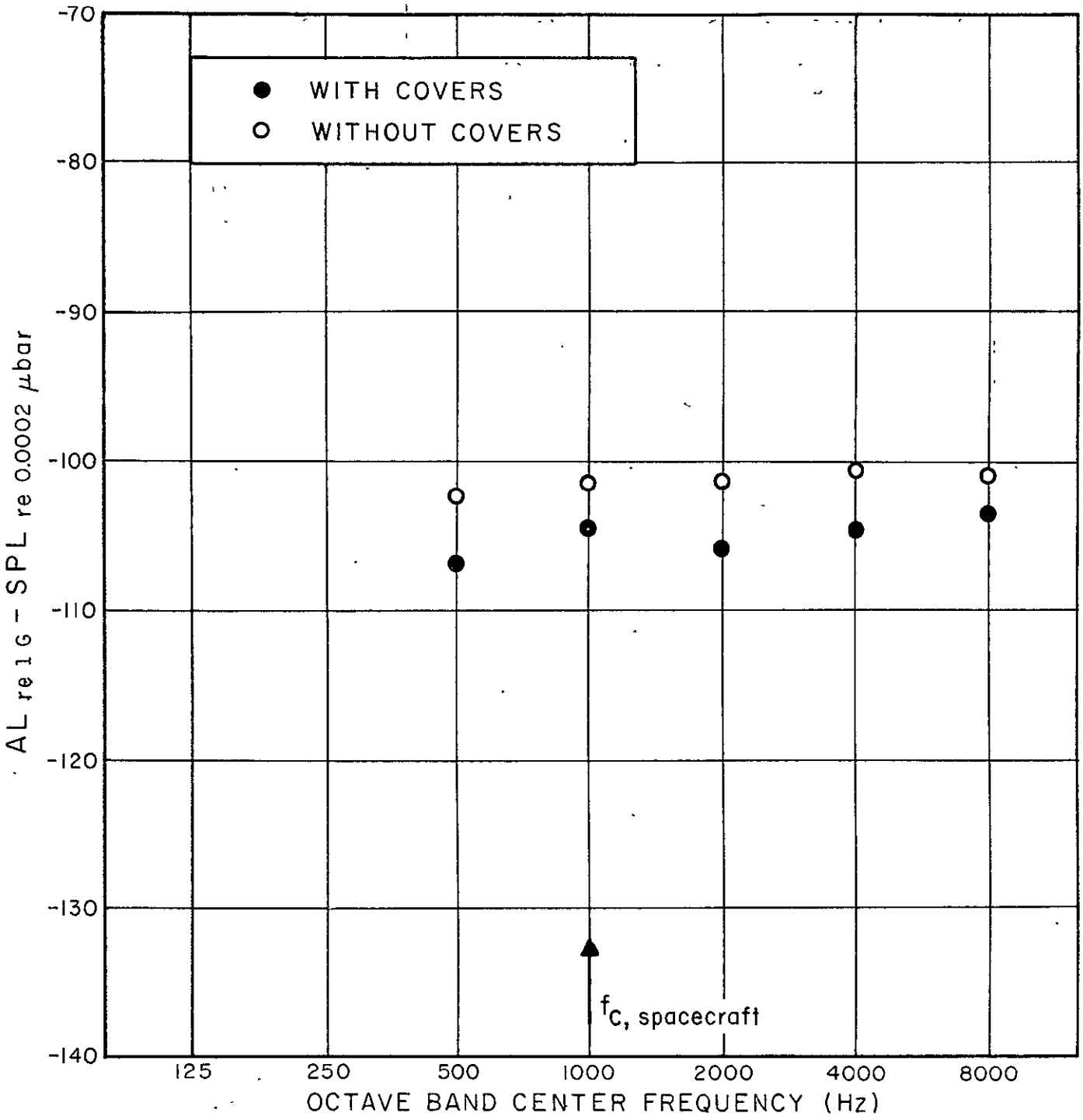

FIGURE 42. EFFECT OF COVERS ON THE SPACECRAFT RESPONSE TO ACOUSTIC EXCITATION

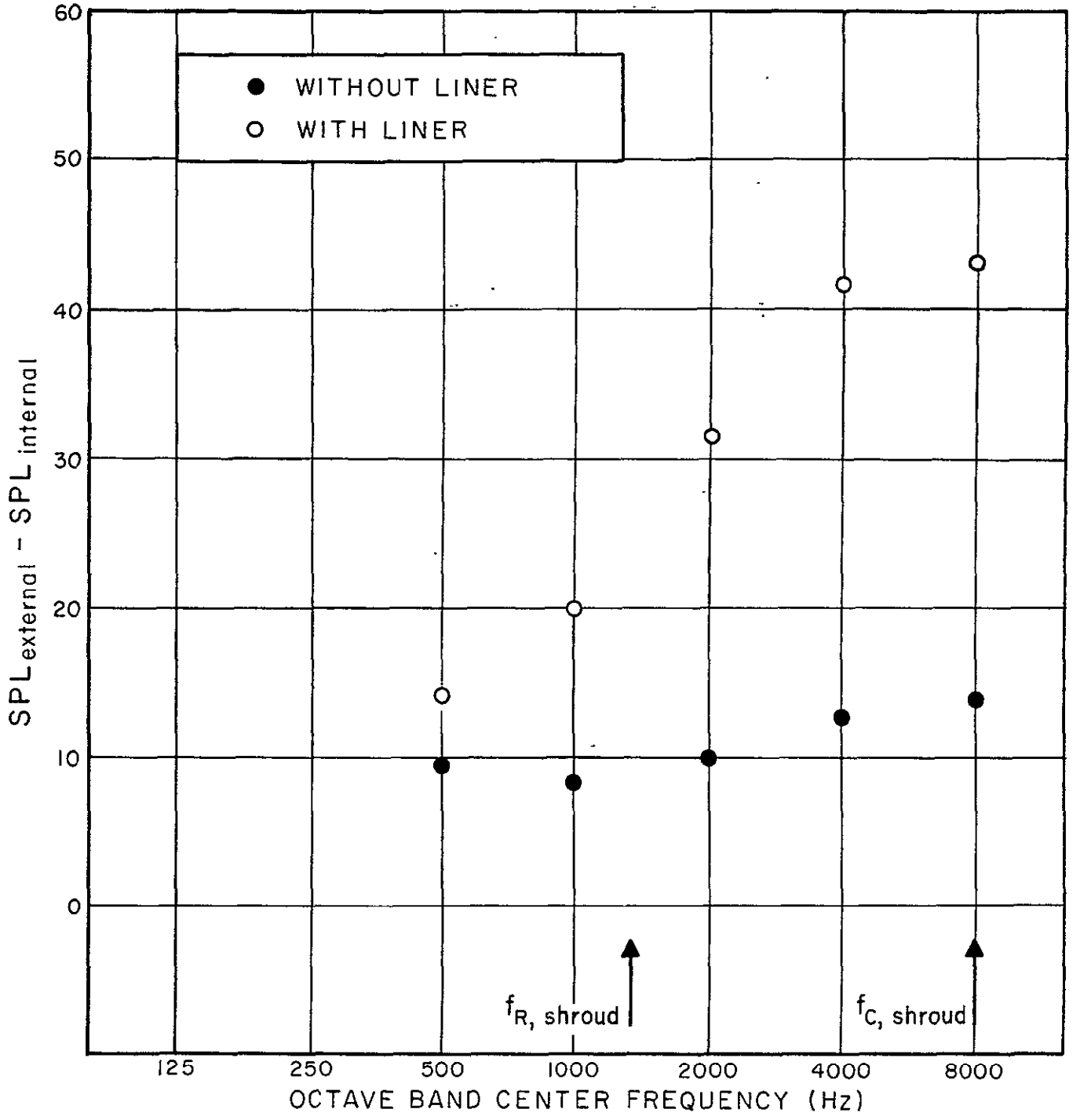

FIGURE 43. EFFECT OF THE ABSORPTIVE LINER ON SHROUD NOISE REDUCTION

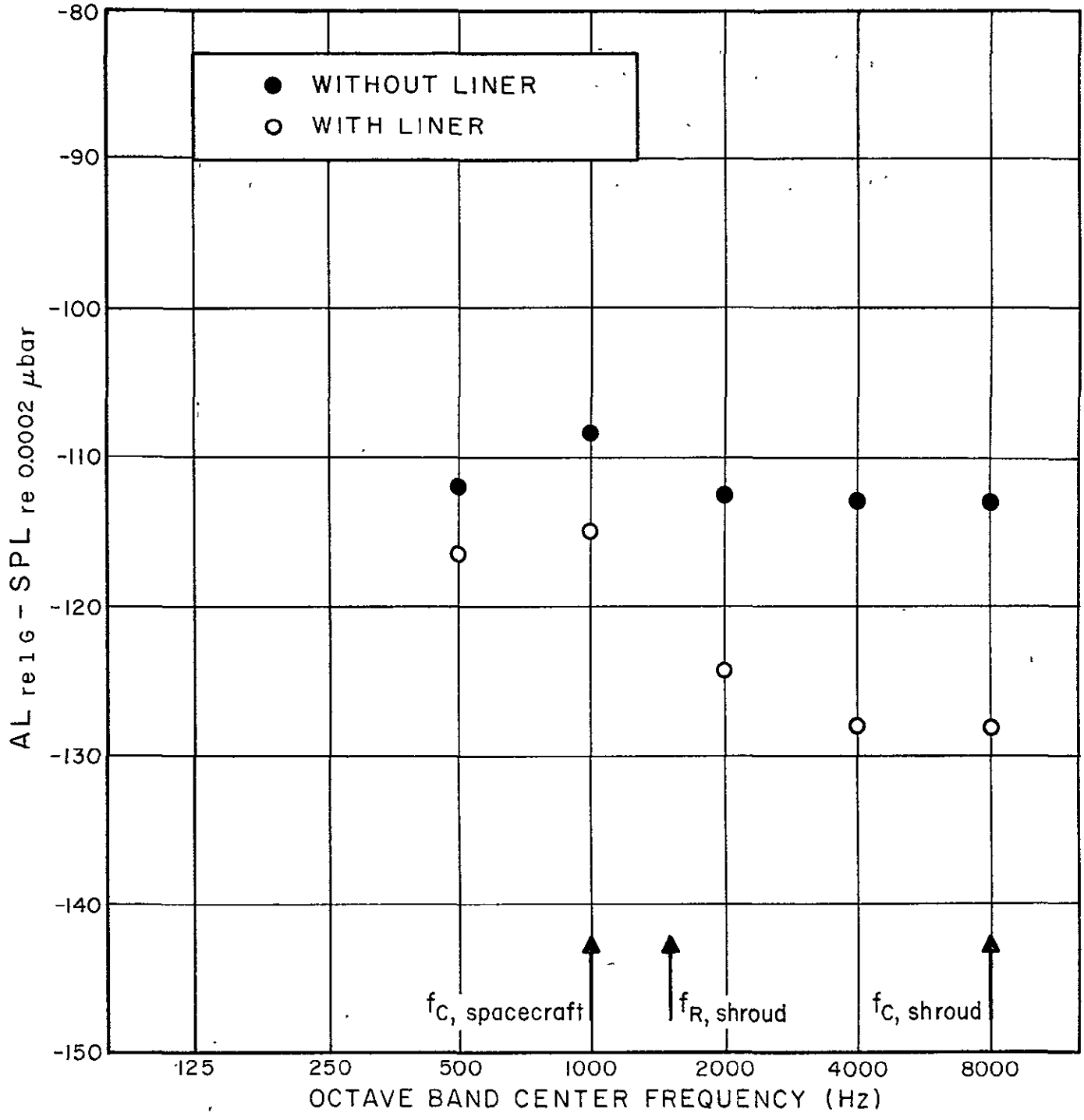

FIGURE 44. EFFECT OF THE ABSORPTIVE LINER ON THE SPACECRAFT RESPONSE TO ACOUSTIC PATH VIBRATION TRANSMISSION

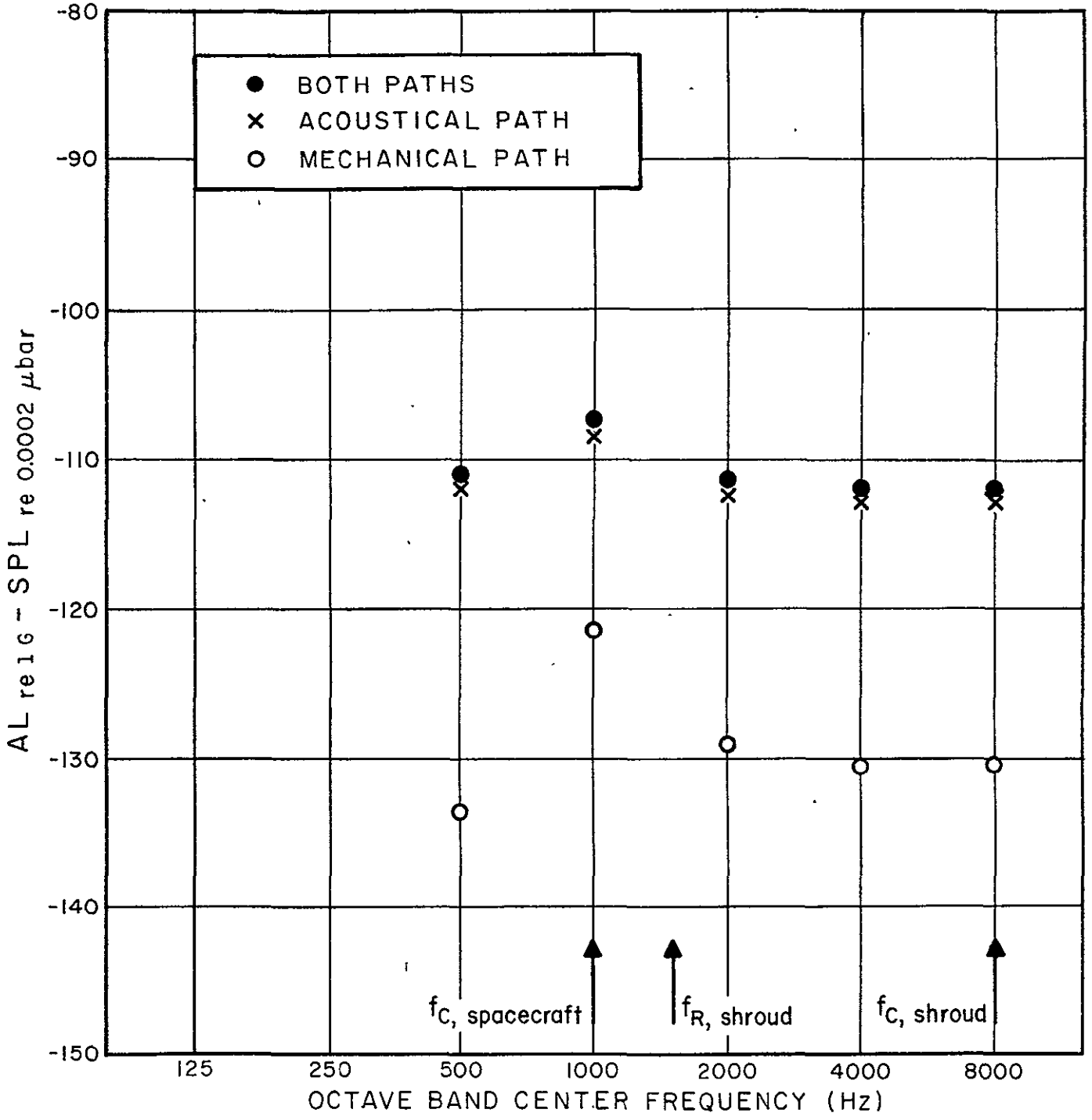

FIGURE 45. SPACECRAFT RESPONSE TO VIBRATION TRANSMITTED BY THE ACOUSTIC AND MECHANICAL PATHS — NO ABSORPTIVE LINER

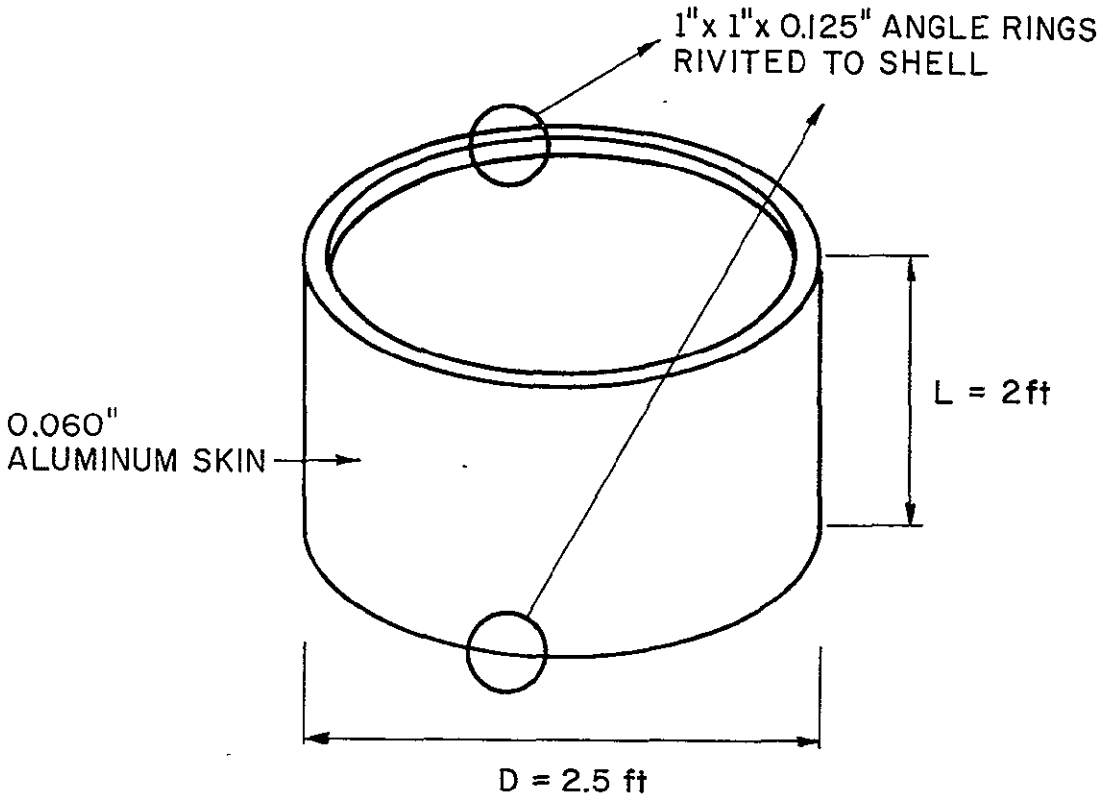

FIGURE 46. THE ADAPTOR

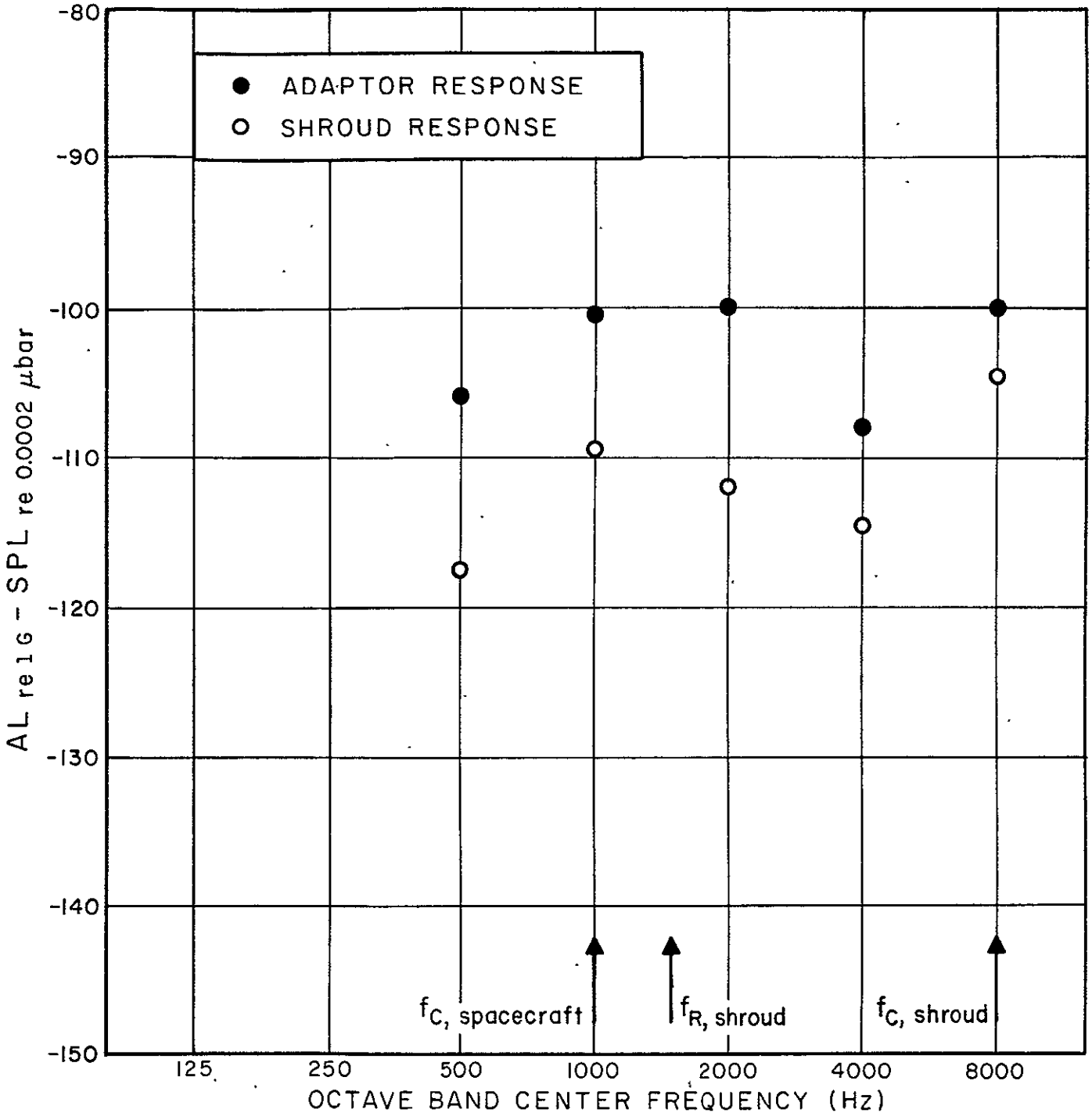

FIGURE 47. ADAPTOR RESPONSE TO ACOUSTIC EXCITATION

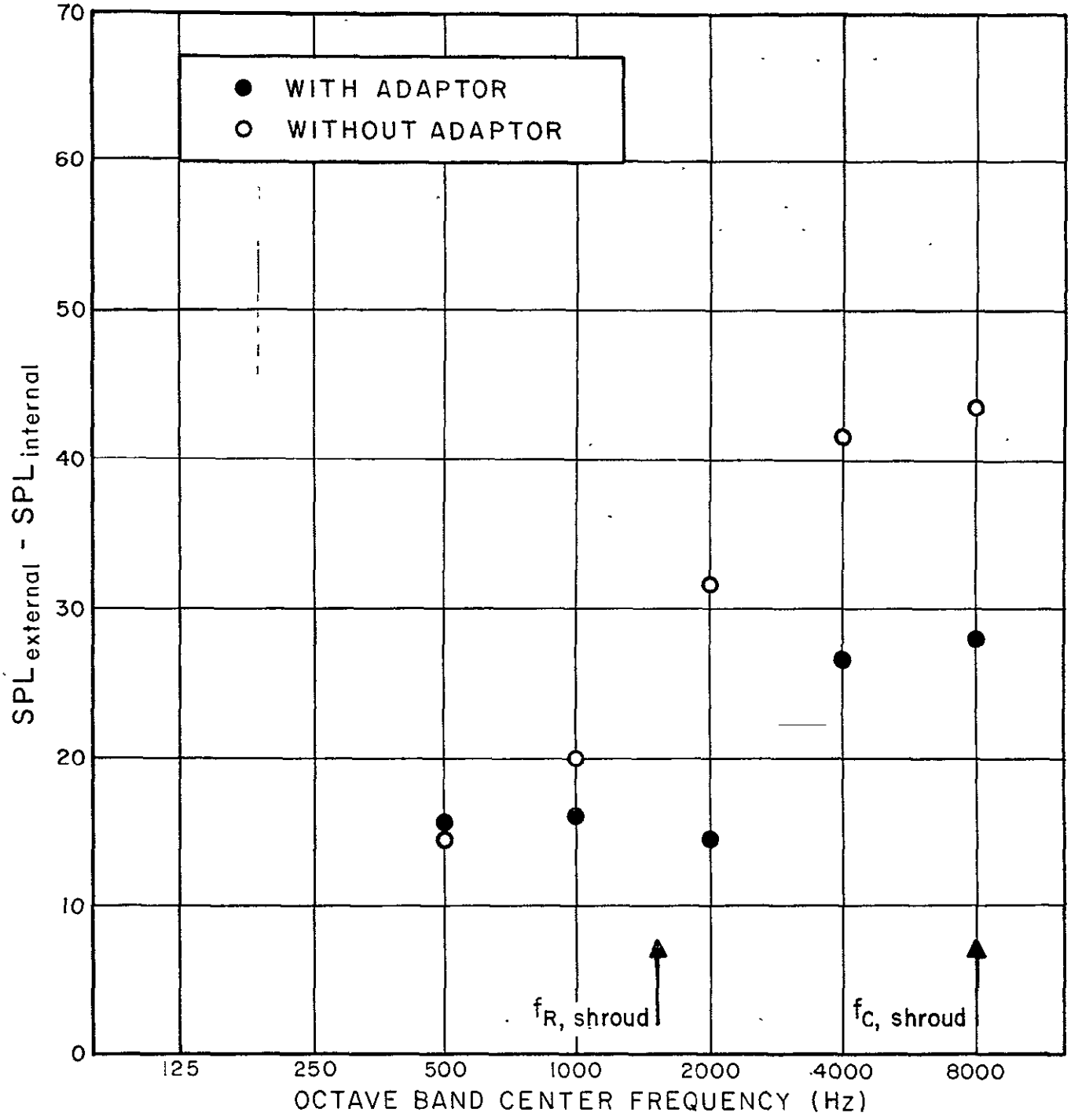

FIGURE 48. NOISE REDUCTION BY THE SHROUD-ADAPTOR ASSEMBLY

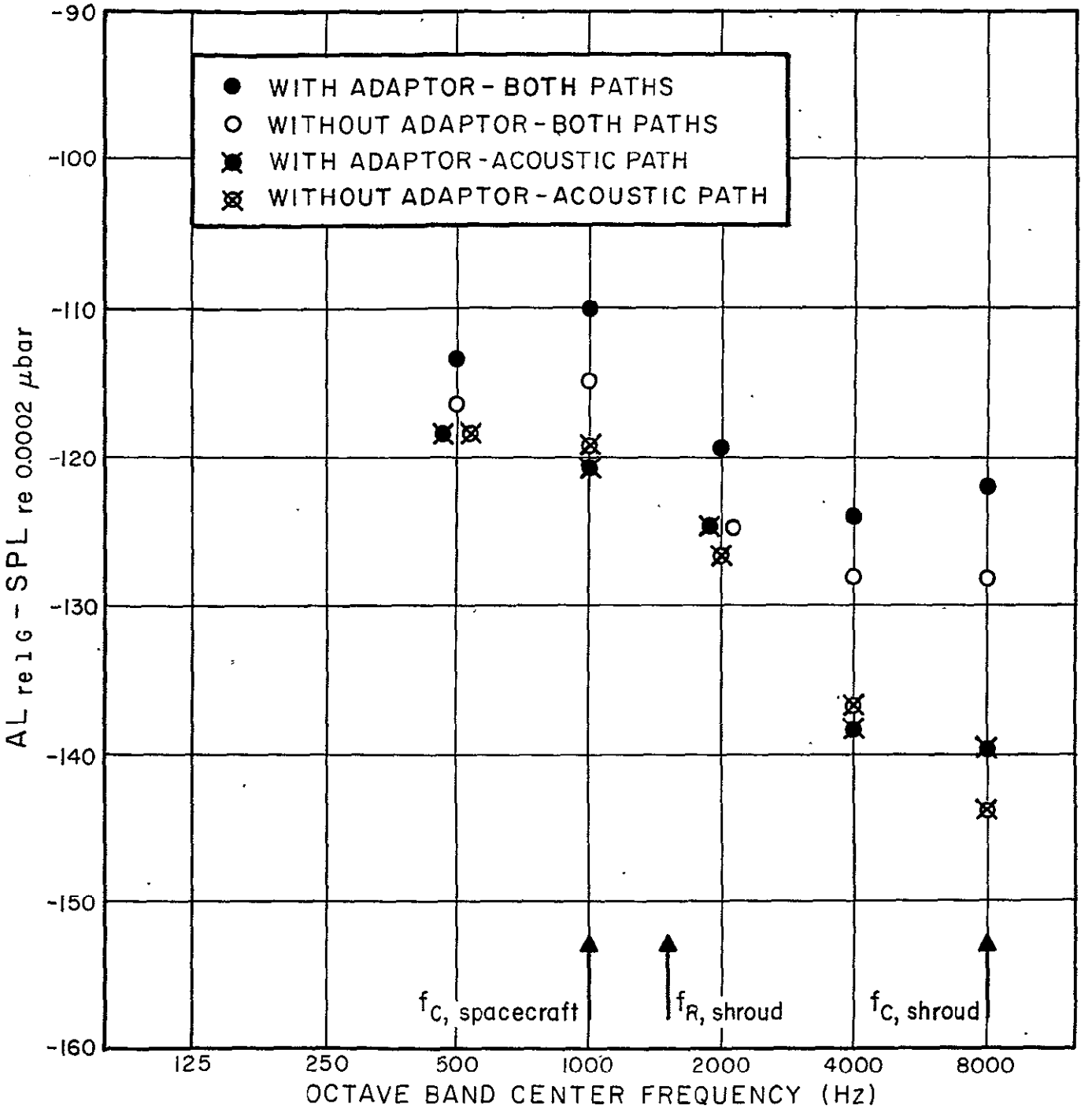

FIGURE 49. SPACECRAFT RESPONSE TO VIBRATIONS TRANSMITTED BY THE ACOUSTIC PATH AND BOTH PATHS COMBINED — WITH ADAPTOR

Unclassified
Security Classification

DOCUMENT CONTROL DATA - R & D

(Security classification of title, body of abstract and indexing annotation must be entered when the overall report is classified)

1 ORIGINATING ACTIVITY *(Corporate author)* BOLT BERANEK AND NEWMAN INC. 50 Moulton Street Cambridge, Massachusetts 02138	2a. REPORT SECURITY CLASSIFICATION Unclassified 2b. GROUP

3 REPORT TITLE

A THEORETICAL AND EXPERIMENTAL MODEL-STUDY OF THE SOUND-INDUCED VIBRATION TRANSMITTED TO A SHROUD-ENCLOSED SPACECRAFT

4 DESCRIPTIVE NOTES *(Type of report and inclusive dates)*
Final Report – 20 January 1967 – 20 July 1969

5 AUTHOR(S) *(First name, middle initial, last name)*

Jerome E. Manning

6. REPORT DATE	7a. TOTAL NO OF PAGES	7b. NO OF REFS
1 May 1970	136	11

8a. CONTRACT OR GRANT NO NAS5-10302 b. PROJECT NO. c. d.	9a ORIGINATOR'S REPORT NUMBER(S) BBN Report No. 1891 9b. OTHER REPORT NO(S) *(Any other numbers that may be assigned this report)*

10 DISTRIBUTION STATEMENT
Distribution of this report is provided in the interest of information exchange. Responsibility for the contents resides in the authors or organization that prepared it.

11 SUPPLEMENTARY NOTES	12. SPONSORING MILITARY ACTIVITY National Aeronautics and Space Administration Goddard Space Flight Center Greenbelt, Maryland 20771

13. ABSTRACT

Results are presented from a three year study of the vibration transmitted to a shroud-enclosed spacecraft from an external acoustic field. The study included both a theoretical prediction of the vibration transmission and an experimental study of a 1/2-scale model of a typical spacecraft assembly. The theoretical predictions were obtained using a statistical energy analysis. Data from the experiments are compared with the predictions to establish the validity and accuracy of the prediction technique. Experiments were also conducted to determine the effect of changes in the model configuration on the vibration transmission. The results of the study indicate that the vibrations transmitted via the internal acoustic space and those transmitted via the mounting trusses are comparible.

14. KEY WORDS	LINK A		LINK B		LINK C	
	ROLE	WT	ROLE	WT	ROLE	WT
Vibration						
Sound						
Spacecraft						